ENGINEERING RESEARCH INSTITUTE
UNIVERSITY OF MICHIGAN
ANN ARBOR

Technical Report No. 3

THE INFRARED SPECTRUM OF

GYPSUM, $CaSO_4 \cdot 2H_2O$

Marvin Hass

PREFACE

The following text has been approved as a dissertation for the doctorate at the University of Michigan. Since the author has derived support (mainly in funds for equipment and computations) from a Signal Corps contract from June, 1954, to May, 1955, the full account of the work is being submitted as a report to the Signal Corps.

The principal financial aid, however, was received from a University of Michigan Teaching Fellowship (1953-54) and from a University of Michigan Research Fellowship (1954-55).

The author would like to thank the following for their aid:

Professor D. Wood for his advice on crystal spectra and infrared instrumentation.

Mr. K. T. Hecht for many helpful discussions in connection with the theoretical aspects.

Professor T. Venkatarayudu for his stimulating discussions of group theory given during his stay at Michigan.

The staff of the MIDAC Computation Group of the Willow Run Research Center for their aid on calculations.

Mr. A. Dockrill for his talents on construction of equipment.

TABLE OF CONTENTS

LIST OF TABLES

LIST OF FIGURES

ABSTRACT

This investigation is concerned with the infrared spectrum of gypsum, $CaSO_4 \cdot 2H_2O$, and its relation to the crystal structure. Both the experimental methods and analysis of the spectrum may be of interest in similar problems. The study may be divided into the following three parts:

1. Determination of the infrared transmission and reflection spectrum of the gypsum for various orientations of the crystal.

2. Conversion of the reflection spectrum into the absorption spectrum.

3. Interpretation of the absorption spectrum in terms of the structure and determination of the orientation of the molecules of water of crystallization.

The infrared transmission and reflection spectrum of gypsum for various orientations was determined using polarized radiation over the frequency range $450 - 4000$ cm^{-1}. Transmission spectra were obtained using sections parallel to the principal cleavage. Suitable transmission samples for the other orientations could not be prepared. Reflection spectra at nearly normal incidence were obtained using three different crystal orientations. Reflection bands corresponding to the stronger infrared active fundamentals of the sulfate ions and water molecules could be identified.

The reflection spectra were converted into absorption spectra using the method reported recently by T. S. Robinson. This requires measurements of the reflection spectrum at normal incidence in contrast to pre-

vious methods which require measurements at two different angles of incidence. The previous methods are not suitable for anisotropic crystals such as gypsum. The theory underlying this method is discussed and the experimental errors are reviewed. Since the calculations are tedious, they were programmed for MIDAC, MIchigan Digital Automatic Electronic Computer.

The various infrared absorption bands can be classified in terms of the symmetry species associated with the space group of gypsum. Since the symmetry of both the sulfate ions and water molecules is lower in the crystal than for the isolated system certain differences in the form of the normal vibrations will occur between the crystal and the isolated system. For the sulfate ion these changes are large since the degenerate vibrations of the isolated system are split in the crystal. The direction and magnitude of crystal perturbations on the sulfate ion can be estimated from a study of the resulting non-degenerate fundamentals. For the water molecules, the fixed orientation in space in the crystal allows prediction of the intensity ratio of the two infrared active crystal fundamentals arising from each molecular fundamental. Good agreement between the observed and predicted values was obtained for the ν_2 (deformation) fundamental and poor agreement was obtained for the ν_1 and ν_3 (stretching fundamentals). The reason for the discrepancy is discussed.

In general, this investigation shows that infrared spectroscopy provides a powerful method for examining the motions of molecules and ions in crystals. However, any conclusions about the positions of molecules deduced from infrared intensities must be examined with care.

OBJECT

The object of this investigation is to utilize infrared spectroscopy in order to elucidate details of crystal structure. In particular, infrared methods show great promise for the location of hydrogen atoms, which are difficult to locate directly by x-ray diffraction due to their low scattering power. The mineral gypsum was chosen as an example of a substance in which the positions of the hydrogens can be inferred from the results of x-ray diffraction. In this way a comparison of infrared and other structural methods can be obtained.

INTRODUCTION

The study of infrared spectra of crystals has received a fresh impetus within the past few years, the principal reasons being recent improvements in the methods of observation and of the theoretical interpretation. Infrared spectroscopy is now recognized as an important means of supplementing x-ray diffraction in elucidating crystal structures. The most obvious advantage of the infrared method lies in locating hydrogen atoms, which are exceedingly difficult to locate by x-ray diffraction due to their low scattering power. This means that infrared methods will be especially valuable where hydrogen bonding exists and when the crystal contains water of crystallization. A thorough infrared investigation of a hydrated crystal in which the position of the heavy atoms has been established by x-ray diffraction has been chosen as the subject of this investigation. The principal requirements governing the choice of a suitable crystal are the following:

1. The crystal structure should be such that the positions of the hydrogen atoms can be inferred from knowledge of the positions of the heavy atoms.

2. The experimental arrangements are simplified if large single crystals are available.

3. Knowledge of the Raman spectrum allows cross-checks with the infrared spectrum as well as sometimes providing information about certain frequencies which appear weakly or not at all in the infrared.

The selection of the mineral gypsum, $CaSO_4 \cdot 2H_2O$, represents a compromise among these factors. The structure determined by x-ray diffraction permits a good guess to be made as to the location of the hydrogen atoms. These deduced positions are consistent with recent nuclear

1

magnetic resonance measurements. The physical properties of gypsum are such that infrared transmission and reflection spectra are readily obtainable. The Raman spectrum has been studied extensively, but the existing interpretations leave certain features unexplained.

The present investigation may be divided into three parts:

1. Determination of the infrared transmission and reflection spectrum of gypsum for various orientations of the crystal.

2. Conversion of the reflection spectrum into the absorption spectrum.

3. Interpretation of the absorption spectrum in terms of the structure and determination of the orientation of the molecules of water of crystallization.

In Chapter 1, previous work on the structure and spectrum of gypsum is reviewed. The prediction of the infrared spectrum is discussed in Chapter 2. The theory of reflection spectra and conversion of reflection spectra to absorption spectra is outlined in Chapter 3. In Chapter 4 the experimental methods and apparatus are described. The experimental results are collated in Chapter 5. An interpretation of the infrared absorption spectrum and Raman spectrum is given in Chapter 6. The determination of the orientation of the water molecules and a discussion of the various anomalies in the infrared and Raman spectrum is also presented in Chapter 6.

CHAPTER 1

REVIEW OF PREVIOUS WORK

1-1 Occurrence and External Appearance of Gypsum

The variety of gypsum known as selenite* occurs naturally in large

transparent single crystals belonging to the monoclinic system.[1] There

is a principal cleavage parallel to the (010) plane.** Plates parallel

to the principal cleavage can easily be obtained in sections twenty-five

to fifty microns thick and, with some care, as thin as fifteen microns.

There are two other cleavages: namely, a fibrous cleavage parallel to

the ($\bar{1}$11) plane and an imperfect cleavage parallel to the (100) plane.

In thin sections parallel to the (010) plane the crystal fractures in

such a way that the fibrous cleavage looks as if it were parallel to the

($\bar{1}$01) plane. A photograph of the crystals used in this study is given

in Figure 1.

1-2 X-Ray Diffraction Studies

1-2.1 Unit Cell Dimensions

The crystal structure has been determined by x-ray diffraction by

W. A. Wooster.[2] The axes chosen by Wooster differ from those tradition-

---

*There are other varieties of gypsum. These have the same crystal
structure as selenite, but their physical properties make them unsatis-
factory for infrared analysis.

**The numbers inside parentheses indicate the Miller indices of the
plane.
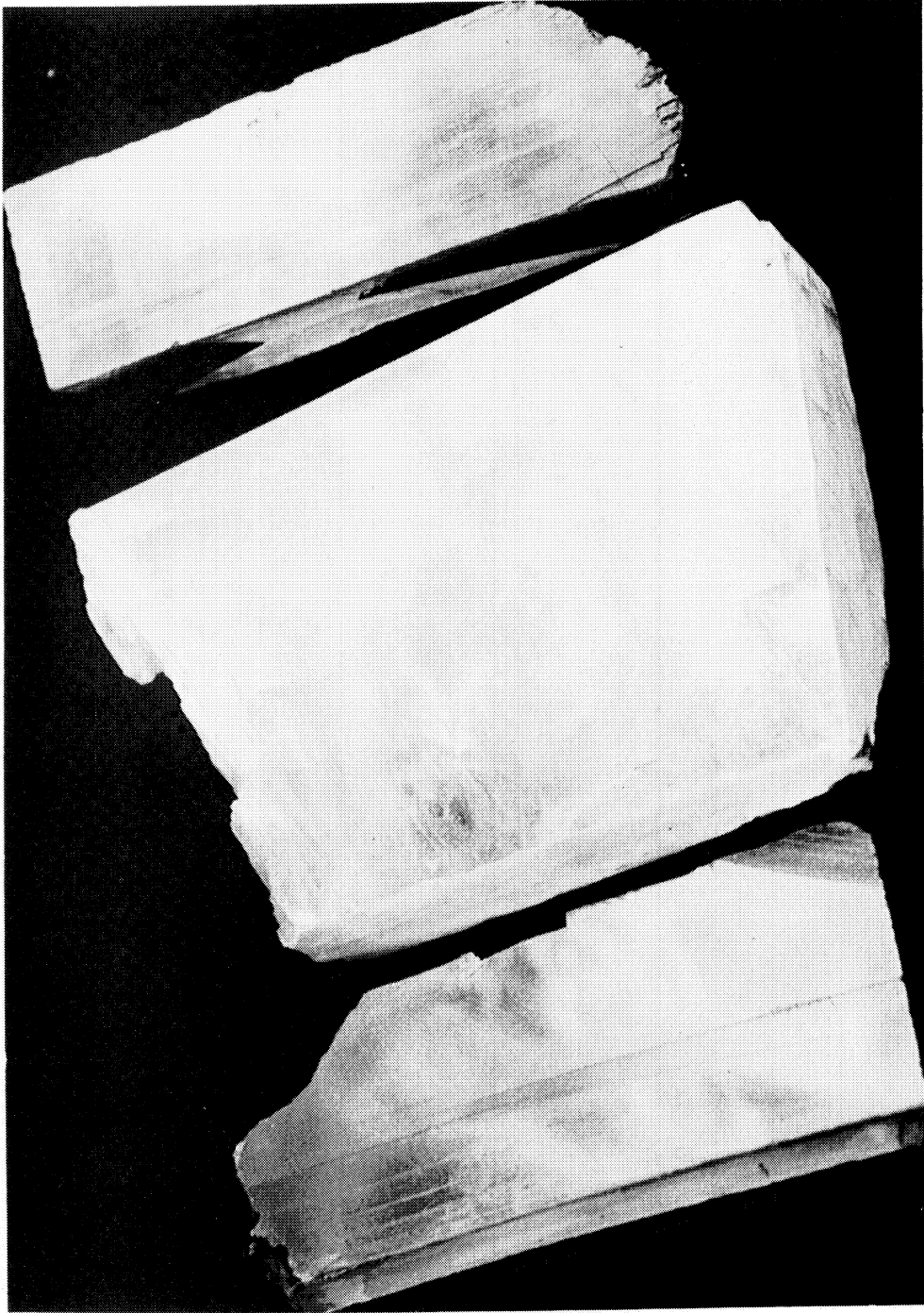
Figure 1. Photograph of Selenite Crystals (actual size).

ally assigned by mineralogists from the external appearance of the crystal. The cell dimensions with respect to the Wooster axes (reduced to Angstrom units from the kX units which we assume were used by Wooster are as follows:

$$\underline{a} = 10.49 \text{ A.U.}, \quad \underline{b} = 15.18 \text{ A.U.}, \quad \underline{c} = 6.52 \text{ A.U.}, \quad \beta = 151°33'$$

This unit cell contains four molecules of $CaSO_4 \cdot 2H_2O$*. The relation between the traditional axes and the Wooster axes is shown in Figure 2. The $\underline{a}$ and $\underline{b}$ axes are the same in both notations, only the $\underline{c}$ axis is different. The traditional axes will be used for describing the spectroscopic results since it was found empirically that the spectroscopically significant directions are parallel and perpendicular to the $\underline{c}$ axis in the traditional notation. A table containing certain planes written in both notations is given in Table 1. The symbol (K) will follow the Miller indices of any plane written using the traditional axes, which is different when written using the Wooster axes.

TABLE 1

CRYSTAL PLANES

Plane	Traditional Notation (Used in Thesis)	Wooster Notation
Principal Cleavage	010	010
Fibrous Cleavage	$\bar{1}11$	$\bar{1}11$
Imperfect Cleavage	100(K)	$\bar{2}01$

---

*It has been pointed out that a cell having shorter axes and a smaller angle β can be found having the same volume. This cell is preferred by convention but will not be given here[3,4].
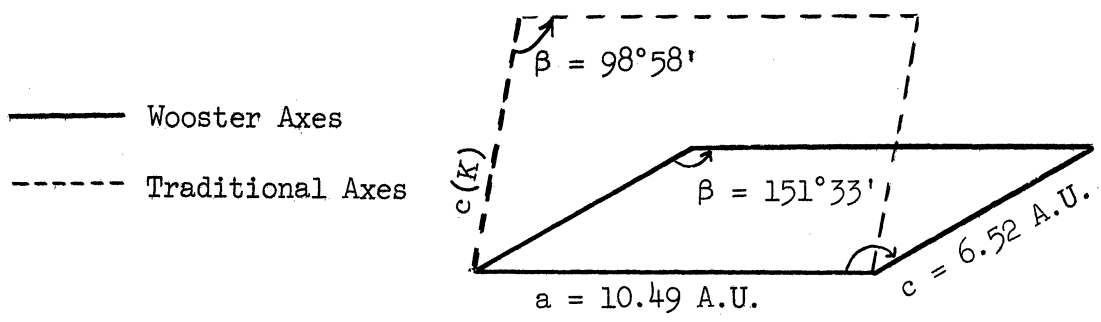
Figure 2. Projection of Unit Cell on (010) Plane

1-2.2 Space Group

From a careful study of the x-ray diffraction pattern, Wooster con-
cluded that the crystal belongs to the space group C_{2h}^6 in the Schoenflies
notation (or $C2/c$ in the Hermann-Mauguin notation). In the standard
treatises on space group theory it is shown that any space group can be
regarded as the product of an invariant subgroup containing the symmetry
elements of pure translation and a factor group containing the symmetry
elements of the Bravais unit cell. The factor group of the space group
of gypsum contains the symmetry elements E, C_2, i, and $C_2 \cdot i = \sigma_g$.
Whereas in point groups the identity operation E transforms a point only
into itself, in factor groups the meaning is generalized to include trans-
formations to a corresponding position in all the other unit cells. The
center of inversion i does not lie on the two-fold axis C_2. Consecutive
application of the C_2 operation and the inversion operation gives rise
to a glide plane σ_g perpendicular to the C_2 axis. A glide plane corres-
ponds to a reflection across the plane followed by a translation parallel
to the plane.

At this point it might be helpful to explain the meaning of the
space group symbols. The part C_{2h} of the Schoenflies symbol indicates
that it is related to the point group C_{2h}. The superscript 6 is an index
number of space groups isomorphous to the point group. In the Hermann-
Mauguin notation the symbol 2/c refers to a C_2 axis perpendicular to a
c type glide plane, or one having a translation in the direction of the c
axis. The capital C indicates an end-centered Bravais lattice with the
end positions located on (001) planes.

Gypsum has an end-centered Bravais lattice. For end-centered,
body-centered, and face-centered Bravais lattices, the unit cell of
spectroscopic interest differs from that usually reported from x-ray

data. The unit cell of spectroscopic interest is called the Bravais unit
cell and is defined as the smallest unit under which no two atoms become
equivalent under simple translations. In cases where the lattice is
primitive, the Bravais unit cell and the crystallographic unit cell are
identical. In all other cases, the Bravais unit cell is either one-
quarter or one-half the size of the crystallographic unit cell.[5] This
is illustrated in Figure 3, which shows an end-centered Bravais lattice.
The crystallographic unit cell is the rectangular parallelopiped defined
by ABCDA'B'C'D', while the Bravais unit cell is outlined by AEDFA'E'D'F'.
The Bravais unit cell in this case is one-half the size of the crystallo-
graphic unit cell. The crystallographic unit cell contains four mole-
cules of $CaSO_4 \cdot 2H_2O$, but the Bravais unit cell contains only two mole-
cules of $CaSO_4 \cdot 2H_2O$. This will become obvious when the atomic structure
is considered.

1-2.3 Positions of the Calcium and Sulfate Ions

A photograph of a scale model of a Wooster unit cell is shown in
Figure 4. In the photograph the black rods outline the unit cell with
the b axis vertical. The light-colored vertical rods represent C_2 axes.
The calcium (black) and sulfur (light) nuclei are located on C_2 axes.
Each sulfur is surrounded by four oxygens in a tetrahedral configuration.
Each black ball located near two small white balls (representing protons)
is a water oxygen. The water molecules occur in layers centered at dis-
tances of $b/4$ and $3b/4$ units above the base. The calcium and sulfate
ions also occur in layers centered at 0, $b/2$ and b units above the base.
These layers are parallel to the principal cleavage of the crystal.

A projection on the (010) plane (base of model) reproduced from
Wooster's paper is shown in Figure 5. The sulfate tetrahedra project
as squares. The sulfate ions lie in rows parallel to the c(K) axis.
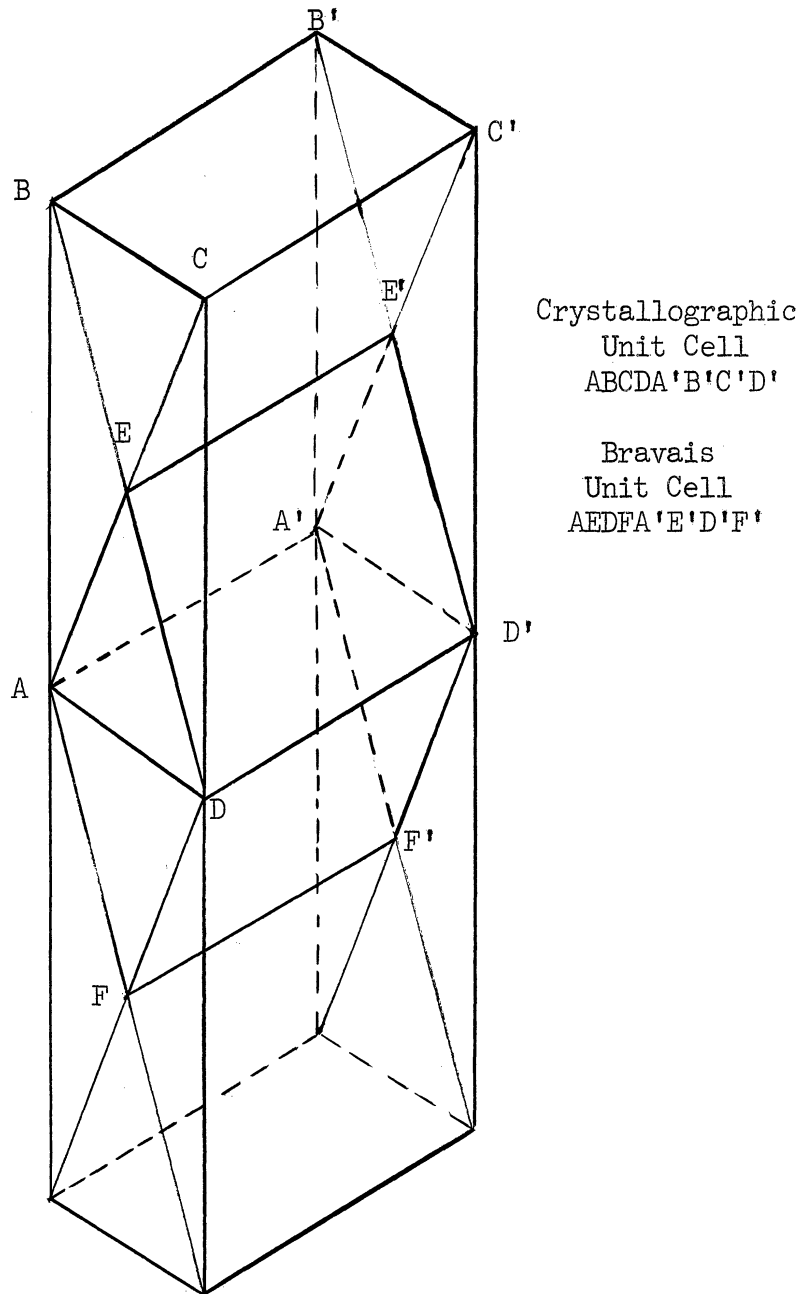
Figure 3. Crystallographic and Bravais unit cell
for end-centered lattice.
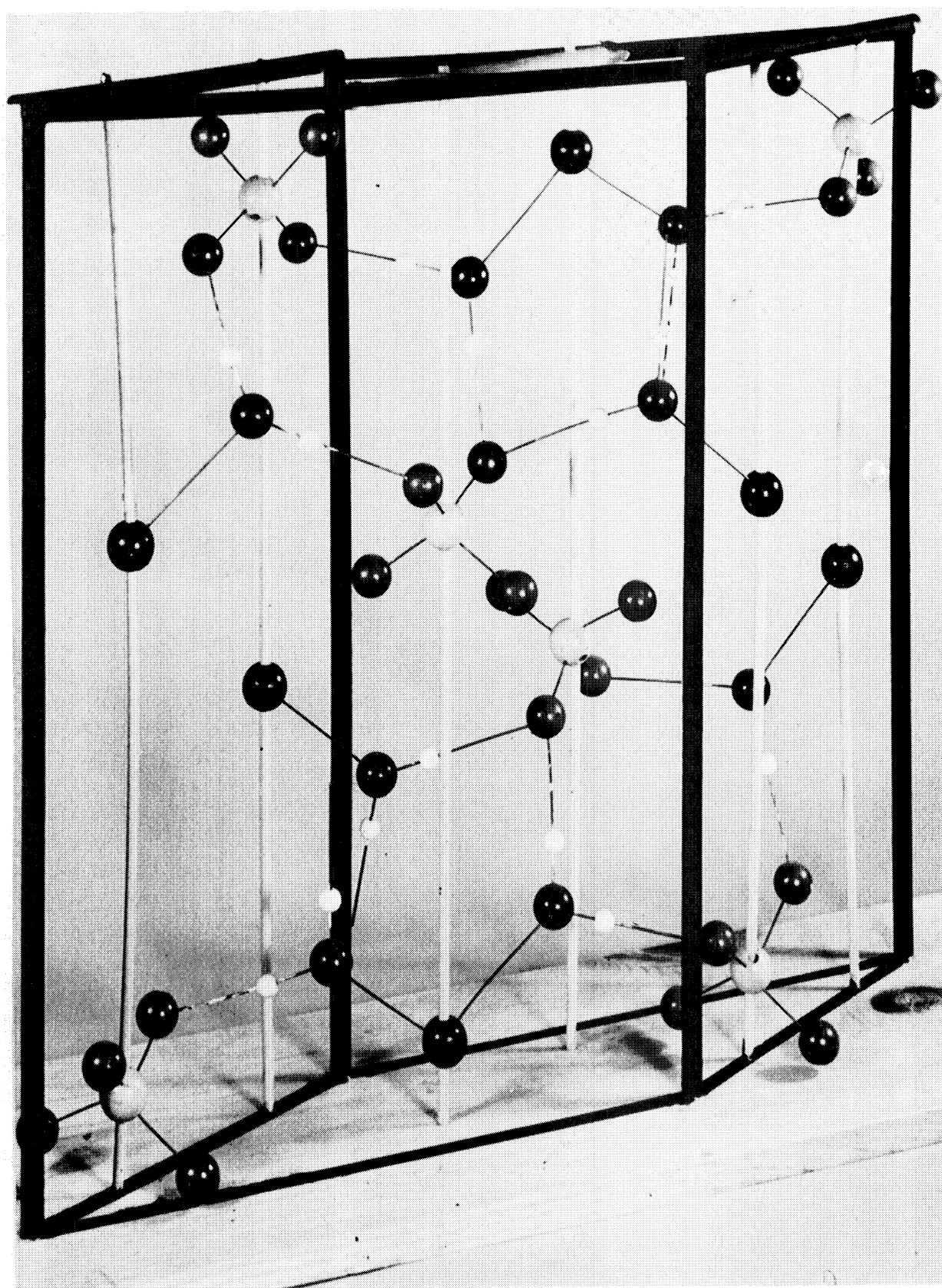
Figure 4. Photograph of scale model of unit cell
of gypsum (the _b_ axis is vertical).
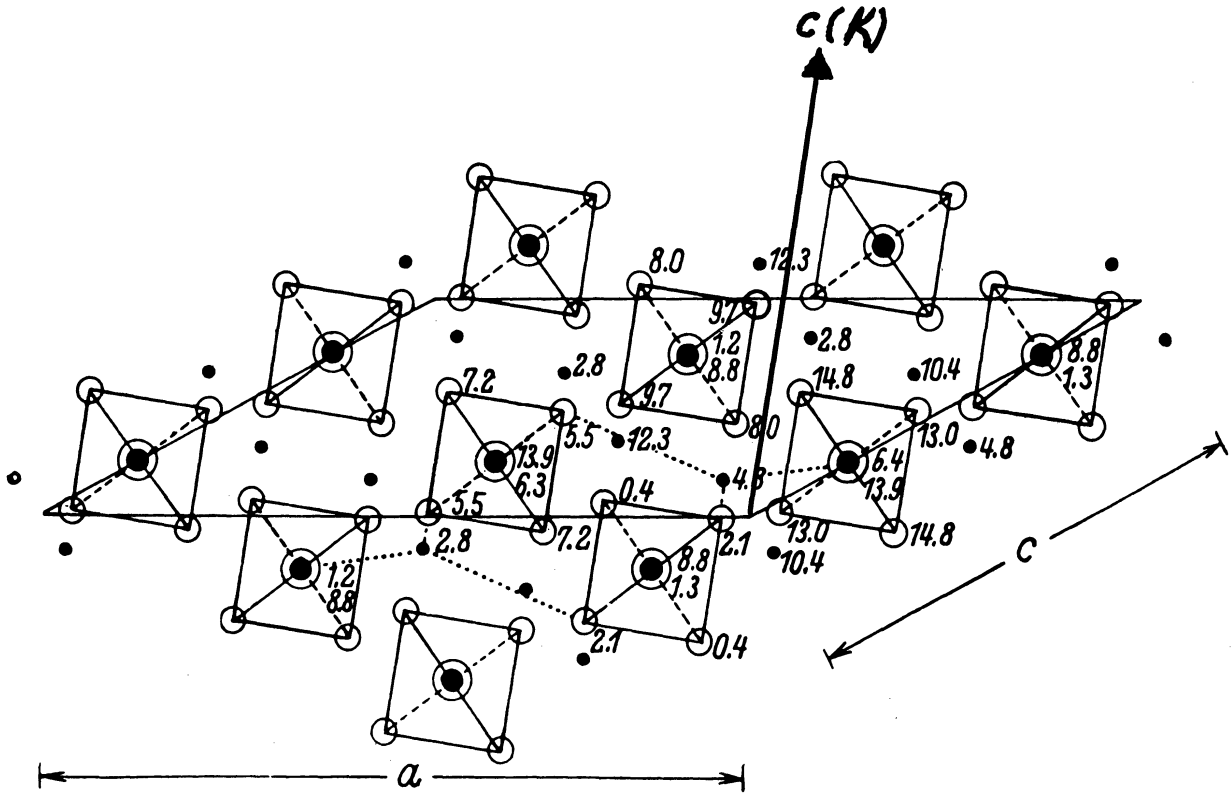
Figure 5. Projection of the structure on the (010)
plane. Heights are given in Ångstrom units.
Squares indicate sulfate tetrahedra. The upper of
the two numbers beside the symbol ◉ gives the
height of Ca, and the lower gives the height of the
S [reproduced from W. A. Wooster, Z. Krist. 94, 375
(1936)]. The c(K) axis has been drawn over Wooster's
diagram.

This feature of the structure will be referred to later in discussing the spectroscopic results.

A projection perpendicular to the Wooster c axis reproduced from Wooster's paper is shown in Figure 6. This corresponds to looking along the AA' axis in Figure 3. The diamond-shaped Bravais unit cell is outlined. In this projection the sulfate ions are of two orientations. Members of each kind can be transformed into each other by a simple translation. For this reason there are only two sulfate ions in the Bravais unit cell, while there are four in the crystallographic unit cell.

The sulfate oxygens are of two kinds, designated as O_I or O_{II}. The O_I atoms are nearer to the water oxygens than the O_{II} atoms. Each Ca^{++} ion is surrounded by six sulfate oxygens and two water oxygens. Two of the sulfate oxygens are nearer than any of the others.

A list of interionic distances given by Wooster is shown in Table 2. These distances may indicate directions and relative magnitudes of forces which will be of interest later on in interpreting the spectrum.

1-2.4 Positions of the Water Molecules

The presumed location of the water molecules in the unit cell is shown in the photograph of the model. There are four molecules of H_2O in the Bravais unit cell although there are eight in the crystallographic unit cell. This can be shown in a similar way, as was done in the previous section for the sulfate ions.

The hydrogens can not be directly located by x-ray diffraction. Knowledge of the positions of the other atoms of the crystal provides a clue to the location of the hydrogens. The distance between the water oxygen and the nearest sulfate oxygen is listed in Table 2 at about 2.70 A.U. This is comparable with the oxygen-oxygen distance of 2.76 A.U. in ice. If the protons are located on the lines joining the water
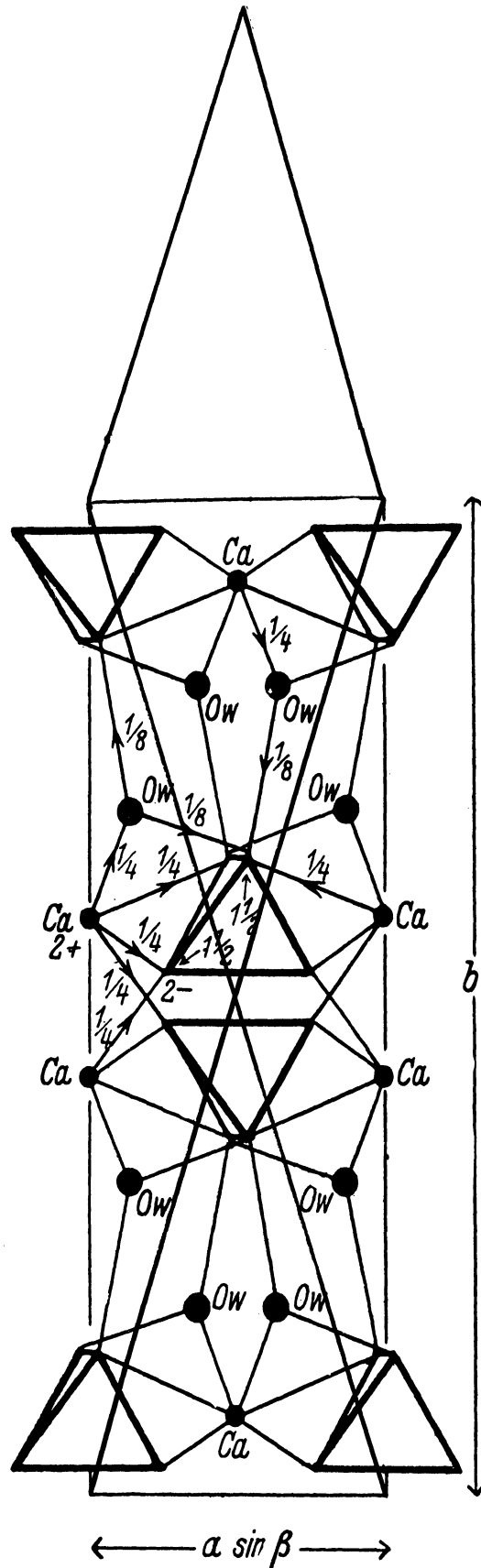
Figure 6. Projection of the structure with the Wooster c axis perpendic-
ular to the paper. Numbers indicate the distribution of valency bonds
[reproduced from W. A. Wooster, Z. Krist. 94, 375 (1936)]. The outline
of the diamond-shaped Bravais unit cell has been drawn over Wooster's
diagram.

oxygens and the nearest sulfate oxygens, then the $H \diagdown O \diagdown H$ angle is 108°, which differs only slightly from the value of 104°27' given by infrared analysis for water vapor[6].

TABLE 2

IONIC ENVIRONMENTS**

Central Ion	Surrounding Ions		Separation in A.U.
	Nature	Number	
Ca	O_I	2	2.59
	O_{II}	2	2.38
	O_{II}	2	2.57
	O_W	2	2.44
O_I	O_I*	1	2.43
	O_{II}*	1	2.43
	O_{II}*	1	2.43
	S*	1	1.49
	O_W	1	2.70
	O_W	1	2.71
	O_W	1	3.06
	Ca	1	2.59
	O_I	1	4.11
O_{II}	O_I*	1	2.43
	O_I*	1	2.43
	O_{II}*	1	2.43
	S*	1	1.49
	Ca	1	2.38
	Ca	1	2.57
	O_W	1	3.11
	O_{II}	1	3.35
O_W	Ca	1	2.44
	O_I	1	2.70
	O_I	1	2.71

*within the same sulfate group

**taken from W. A. Wooster[2]

1-3 Nuclear Magnetic Resonance Studies

The results of an investigation by G. E. Pake[7], using nuclear magnetic resonance, are consistent with the deduced structure. This tech-

nique allows measurement of the distance between the proton pairs of the water of crystallization in gypsum, as well as the orientations of the lines joining the proton pairs with respect to the crystallographic axes. The experiment is best explained by the following quotation from Pake's paper.

> Since the interaction between magnetic dipoles falls off as the inverse cube of the separating distance, nuclear moments in certain crystals, e.g., protons in water molecules of hydration, may possibly occur in pairs the members of which are so closely spaced that each nucleus finds itself predominently in the local field of its partner. Classically we should then expect each nuclear dipole to produce at its partner a field of several gauss, the component of which along the H_O field of several thousand gauss will alter somewhat the effective large field. In fact, if θ is the angle between H_O, taken in the z direction, and the line joining the two interacting nuclei, this local field component varies as $3 \cos^2 \theta - 1$ and space quantization of the nuclear spin in the H_O field should produce nuclear resonance fine structure governed by this angular factor. In particular, for spin 1/2, we may naively write the magnitude of the effective field at one nucleus of the pair as
>
> $$H_{eff} = H_O \pm \alpha \, (3 \cos^2 \theta - 1)$$
>
> where the $\pm$ sign attempts to account for the two possible values of the z component of the partner's magnetic moment, and α is an interaction field parameter to be fixed by a more careful analysis. Thus, the naive picture predicts a pair of nuclear resonance lines symmetrically disposed about the field value at which a simple resonance line would occur.

The maximum change in the effective field will occur when the angle between the magnetic field and the line joining the proton pair is at a minimum for the crystal orientation used. The orientation of the crystal when the effective field is at an extremum can be related to the orientation of the lines joining the proton pairs in the crystal. Evaluation of the interaction constant α allows determination of the H-H distance r from the equation $\alpha = \frac{3}{2} \mu r^{-3}$ in which μ is the magnetic moment.

The H-H distance was found to be 1.58 A.U. If the protons are assumed to lie on the lines joining the sulfate and water oxygens, then the OH distance comes out to 0.98 A.U., compared to 0.96 A.U. in the water vapor.

1-4 Spectroscopic Investigations

1-4.1 Infrared Studies

There have been a number of infrared studies of gypsum reported in the literature. The papers on transmission spectra are listed in Table 3 and those on reflection spectra in Table 4.

TABLE 3

LITERATURE SURVEY
TRANSMISSION SPECTRA OF GYPSUM

Investigator and Year	Reference	Orientation	Region cm^{-1}	Remarks
Coblentz (1905-21)	8,9,10,11	(010)	800-10,000	NaCl prism; compared $CaSO_4 \cdot 2H_2O$ and $CaSO_4$
Goens (1921)	12	(010)	1200-4000	Used polarized light
Ellis (1931)	13	(010)	5000-10,000	
Carrelli (1937)	14	(010) (Ī01)	5000-10,000	
Louisfert (1947)	15,16	(010) (Ī01)	4300-11,000	Used polarized light Quartz prism
Pain, Duval and Lecomte (1953)	17	(010) crystal and mull	2000-4000	Mulls of $CaSO_4 \cdot 2H_2O$ and $CaSO_4 \cdot 2D_2O$ P-E Model 12C Spectrometer-LiF prism
Webber (1954)	18		3000-9000	Used polarized light Prism-grating spectrometer Results unpublished
Hunt, et al., (1950) Miller and Wilkins (1952) Keller, et al., (1953)	19 20 21	powder	650-5000	NaCl prism

TABLE 4

LITERATURE SURVEY
REFLECTION SPECTRA OF GYPSUM

Investigator and Year	Reference	Orienta- tion	Region cm^{-1}	Remarks
Aschkinass (1900)	22	(010)	1150	
Coblentz (1906)	8	(010)	1150	
Koch (1908)	23	(010)	1150	
Randall (1911)	24	(010)	1150	
Schaefer and Schubert (1916)	25	(010)	600- 10,000	Examined other sulfates; used polarized light near 1150 cm^{-1}
Rubens (1920)	26		32- 450	Used polarized light
Goens (1921)	12	(010)	850- 1250	Used polarized light

Most of the transmission spectra and all of the reflection spectra were reported more than thirty years ago. The transmission spectrum reported by Coblentz[8] consists of strong absorption below 800 cm^{-1}, strong absorption near 1150 cm^{-1}, bands near 1600 cm^{-1}, 3500 cm^{-1}, and a weaker doublet near 2200 cm^{-1}. Additional weaker bands above 3800 cm are also given. Since $CaSO_4$ and $CaSO_4 \cdot 2H_2O$ which was heated to expel the water did not show strong bands near 1600 cm^{-1} and 3500 cm^{-1}, Coblentz concluded that these bands were associated with the water of crystallization. From a study of reflection spectra of sulfates, Schaefer and Schubert[25] showed that a complex band near 1150 cm^{-1} and a simple band near 670 cm^{-1} are common to gypsum and other sulfate crystals. The work of Rubens[26]

and Goens[12] is interesting in that plane-polarized radiation was employed. The intensities of the bands was found to depend markedly on the angle of polarization with respect to the orientation of the crystal. The measurements of Rubens extended to very long wavelengths.

Detailed information on the polarized transmission and reflection spectra at high resolution and for various crystal orientations is lacking. The available results indicate a considerable dependence on these factors. No work has been reported on the spectrum at various temperatures.

1-4.2 Raman Studies

The Raman spectrum of gypsum has been examined by many investigators. A bibliography of the work done before 1945 (16 references) is given by Krishnan.[29] A list of all subsequent papers and earlier papers which will be referred to later is given in Table 5. An excellent Raman spectrum published by Krishnan is reproduced in Figures 7 and 8, along with the microphotometric records.

The assignments next to the microphotometric records have been written in by the author (M. H.). Depolarization ratios of the strong fundamentals of the sulfate ions and water molecules have been measured. The discussion of the assignments and depolarization ratios will be postponed until Chapter 6. It is worth stating at this time that gypsum is among the few crystals whose Raman spectrum has been studied extensively.

TABLE 5

LITERATURE SURVEY
RAMAN SPECTRA OF GYPSUM

Investigator and Year	Reference	Subject
Cabannes and Aynard (1942)	27	Theory and experimental results on 3400 cm^{-1} water band
Rousset and Lochet (1945)	28	Depolarization ratios of sulfate frequencies
Krishnan (1945)	29	General survey and combinations and overtones
Gross and Val'kov (1948)	30	Low frequency lattice oscillations
Stekhanov (1953)	31	Low temperature study of 3400 cm^{-1} band
Aynard (1953)	32	High temperature study of 3400 cm^{-1} band
Cabannes, Couture, and Mathieu (1953)	33	Depolarization ratios of 3400 cm^{-1} band
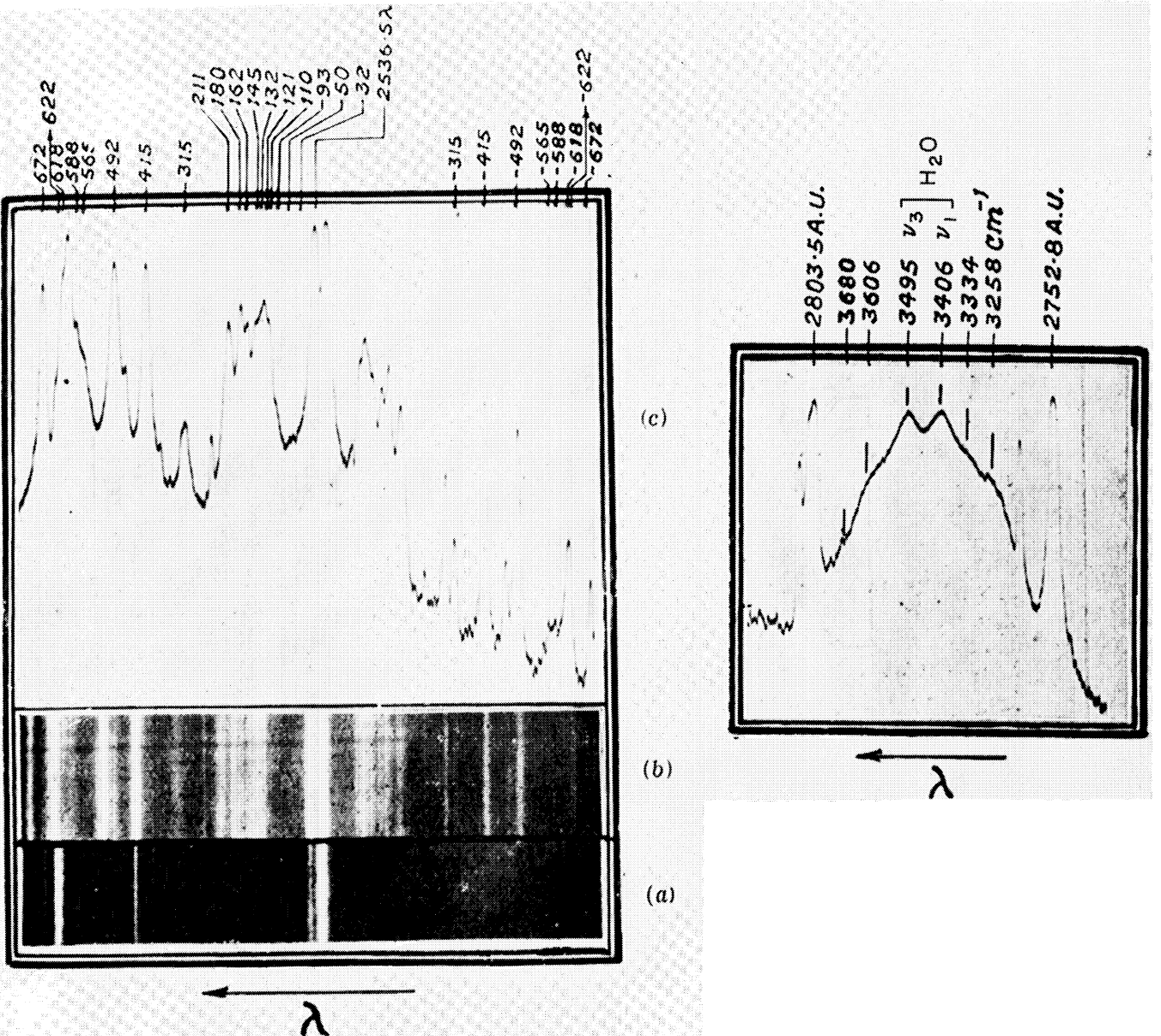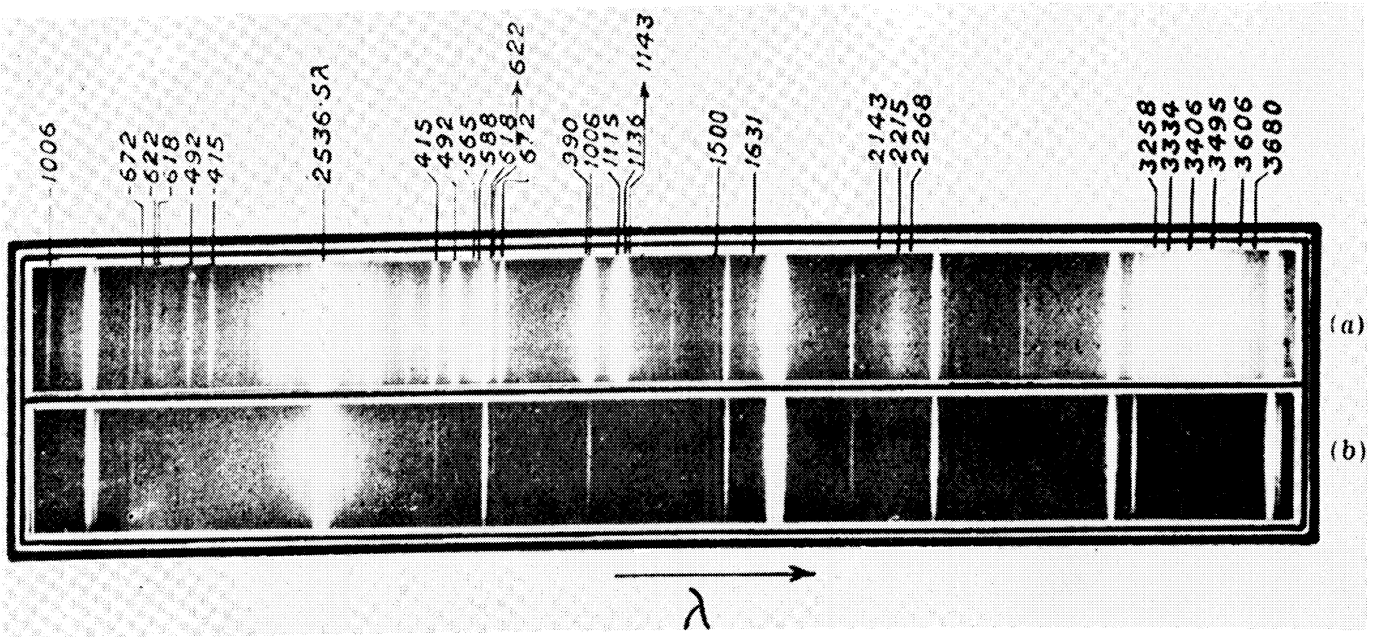
Figure 7. Raman Spectrum of Gypsum.
[Reproduced from R. S. Krishnan, Proc. Indian Acad. Sci. 22A, 274 (1945)]

λ2536·5
32
50
93
110 121
132
145
162
180
211

315

415
λ2563·9

492

565
588
λ2576·3
618
622
672

990
1006

1115
1136
1143

2536·5

32
50

93

110
121
132
145

162
180

211

315

415

492

565
588

λ
618
622

672

990
1006

1115
1136
1143

Lattice
Oscillations

SO_4: ν_2

SO_4: ν_2

H_2O: ν_R

SO_4: ν_4

SO_4: ν_4

SO_4: ν_1

SO_4: ν_3
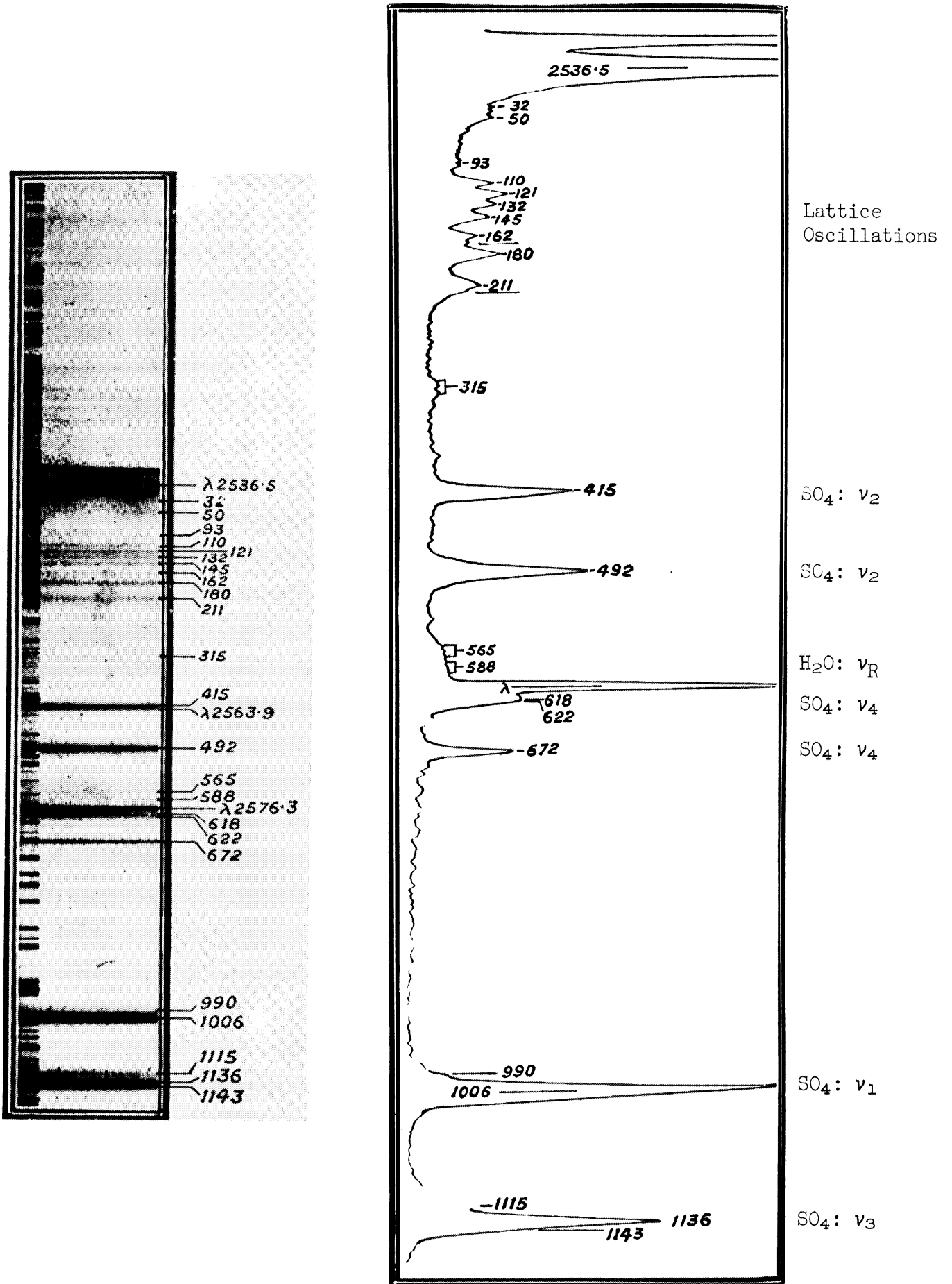
Figure 8. Raman Spectrum of Gypsum.
[Reproduced from R. S. Krishnan, Proc. Indian Acad. Sci. 22A, 274 (1945)]

PREDICTION OF CERTAIN ASPECTS OF
THE INFRARED AND RAMAN SPECTRUM

2-1 Classification of Crystal Fundamentals

A crystal consisting of N atoms has $3N$ degrees of freedom. Three of these correspond to pure translations, leaving $3N - 3$ fundamental modes of vibration to be considered. Only a very small number of these modes are potentially infrared or Raman active. In fact, it can be shown that if the unit cell* of a crystal contains p atoms, then there will be only $3p - 3$ fundamental modes which are potentially infrared or Raman active.** This analysis also shows that the classification of the motions of these modes can be made by considering only the factor group (unit cell group) of the crystal rather than the entire space group. In other words, the atoms in the unit cell can be regarded as forming one large "molecule" having the symmetry of the factor group. The selection rules and classification of modes can be carried out in a similar way as for molecules.

Methods for classification of fundamentals and selection rules in crystals have been approached from two main points of view. Bhagavantam and Venkatarayudu[35,36] have sought to analyse spectra by considering the motions of molecules in a particular unit cell. Halford[37] suggested use of the site approximation in which attention is focused on the local symmetry of a molecule in the unit cell. Hornig[38] has shown how to

---

*Unit cell will hereafter refer to Bravais unit cell.
**See for example, Born and Goeppert-Mayer.[34]

proceed from the site approximation to obtain the same results as Bhaga-
vantam and Venkatarayudu. Winston and Halford[39] have derived both
methods by considering the motions of a crystal segment composed of an
arbitrary number of unit cells and subject to the Born-Karman boundary
conditions.

The classification of the fundamental vibrations of gypsum will be
carried out in the way indicated by Bhagavantam and Venkatarayudu. Gyp-
sum may be regarded as composed of three types of structural groups:
(1) simple ions, Ca^{++}; (2) complex ions, $SO_4^=$; (3) neutral molecules,
H_2O. The forces holding the atoms within a group together may be assumed
much stronger than those holding the various groups together in the crys-
tal. With the aid of this assumption, it is possible to classify the
various vibrations as either internal or external. The internal vibra-
tions are those in which the motions are essentially those of the atoms
within a group. The internal vibrations of $SO_4^=$ and H_2O in the crystal
will occur at approximately the same frequency as for the isolated sys-
tems $SO_4^=$ and H_2O. There will be no internal vibrations of the Ca^{++} ions
since the isolated system possesses only translational freedom. The
external or more commonly called lattice vibrations are due to motions
of the groups against each other. The lattice vibrations may be further
subdivided into those of a translatory type and those of a rotary type
corresponding to the limiting cases of pure translations and pure rota-
tions in the absence of forces among the groups. Since the forces among
the groups are assumed much weaker compared to those within an individual
group, the lattice vibrations may be expected to occur at much lower fre-
quencies than the internal vibrations. The division described above may
be illustrated in the following way:

crystal fundamentals belonging
to a particular factor group
symmetry species

internal   external

water   sulfate   translatory   rotary
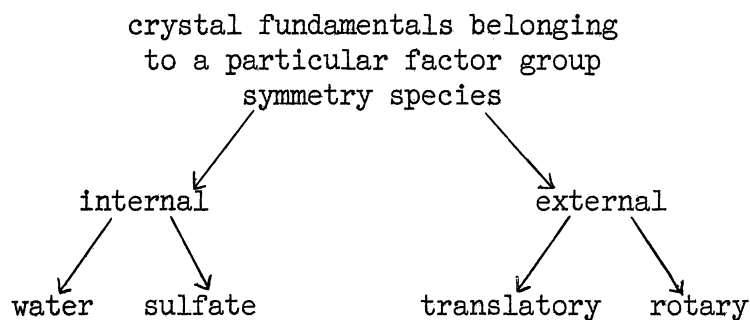
A physical meaning can be ascribed to these various types of modes by considering the motions of molecules and ions in the unit cell. Some diagrams of the internal modes are shown in Sections 2-2 and 2-3. Most of the external modes occurred at too low a frequency to be measured in the infrared spectrum. A classification of the various modes was carried out with the aid of group theory by the method of Bhagavantam and Venkatarayudu.[36] Only the results will be given. These are shown in Table 6, using the following symbols:

n_i = total number of modes belonging to the ith irreducible representation

n_i' = total number of internal vibrations belonging to the ith irreducible representation

T = number of pure translations

T' = number of translatory lattice vibrations

R' = number of rotary lattice vibrations

$U_R(n_i)$ = number of atoms remaining invariant under the symmetry operation R

$U_R(s)$ = number of groups remaining invariant under the symmetry operation R

$U_R(s-v)$ = number of polyatomic groups remaining invariant under the symmetry operation R

h = order of group (this is 4 for C_{2h}^6)

$\chi(n_i)$ = character of representation defined by the $3p$ Cartesian coordinates

$\chi(T)$ = character of a vector defined by the three Cartesian coordinates of a vector

$\chi(T')$, $\chi(R')$ = characters of representations used to find T' and R'

T_x, T_y, T_z = pure translations in the three Cartesian directions

α_{xy}, etc. = components of a symmetric tensor

IR = infrared

TABLE 6

DISTRIBUTION OF MODES

C_{2h}^6	E	C_2	i	$C_2^{\sigma_g=} \cdot i$	IR	Raman	n_i	T	T'	R'	n_i' SO$_4^=$	n_i' H$_2$O
A_g	1	1	1	1	..	$\alpha_{xx}; \alpha_{yy}$ $\alpha_{zz}; \alpha_{xz}$	17	0	5	4	5	3
A_u	1	1	-1	-1	T_y	.....	17	1	4	4	5	3
B_g	1	-1	1	-1	..	$\alpha_{xy}; \alpha_{yz}$	19	0	7	5	4	3
B_u	1	-1	-1	1	T_x T_y	.....	19	2	5	5	4	3
$U_R(n_i)$	24	4	0	0								
$U_R(s)$	8	4	0	0								
$U_R(s-v)$	6	2	0	0								
$h\chi(n_i)$	72	-4	0	0								
$h\chi(T)$	3	-1	-3	1								
$h\chi(T')$	21	-3	3	-1								
$h\chi(R')$	18	-2	0	0								

The method of Bhagavantam and Venkatarayudu is most successful for classifying the lattice vibrations. The number of internal vibrations is obtained by subtracting the number of lattice vibrations from the total number of vibrations belonging to any particular irreducible representation. This leads to difficulties when there are two types of polyatomic groups as in gypsum ($SO_4^=$ and H_2O). The number of internal vibrations must be divided into those belonging to $SO_4^=$ and H_2O. In order to deter-

mine the number belonging to each kind of group it is necessary to resort to some sort of artifice. To obtain the number of $SO_4^=$ fundamentals the lattice is considered to be composed only of $CaSO_4$. The number of $SO_4^=$ internal vibrations belonging to each irreducible representation is then calculated.[40] The lattice is next considered to be composed only of H_2O molecules ignoring the $CaSO_4$. This procedure is legitimate since the number of internal fundamentals of each kind of molecules depends only on the number of each kind of molecule in the unit cell. This artificiality can be avoided by use of the site method introduced by Halford. Here the starting point is the number of molecular fundamentals. The number of internal crystal fundamentals is calculated directly from the number of molecular fundamentals. Such a procedure is used to some extent in the next two sections where the form of the fundamental vibrations is considered.

2-2 The Water Frequencies

In this subsection, attention is focused on the internal vibrations of the water of crystallization in gypsum. Each crystal internal fundamental will be assumed to consist of the superposition of molecular fundamentals of the four H_2O molecules in the unit cell with the phases so chosen as to satisfy symmetry requirements.

The fundamental vibrations of an isolated water molecule are shown in Figure 9. The fundamental vibrations designated as v_1 and v_2 have transition moments along the molecular symmetry axis, while the fundamental vibration designated as v_3 has its transition moment perpendicular to the molecular symmetry axis (or parallel to a line joining the proton pair). All three fundamentals are potentially active in both the infrared
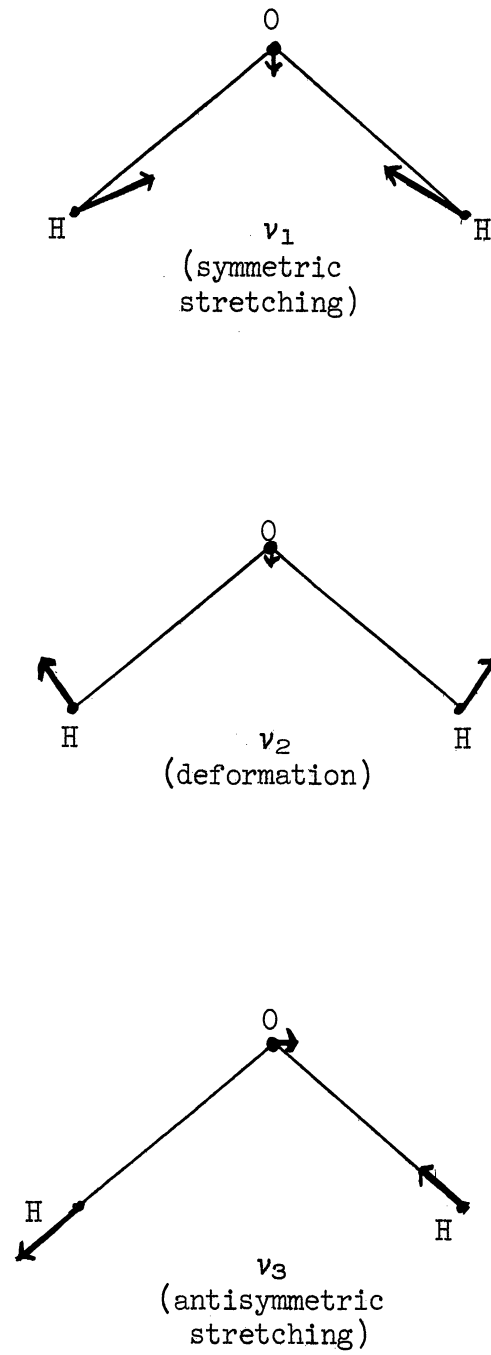
Figure 9. Normal vibrations of the water molecule (not drawn to scale).

and Raman spectrum. The infrared spectrum of all three bands is observed, with ν_2 and ν_3 being more intense than ν_1. In the Raman spectrum, only the ν_1 band is of sufficient intensity to be definitely observed. Table 7 summarizes the spectroscopic data on the gas, liquid, and solid phases of water. The assignments of the ν_1 and ν_3 valence vibrations in the liquid and solid have not been definitely established.

TABLE 7

WATER FUNDAMENTALS

Assign-ment in gas	Gas[41,42]		Liquid		Solid (Ice)	
	IR cm^{-1}	Raman cm^{-1}	IR[43] cm^{-1}	Raman[44] cm^{-1}	IR[43] cm^{-1}	Raman[44] cm^{-1}
ν_2	1595 vs	.....	1646	1630 m	1644	....
ν_1	3657 s	3654.5[a]	3395[b]	3260 s		3147 vs
ν_3	3755.8 vs	....		3426 vs	3256	3264 s
				3610 m		3347 s

s = strong   vs = very strong   m = medium

[a]This band has been reported as a doublet.

[b]A large amount of fine structure in this band has been reported by Andreyev and Balicheva.[45] It is surprising that no one else has observed this.

As an aid in deducing the form of the various crystal internal fundamentals, the four water molecules in the unit cell may be regarded as fixed in space. As a first approximation, the coupling among the molecules will be assumed vanishingly small. Each molecular fundamental now becomes fourfold degenerate in the crystal, since there are four molecules of water in the unit cell. Introduction of a small amount of coupling leads to a splitting of this degeneracy. Each molecular funda-mental leads to four distinct crystal fundamentals, each belonging to

one of the four irreducible representations of the factor group. Since the interaction constants among the various molecules in the unit cell are not known, only the limiting motions in the case of vanishing interaction among the molecules in the unit cell can be given. This can be described as an "oriented gas" model of the crystal.

A projection of the water molecules on the plane perpendicular to the Wooster $\underline{c}$ axis is shown in Figure 10. The diamond-shaped Bravais unit cell is outlined. The $\underline{b}(C_2)$ axes are vertical. Each arrow corresponds to the transition moment of a nearby water molecule for a molecular vibration of the type ν_1 or ν_2. The directions of the arrows are selected so as to satisfy symmetry requirements of the four symmetry species. It can be seen that the A_g and B_g modes will be Raman active, while the A_u and B_u modes will be infrared active. The transition moment for the A_u mode lies parallel to the $\underline{b}(C_2)$ axis of the crystal, while the transition moment of the B_u mode lies perpendicular to the $\underline{b}(C_2)$ axis of the crystal.

Assuming the "oriented gas" model of the crystal, certain predictions about the intensities can be made from a consideration of Figure 10. The four crystal modes corresponding to each molecular mode should occur at slightly different frequencies, the splitting depending on the interaction among the four molecules in the unit cell. If the water symmetry axis* lies inclined at an angle of $45°$ to the crystal $\underline{b}(C_2)$ axis, then one would expect the intensities of the A_u and B_u bands to be equal. In the crystal the angle is not $45°$, but slightly different. The angle θ will be defined as the acute angle between the water symmetry axis and a line parallel to the $\underline{b}(C_2)$ axis passing through the water oxygen. This

---

*In the crystal the C_{2v} symmetry of the water molecules is destroyed and a true molecular symmetry axis no longer exists. For convenience in describing the orientation of the molecules the term molecular symmetry axis will be retained.
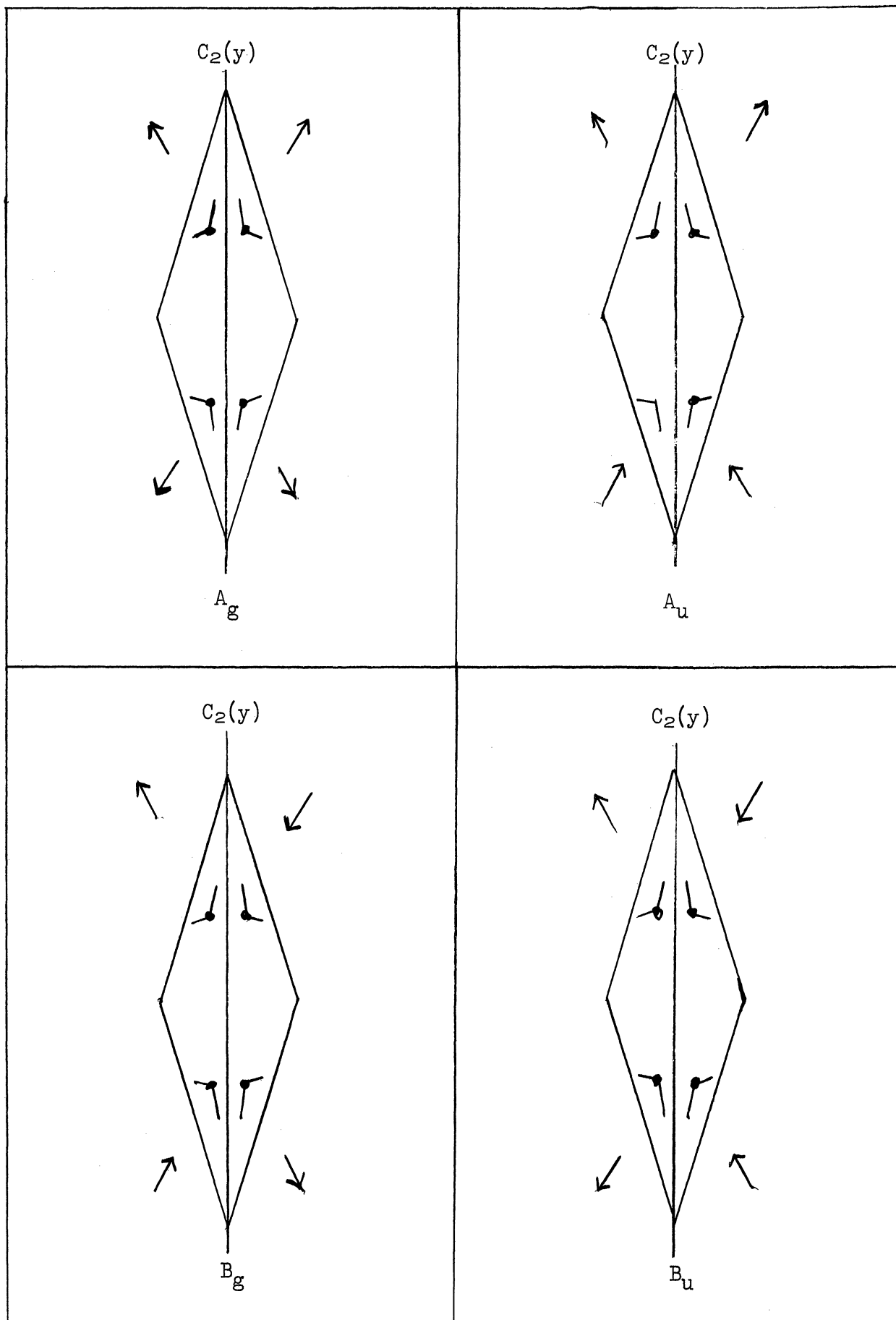
Figure 10. Symmetry species for water vibrations v_1 and v_2 in gypsum.

angle can be found from the x-ray diffraction data. The definition of the angle θ is illustrated in two dimensions in Figure 12. The cotangent of θ gives the ratio of the transition moments of the A_u to B_u bands arising from a particular molecular fundamental. The extinction coefficient is proportional to the square of the transition moment. Hence, $\cot^2 \theta$ should give the ratio of the extinction coefficients of the A_u to B_u bands. This quantity will be known as the dichroic ratio. The angle θ in gypsum is $52°$, predicting a dichroic ratio of 0.613 for the A_u and B_u crystal modes corresponding to the molecular fundamentals ν_1 and ν_2.

A similar analysis can be carried through for the ν_3 molecular fundamental. In doing so, the line joining the proton pair in a water molecule is considered, instead of the water symmetry axis. The corresponding symmetry properties of the transition moment is shown in Figure 11. The angle θ for the H-H line is $40°$, predicting a dichroic ratio of 1.40.

The transition moments of the A_u modes must lie parallel to the crystal C_2 axis, as shown in Figures 10 and 11. This direction is unique. However, the only restriction imposed by symmetry on the B_u modes is that the transition moments must lie somewhere in the plane perpendicular to the crystal C_2 axis, i.e., in the (010) plane. This direction in the (010) plane can be predicted from the assumed structure. For the molecular frequencies ν_1 and ν_2 it will be given by the projection of the symmetry axes on the (010) plane. A projection of the water molecules on the (010) plane is shown in Figure 13. The projections of the symmetry axes of all the water molecules in the crystal are parallel and lie at an angle $\phi = 89°21'$ with the $c(K)$ axis as defined in Figure 13. For the ν_3 molecular frequency, the direction of the transition moment is given by the projection of the lines joining the proton pairs. These projections are all parallel and lie at an angle of $\phi = 66°1'$, as shown
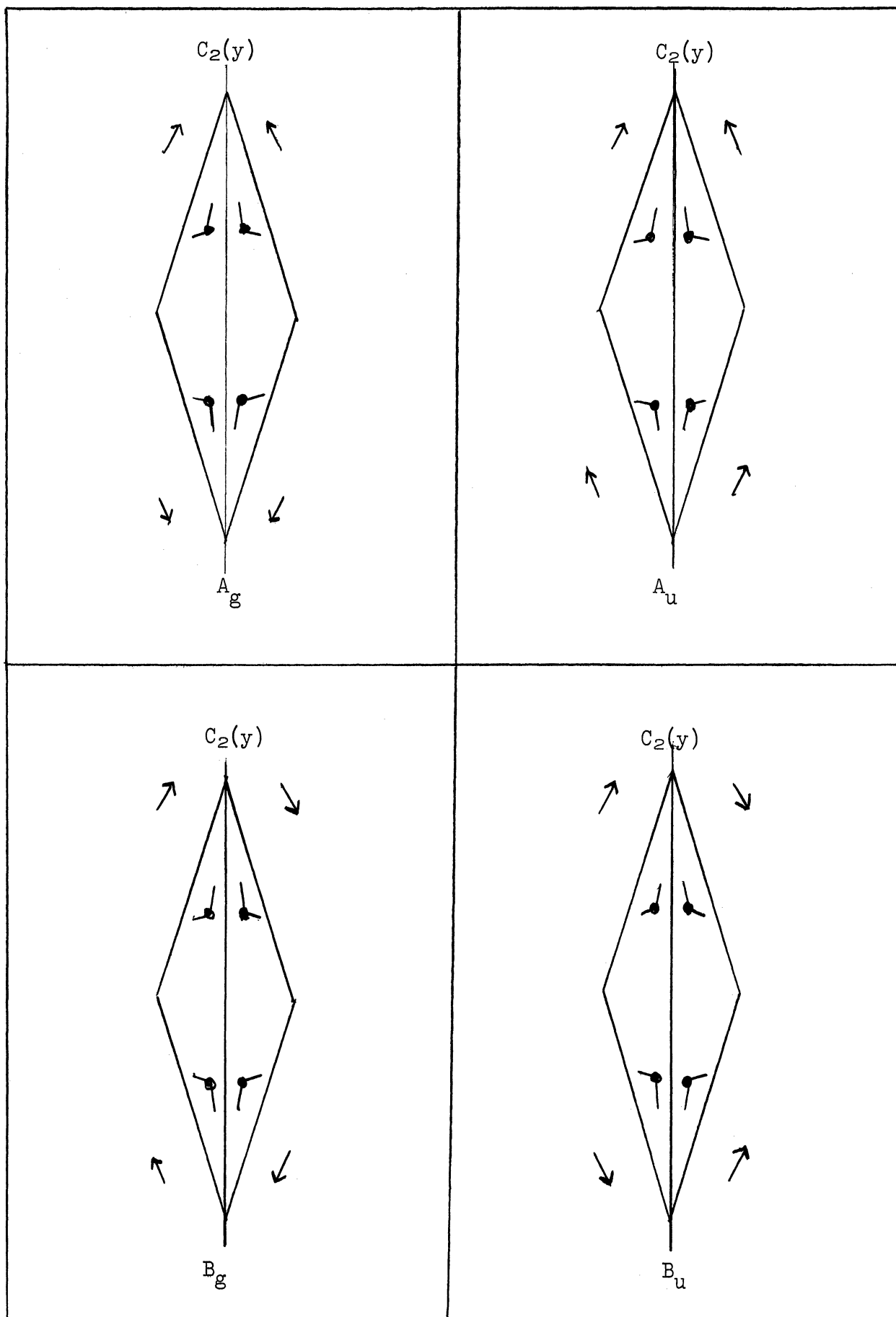
Figure 11. Symmetry species for water vibration ν_3 in gypsum.

$C_2(y)$
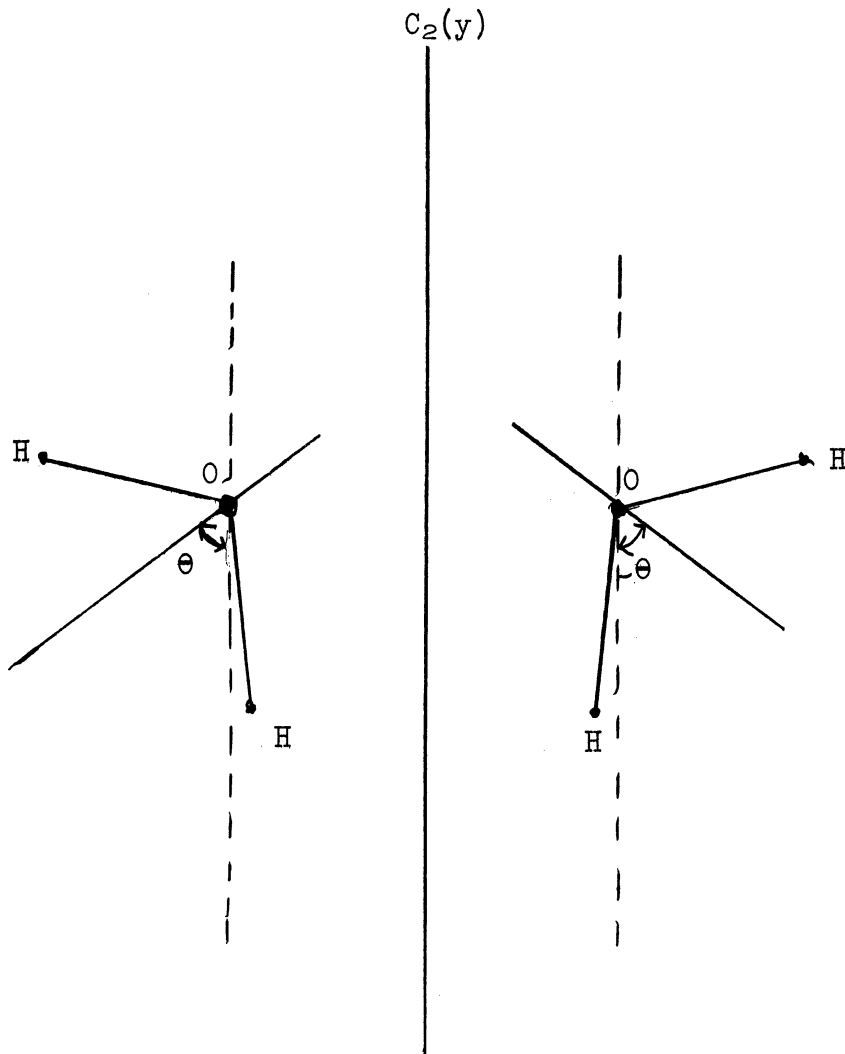
Figure 12. Definition of Angle θ
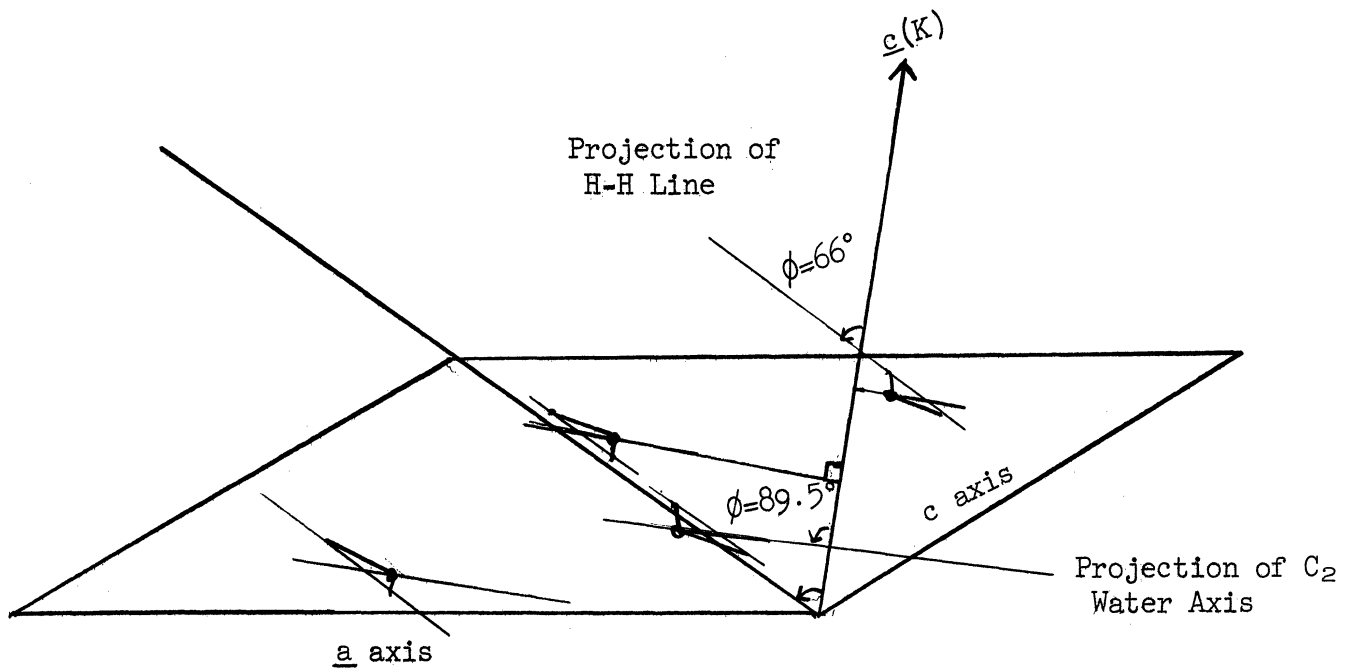
Figure 13. Projection of Water Molecules on the (010) Plane

in Figure 13. The results of this analysis are summarized in Table 8. Although the angles are calculated to the nearest minute from the data given by Wooster,[2] they are probably only accurate to the nearest one-half degree.

TABLE 8

WATER DIRECTIONS IN THE UNIT CELL

	Water C_2 Axis	Water H-H Line
ϕ	89°21'	66°1'
θ	52°7'	40°11'
$\cot^2 \theta$	0.613	1.40

It is interesting to point out that there may be some connection between these directions and the cleavages. For a thin section of gypsum parallel to the (010) plane, the fibrous cleavage direction occurs at an angle $\phi = 66°10'$, which is quite nearly parallel to the projection of the H-H lines. The imperfect cleavage occurs at an angle $\phi = 0°$, which is quite nearly perpendicular to the projection of the water symmetry axes.

2-3 The Sulfate Frequencies

The internal vibrations of the sulfate ions in gypsum will be classified following the site method of Halford.[37] It is desirable to consider first the normal vibrations of a tetrahedral XY_4 molecule. The point group is T_d, which possesses a very high degree of symmetry. The species and characters of this point group are given in Table 9.

The four normal vibrations are shown in Figure 14. The $\nu_1(A_1)$ and $\nu_2(E)$ modes are Raman active and infrared inactive, while the two F_2
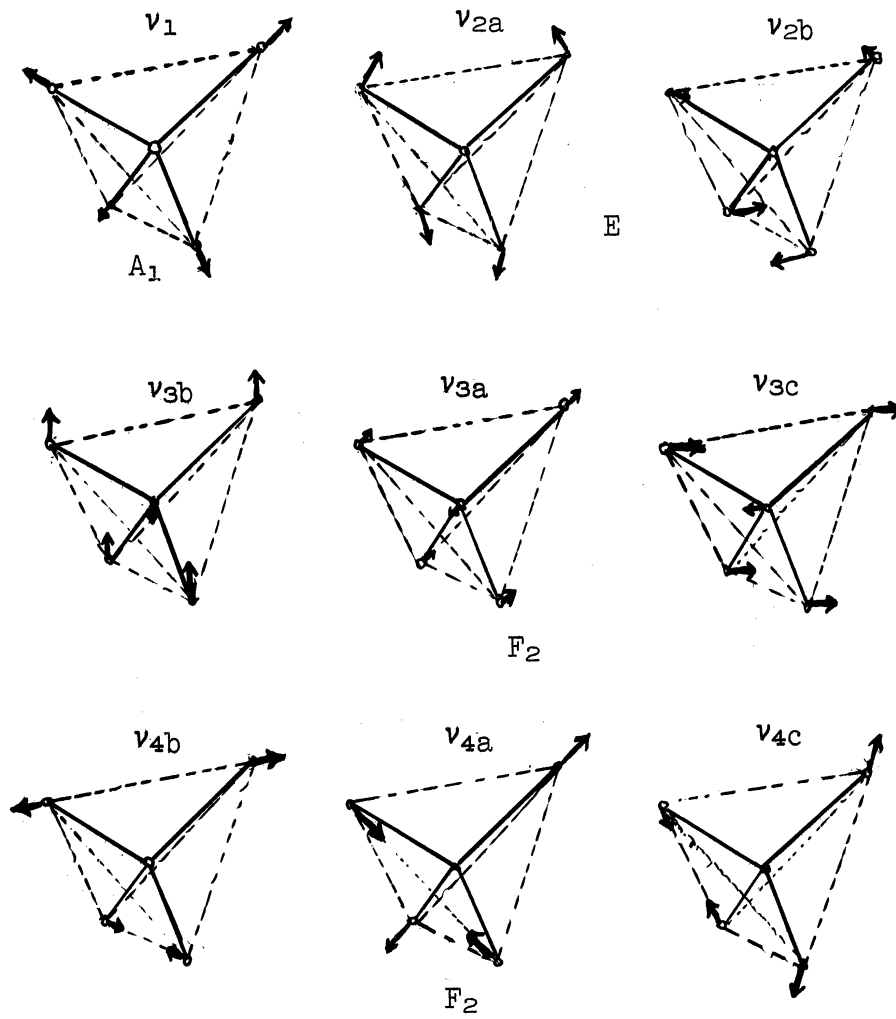
Figure 14. Normal Vibrations of a Tetrahedral XY_4 Molecule

triply-degenerate modes are infrared as well as Raman active. The $\nu_1(A)$ or breathing frequency is a radially inward and outward motion of the peripheral atoms. In the $\nu_2(E)$ doubly degenerate vibrations the peripheral atoms describe circles on the surface of a sphere. In the F_2 triply degenerate mode known as ν_3, the peripheral atoms move as a unit in opposition to the central atom. For the $\nu_4(F_2)$ vibration, the peripheral atoms move against each other along the edges of a tetrahedron. The numerical values of the frequencies are given in Table 10.

TABLE 9

SYMMETRY SPECIES AND CHARACTERS FOR THE POINT GROUP T_d

T_d	E	$8C_3$	$6\sigma_d$	$6S_4$	$3S_4^2{=}3C_2$	n	Activity	
							IR	Raman
A_1	1	1	1	1	1	1	...	$\alpha_{xx};\alpha_{yy};\alpha_{zz}$
A_2	1	1	-1	-1	1	0	...	....
E	2	-1	0	0	2	1	...	$\alpha_{xx};\alpha_{yy};\alpha_{zz}$
F_1	3	0	-1	1	-1	0	...	....
F_2	3	0	1	-1	-1	2	$T_x;T_y$ T_z	$\alpha_{xy};\alpha_{yz};\alpha_{xz}$

TABLE 10

SULFATE FUNDAMENTALS

Assign-ment	Species	Freq.Shift cm^{-1}	Relative Intensity
ν_1	A_1	981	4
ν_2	E	451	2
ν_3	F_2	1104	1
ν_4	F_2	613	1

Taken from Kohlrausch.[46]

In the crystal, the sulfate ions are located such that the C_2 crystal axes coincide with a C_2 axis of each tetrahedral $SO_4^=$ group. The crystal potential energy function has twofold symmetry about these axes. The motions of the sulfate ion can thus be classified as those of a molecule having only C_2 symmetry. Since the intermolecular forces giving rise to this reduction in symmetry are assumed weak compared to the intramolecular forces in the sulfate ion, the internal vibrations of the ions may be regarded as essentially those of a tetrahedral molecule subject to a small perturbation having the symmetry of the lattice. The symmetry types and characters of the C_2 point group are shown in Table 11. The four fundamental vibrations of the tetrahedral ion $SO_4^=$ can be thought of as splitting into nine non-degenerate fundamentals to be distributed over the two symmetry species of point group C_2. This distribution is illustrated in Figure 15 and can be derived from the following considerations. It can be seen from Figure 14, giving the form of the normal vibrations, that the $\nu_1(A_1)$ and $\nu_2(E)$ fundamentals will correlate with the A species of the C_2 point group, since these fundamentals are completely symmetric with respect to the twofold rotation operation. The triply degenerate vibrations are somewhat more complicated. However, it can be seen from Figure 14 giving the form of the normal vibrations that it is possible to find a set of linear combinations one member of which is symmetric

TABLE 11

SYMMETRY SPECIES AND CHARACTERS FOR THE POINT GROUP C_2

| C_2 | E | $C_2(y)$ | n | Activity | |
				IR	Raman
A	1	1	5	T_y	$\alpha_{xx}\alpha_{yy}\alpha_{zz}$ α_{xz}
B	1	-1	4	$T_x;T_z$	$\alpha_{xy}\alpha_{yz}$

n = number of internal sulfate vibrations.
IR = infrared.

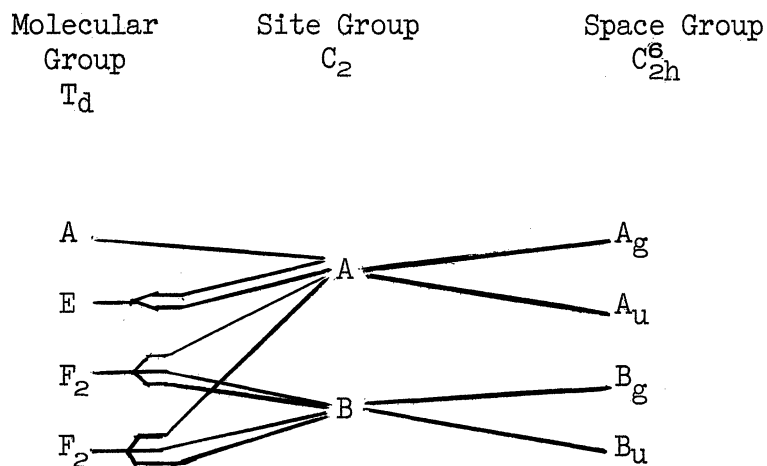| Molecular Group T_d	Site Group C_2	Space Group C_{2h}^6

Figure 15. Correlation chart for sulfate fundamentals.

with respect to the C_2 axis and the other two antisymmetric. In Figure 14, ν_{3b} and ν_{4b} are chosen symmetric, while ν_{3a}, ν_{3c}, ν_{4a}, and ν_{4c} are chosen antisymmetric with respect to the C_2 molecular axis which is assumed to coincide with one of the C_2 crystal axes. On application of a small perturbation with C_2 symmetry, it is expected that the triply degenerate vibrations will split into three single frequencies, one of which will be symmetric and the other two antisymmetric with respect to the twofold axis.

The above classification scheme considers a stationary molecule subject to a perturbation having the symmetry of the lattice. While this method is useful for classification, it is necessary to investigate the motions of all the molecules in the unit cell in order to secure more detailed information. Consider the lattice as composed only of $CaSO_4$. There are two molecules of $CaSO_4$ in the unit cell. The molecular modes can be combined in the way indicated in Figure 16.

A distinction exists between those frequencies arising from the F_2 molecular species and those arising from the A and E molecular species. In the former case, an infrared active mode remains infrared active in
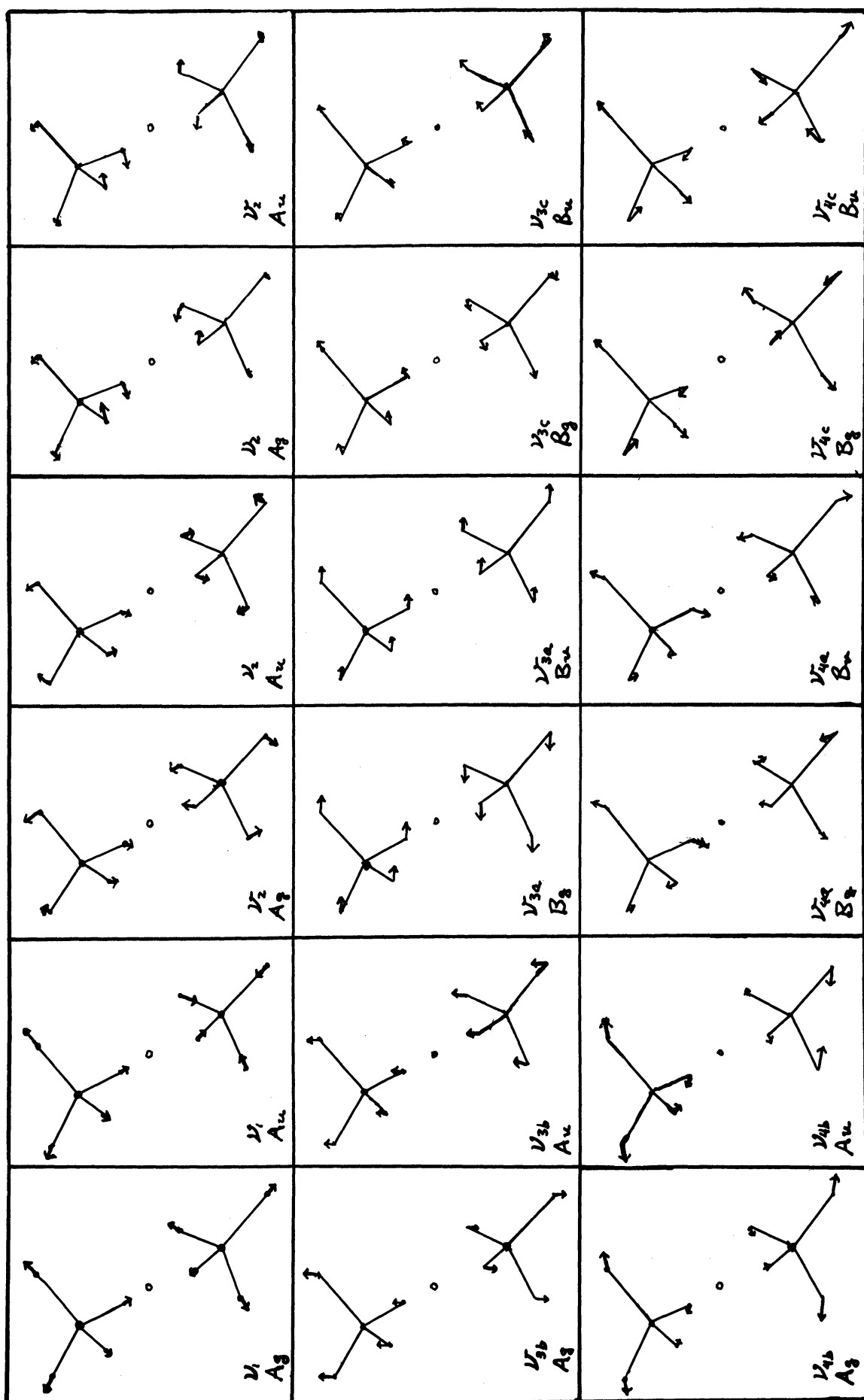
Figure 16. Symmetry species of the sulfate vibrations. The symbol o in the center of each rectangle represents a center of inversion.

the crystal. In the latter case, an infrared inactive mode now becomes permitted. If the coupling forces are weak, these modes will appear only weakly or not at all, in the case of vanishing coupling.

The results will now be summarized:

1. The $\nu_1(A)$ and $\nu_2(E)$ molecular modes become permitted in the crystal and the transition moment will lie along crystal C_2 axis.

2. The $\nu_3(F)$ and $\nu_4(F)$ triply degenerate molecular modes each split into three non-degenerate modes in the crystal. For each set, one transition moment lies along the C_2 axis and the other two lie perpendicular to the C_2 axis.

CHAPTER 3

REFLECTION SPECTRA

3-1 Advantages of Reflection Spectra

The fundamental absorption bands of ionic crystals may be quite in-
tense. For this reason it may be necessary to procure extremely thin
samples of the order of tenths of microns in order to obtain satisfactory
results by the usual transmission method. With available techniques it
is difficult, if not impossible, to secure single crystals of this thick-
ness in various orientations. An alternative approach to the problem is
offered by measuring the reflection spectrum instead of the transmission
spectrum. It is well known that intense absorption in solids is always
accompanied by corresponding variations in the reflecting power. From
Maxwell's theory, it is possible to relate the observed reflection spec-
trum to the desired absorption spectrum.

The standard method for obtaining an absorption spectrum from a re-
flection spectrum requires measurements at two angles of incidence at
every frequency. The experimental procedure and calculations are re-
viewed by Simon.[47] In practice these angles must differ considerably,
e.g., 20° and 70°. This method works well for isotropic solids; however,
it is not suited for anisotropic crystals since here the extinction co-
efficient depends on the angle of incidence.

The difficulties encountered with measurements at oblique incidence
are avoided by taking measurements at normal incidence. However, it is

only recently that the conversion of measurements of the reflecting power at normal incidence to the corresponding optical constants has been carried out. Simon[47] attempted to show how this could be done for a single band arising from a set of identical Lorentz oscillators. Robinson[48,49,50] revised and extended the concepts of Simon to permit the evaluation of the optical constants for bands of arbitrary shape. The method is limited to non-ferroelectric substances where saturation effects are negligible. The method is rigorously applicable only to crystals of orthorhombic or higher symmetry for reasons similar to those given in Section 4-4, but under certain conditions the method may also be applied to crystals of lower symmetry (see Section 5-4). We have used Robinson's method and, since the theory on which it rests has not been given explicitly, we will attempt to justify it in the following sections.

3-2 Relations Between the Optical Constants and Reflecting Power

The reflection coefficient r is defined as the ratio of the reflected amplitude of light to the incident amplitude. The square of the reflection coefficient, r^2, is the experimentally observed reflecting power (i.e., the ratio of the reflected to incident light intensity). The reflection coefficient of light normally incident on a semi-infinite slab of a non-absorbing medium is given by

$$r = \frac{n - 1}{n + 1} \qquad (3-1)$$

where n is the ordinary index of refraction. When absorption occurs, the ordinary index of refraction must be replaced by a complex index of refraction $\underline{N}$ in which

$$\underline{N} = n - ik \qquad (3-2)$$

where k is the extinction coefficient. The extinction coefficient, k, is related to the more familiar absorption coefficient α appearing in Lambert's law $(T = e^{-\alpha x}$, where T is the fractional transmission and x is the sample thickness) by the relation

$$\alpha = \frac{4\pi k}{\lambda} ,\qquad (3\text{-}3)$$

where λ is the wavelength of the light. Similarly, a complex reflection coefficient

$$\underline{R} = re^{i\Theta} \qquad (3\text{-}4)$$

must be employed to allow for a phase difference between the incident and reflected wave. The reflection equation for an absorbing medium can be written as

$$re^{i\Theta} = \underline{R} = \frac{\underline{N} - 1}{\underline{N} + 1} = \frac{n - ik - 1}{n - ik + 1} . \qquad (3\text{-}5)$$

Solving for n and k yields*

$$n = \frac{1 - r^2}{1 + r^2 - 2r\cos\Theta} \qquad k = \frac{-2r\sin\Theta}{1 + r^2 - 2r\cos\Theta} . \qquad (3\text{-}6)$$

Consequently, if r and Θ are known over the frequency range covered by the absorption bands, the optical constants n and k for this range can be calculated. The quantity r^2 is measured directly from observations of the reflection spectrum at normal incidence. Although there is no direct way of measuring Θ it is possible to show that

$$\Theta_c = \frac{1}{\pi} \int_0^\infty \frac{d \ln r}{d\omega} \ln \left| \frac{\omega + \omega_c}{\omega - \omega_c} \right| d\omega , \qquad (3\text{-}7)$$

where Θ_c is the value of Θ at frequency ω_c.

Robinson[48] pointed out that equation (3-7) can be obtained by analogy

---

*This can also be solved graphically using a Smith chart (see Robinson and Price[49]).

from a similar problem which was solved by Bode[51] for electric networks.
The corresponding problem in an electrical network is concerned with the
complex impedance of a system. This is defined by

$$\underline{Z} = R + iX \quad , \tag{3-8}$$

in which R is the resistance of the system and X is the reactance. For
linear networks (those composed only of resistance, capacitance, and in-
ductance and where these remain independent of the magnitude of the
applied field), Bode has shown how to calculate X when R is known as a
function of frequency. The analogy with the reflection problem is seen
in the complex function

$$\ln \underline{R} = \ln r + i\Theta \quad . \tag{3-9}$$

In treating electrical networks, a simple resonant circuit as shown
in Figure 17, containing an inductance L, resistance R, and capacitance C
is first considered. The differential equation for the instantaneous
charge q on the condenser is given by

$$L\frac{d^2q}{dt^2} + R\frac{dq}{dt} + Cq = E_0 e^{i\omega t} \quad , \tag{3-10}$$

in which $E_0 e^{i\omega t}$ is the exciting electric voltage of frequency ω. This
is the usual differential equation of a damped oscillator and was used
by Lorentz to explain absorption and dispersion in insulators.

3-3 The Lorentz Oscillator

In this section it will be indicated how to obtain the phase angle Θ
for a simple absorption band having a Lorentz shape.

Lorentz[52] postulated that insulating materials contain electrons
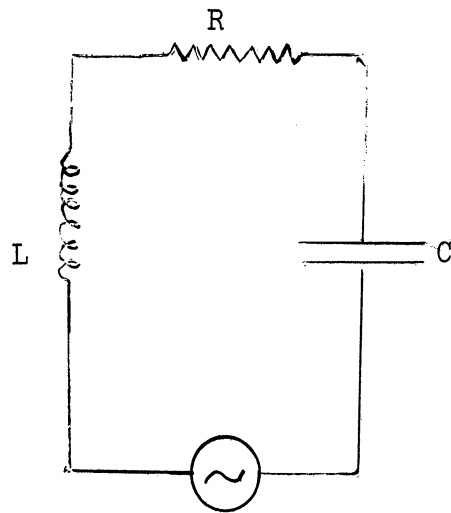
Figure 17. Simple Electrical Circuit

that are bound to their equilibrium positions by Hooke's law forces. These forces will be assumed isotropic for simplicity. The electrons will also be assumed subject to a retarding force proportional to their velocity. The equation of motion of such an electron in the periodic electric field of the incident light wave is therefore given by[53]

$$m\frac{d^2y}{dt^2} + mg\frac{dy}{dt} + m\omega_0^2 y = -eE_0e^{i\omega t} , \qquad (3\text{-}11)$$

where y is the displacement of the electron along the y axis, g is the damping constant, $m\omega_0^2$ is Hooke's constant, and E_0 is the magnitude of the electric vector of the exciting field, e is the charge of the electron, and m is the mass. The solution of this equation is of the form

$$y = -\frac{eE_0e^{i\omega t}}{m(\omega_0^2 - \omega^2 + ig\omega)} + \text{transient terms} \qquad (3\text{-}12)$$

$$= -\frac{eE_0e^{i\omega t}e^{-i\phi}}{m\sqrt{(\omega_0^2 - \omega^2) + g^2\omega^2)}} + \text{transient terms} \qquad (3\text{-}13)$$

where $\quad \phi = \arctan \dfrac{g\omega}{\omega_0^2 - \omega^2} .$ $\qquad (3\text{-}14)$

The steady state current per unit area J is given by

$$J = -n_0e\dot{y} = \frac{n_0e^2}{m} \frac{\omega e^{i(-\phi + \frac{\pi}{2})}}{\sqrt{(\omega_0^2 - \omega^2) + g^2\omega^2}} E_0e^{i\omega t} , \qquad (3\text{-}15)$$

where n_0 is the number of oscillators per unit volume. The coefficient of $E_0e^{i\omega t}$ is the complex conductivity $\underline{\sigma}$ and is given by

$$\underline{\sigma} = \frac{n_0e^2}{m} \frac{\omega e^{i(-\phi + \pi/2)}}{\sqrt{(\omega_0^2 - \omega^2) + g^2\omega^2}} . \qquad (3\text{-}16)$$

The modulus of $\underline{\sigma}$ is given by

$$\frac{n_0e^2}{m} \frac{\omega}{\sqrt{(\omega_0^2 - \omega^2) + g^2\omega^2}} \qquad (3\text{-}17)$$

and the phase angle between J and E_0 is given by

$$-\phi + \pi/2 = \arctan\left(\frac{-g\omega}{\omega_0^2 - \omega^2}\right) + \pi/2 \quad . \tag{3-18}$$

Thus for a simple band arising from a number of identical independent Lorentz oscillators it is possible to express the amplitude and phase as functions of the frequency ω having the parameters ω_0, g, and $n_0 e^2/m$. These are shown graphically in Figures 18A and 18B for a typical case.

If the modulus of $\underline{\sigma}$ shown in Figure 18B is known, then the parameters g, ω_0, and $n_0 e^2/m$ can be found. Using these parameters, the phase angle ϕ can be reconstructed.

The connection of the foregoing with reflection follows through Maxwell's equations from which the relation (3-19) can be derived.[53]

$$\underline{N}^2 = 1 + \frac{4\pi\underline{\sigma}}{i\omega} \tag{3-19}$$

The complex function $\underline{\sigma}$ may be written in terms of its real and imaginary parts,

$$\underline{\sigma} = \sigma + \frac{i\omega}{4\pi}(\epsilon - 1) \quad , \tag{3-20}$$

in which σ is the real conductivity and ϵ is the real dielectric constant. The quantities n and k can then be expressed in terms of σ and ϵ, giving

$$n^2 - k^2 = \epsilon$$
$$nk = \frac{2\pi\sigma}{\omega} \quad . \tag{3-21}$$

These two equations can be solved for n and k, giving

$$n^2 = \frac{\epsilon \pm \sqrt{\epsilon^2 + 4\left(\frac{2\pi\sigma}{\omega}\right)^2}}{2}$$

$$k^2 = \frac{-\epsilon \pm \sqrt{\epsilon^2 + 4\left(\frac{2\pi\sigma}{\omega}\right)^2}}{2} \tag{3-22}$$
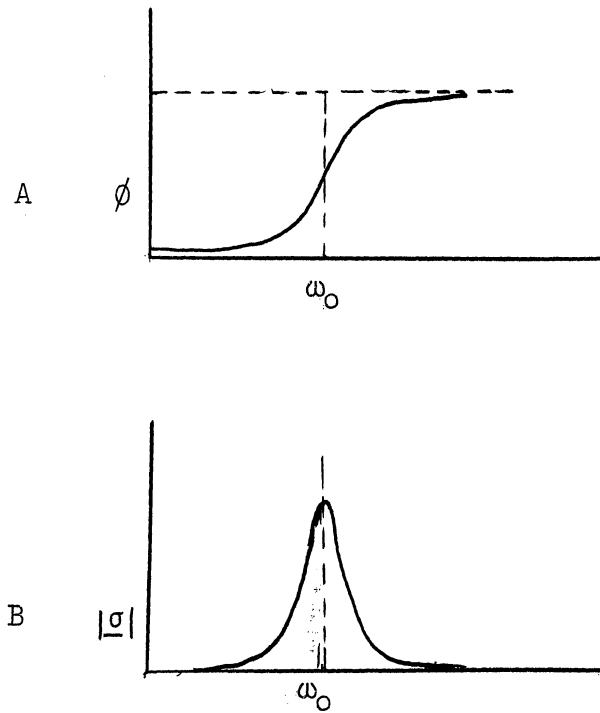
Figure 18. Modulus and phase angle of the
complex conductivity.
A: Phase Angle
B: Modulus

For a Lorentz oscillator, σ and ϵ can be obtained by rationalizing the value of $\underline{\sigma}$ contained in (3-16), giving

$$\sigma = \frac{n_o e^2}{m} \frac{g\omega^2}{(\omega_0 - \omega^2)^2 + g^2\omega^2}$$

$$\epsilon = 1 + 4\pi \frac{n_o e^2}{m} \frac{\omega_0^2 - \omega^2}{(\omega_0^2 - \omega^2)^2 + g^2\omega^2} \quad .$$

(3-23)

Having expressed n and k in terms of ω, it is now possible to substitute in the reflection equation (3-5)

$$r e^{i\Theta} = R = \frac{N-1}{N+1} = \frac{n - ik -1}{n - ik +1} \quad . \quad (3-5)$$

In terms of n and k, r and Θ are found by rationalizing (3-5), giving

$$r = \sqrt{\frac{(n^2 + k^2 - 1)^2 + 4k^2}{(n + 1)^2 + k^2}} \qquad \tan^{-1}\Theta = \frac{-2k}{n^2 + k^2 - 1} \quad . \quad (3-24)$$

Some idea of the frequency dependence of r and Θ can be obtained by considering the case where the absorption is weak. It can be seen from equation (3-24) that where k is much less than n, the value of Θ will be proportional to k in first order. Similarly, r will be largely influenced by the value of n. Consequently, the curves of r and Θ as a function of frequency might be expected to resemble those for n and k.

In this way, the quantities

$$\begin{array}{cc} n & k \\ r & \Theta \end{array}$$

are explicit functions of the frequency ω containing the parameters g, ω_0, and $n_o e^2/m$. Consequently, for a simple Lorentz-shaped band, knowledge of any one of the quantities n, k, r, or Θ as a function of frequency allows the other three to be determined.

The procedure just outlined is practical for the analysis of single isolated absorption bands. However, not all absorption bands are of this type. Many consist of the superposition of more than one band. This can result in doublets or shoulders or other complicated shapes. Extension of the theory just outlined would prove quite difficult. Fortunately, with the aid of complex variable theory it becomes possible to treat such complicated systems. By means of this method, it becomes possible to calculate the imaginary part of certain complex functions when the real part is known as a function of the frequency. Conversely, the real part can be calculated (except for an arbitrary additive constant[54]) when the imaginary part is known as a function of the frequency. The procedure is very briefly sketched in the next section.

3-4 Complex Variable Relations

The quantities $\underline{R}$, $\underline{N}$, and $\underline{\sigma}$ are more easily treated when regarded as complex. For a set of Lorentz oscillators these will be functions of the frequency ω. For mathematical convenience, it is desirable to consider ω also as complex. The complex frequency, p, defined as

$$p = s + i\omega ,$$

(3-25)

where s is some real number, will now replace the real frequency ω. The exciting field, $E_0 e^{i\omega t}$, is replaced by $E_0 e^{pt}$. When s is positive the exciting field is an exponentially increasing sinusoid; when s is negative the exciting field is an exponentially decreasing sinusoid; and when s = 0 the exciting field is the usual sinusoid. There is no difficulty in supposing that all of these cases can be achieved in practice, although only the case where s = 0 is of interest.

It should be emphasized that the complex frequency concept is introduced only for mathematical convenience. The same results can be derived by Fourier analysis with real frequencies, but the mathematics required for such a treatment is more difficult for a rigorous treatment.

Complex frequencies can be represented in the usual Argand diagram as in Figure 19. The right half of the complex frequency plane corresponds to exponentially increasing fields; the left half to exponentially decreasing fields; and the ordinate to the usual sinusoidal fields.

The location of the singularities is of primary importance in problems involving complex variables. If a region does not contain any singularities, it is possible to apply Cauchy's theorem to evaluate certain functions about a closed curve within the region.

If the frequency dependence of $\underline{\sigma}$, $\underline{N}$, and $\ln \underline{R}$ can be explained by a model consisting of any number of Lorentz oscillators, it is possible to show that the singularities of these functions lie in the left half of the complex frequency plane. This result follows for the complex conductivity in the same way as for a complex impedance. By using the relations given by Maxwell's equations expressing $\underline{N}$ and $\underline{R}$ in terms of σ it is shown in Appendix I it holds also for $\underline{N}$ and $\ln \underline{R}$.

By a contour integration over the right half of the complex frequency plane,[55] it is possible to derive relations between the real and imaginary parts of suitable complex functions. This integration is outlined in the Appendix II. The desired result for the phase angle θ is given in the alternative forms, (3-26) and (3-27).

$$\theta_c = \frac{2\omega_c}{\pi} \int_0^\infty \frac{\ln r - \ln r_c}{\omega^2 - \omega_0^2} \, d\omega \qquad (3\text{-}26)$$

$$= \frac{1}{\pi} \int_0^\infty \frac{d \ln r}{d\omega} \ln \left| \frac{\omega + \omega_c}{\omega - \omega_c} \right| d\omega \ . \qquad (3\text{-}27)$$
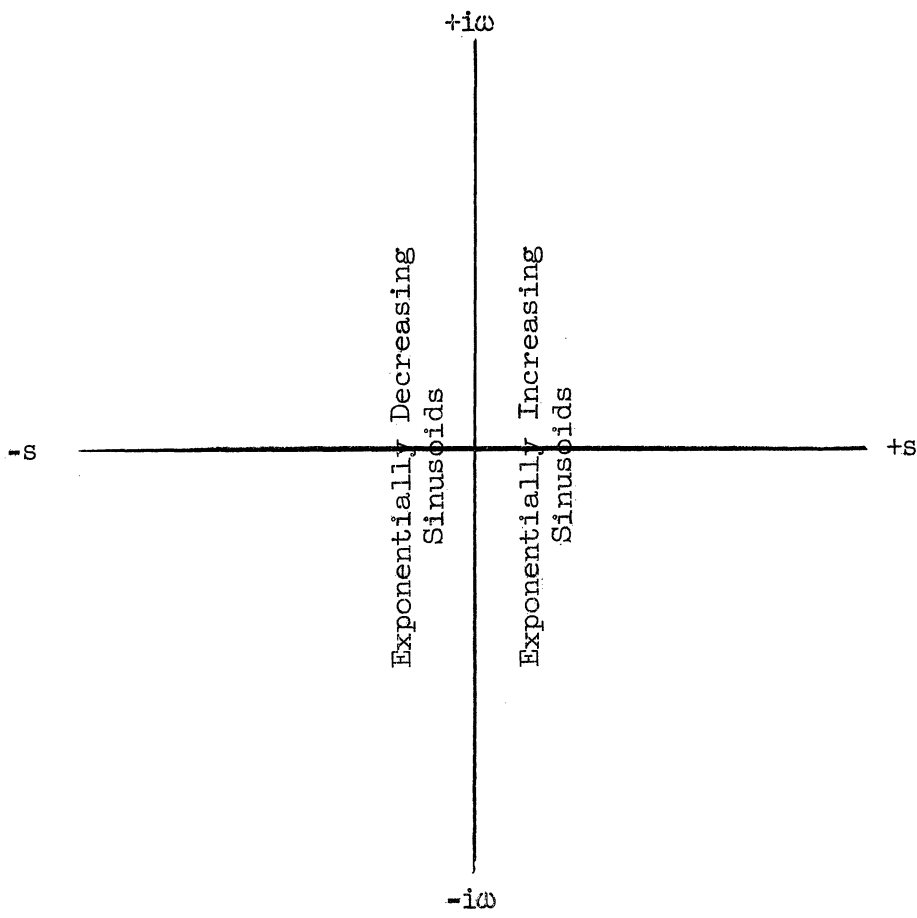
Figure 19. The Complex Frequency Plane

Expression (3-26) is more suitable for calculations near $\omega = \omega_c$ and has been used in our work.

The treatment of absorption and dispersion in solids by considering a series of Lorentz oscillators is a simple classical approximation which enables the location of the singularities of the complex index of refraction and complex reflection coefficient to be specified. It is unsatisfactory since interaction due to neighbors is ignored and since the treatment is classical and not quantum mechanical. Certain simple quantum mechanical modifications can be introduced in the usual way and present no special difficulties. The resonant frequency ω_0 would then be interpreted as the frequency corresponding to the energy difference between the ground state and excited state; the term $n_0 e^2/m$ becomes a measure of the transition moment; while the damping constant g is a measure of the breadth of the two energy levels concerned.

A treatment of the general case of absorption and reflection in insulators would be quite complicated. However, the location of the singularities in the complex frequency plane is the important physical restriction. It can be shown that for complex functions appearing in certain physical problems the singularities are located in the left half of the complex frequency plane. This derivation is based only on the principle of superposition and the assumption of "causality."[*] This approach has been developed most completely by Toll and Wheeler,[56,57] who derived the Kramers-Kronig dispersion formula relating the real and imaginary parts of the complex index of refraction by an integral similar to equation (3-26). (We are grateful to Dr. Toll for the loan of a copy of his thesis containing a discussion of the dispersion formula and its appli-

---

[*]The assumption of "causality" may be stated: "No wave may be scattered before the arrival of a primary wave."

cation to problems involving electron pairs).

There are other applications of the Kramers-Kronig dispersion formula in physics and engineering. The dispersion formula was given by Kronig[58] and Kallman and Mark[59] for x-rays where n is close to unity and k is close to zero, but it appears to be valid for a wide range of frequencies. Kramers[60] pointed out the connection between the analytic properties of the complex index of refraction and complex frequencies. The formula was derived in a more general way by Kronig.[61,62] Recent interest in the dispersion formula has been stimulated by the analogy between the real and imaginary parts of the complex index of refraction, and the total interaction cross section and the differential cross section for forward coherent scattering. This has been discussed by Schutzer and Tiomno;[63] Toll and Wheeler;[56,57] von Kampen;[64] Gell-Mann, Goldberger, and Thirring;[65] and others. The dispersion formula is also of interest in problems of dielectric relaxation where it is desired to find relations between the real and imaginary parts of the complex dielectric constant. Applications in this field are summarized by Frohlich.[66] The dispersion formula has also been applied to relate the real and imaginary parts of the complex magnetic susceptibility.[67,68]

3-5 Digital Computation

The integral (3-27) is not in a convenient form for digital computation. Integrals can not be directly evaluated on a digital computer, but must be expressed in terms of functions involving only the elementary operations of addition, subtraction, multiplication, and division.

The values of ln r, known as the reflection attenuation, are measured as a function of frequency and are usually given as a complicated

curve. If this curve is divided into a series of line segments, the expression (3-27) may be integrated for each of the line segments. Considering one of the line segments extending from ω_1 to ω_2, if one lets $\dfrac{d \ln r}{d\omega} = 0$ outside the limits and $\dfrac{d \ln r}{d\omega} = \dfrac{\ln r_2 - \ln r_1}{\omega_2 - \omega_1}$ for $\omega_1 < \omega < \omega_2$, the expression (3-26) can be evaluated as

$$
\theta_c = \frac{\ln r_2 - \ln r_1}{\pi (\omega_2 - \omega_1)}
\left(
\begin{aligned}
& \left[(\omega_2 + \omega_c)\ln(\omega_2 + \omega_c) - (\omega_2 + \omega_c)\right] \\
& - \left[(\omega_2 - \omega_c)\ln(\omega_2 - \omega_c) - (\omega_2 - \omega_c)\right] \\
& - \left[(\omega_1 + \omega_c)\ln(\omega_1 + \omega_c) - (\omega_1 + \omega_c)\right] \\
& + \left[(\omega_1 - \omega_c)\ln(\omega_1 - \omega_c) - (\omega_1 - \omega_c)\right]
\end{aligned}
\right)
\tag{3-28}
$$

By forming a sum of such terms for each of the line segments, the value of θ_c can be found corresponding to an arbitrary reflection attenuation spectrum. This sum is easy to program on a digital computer. In this way the values of θ at various frequencies can be found from a knowledge of r at all frequencies.

Returning to the original problem, the optical constants n and k can be calculated from the reflection equation (5) once r and θ are known.

3-6 Typical Experimental Results

The results of the preceding sections enable the calculation of the absorption spectrum from a reflection spectrum taken at normal incidence. Some experimental results using this method are shown in Figures 20 and 21. The upper part of these curves shows the experimentally observed reflecting powers* and the lower part the corresponding optical constants

---

*This was not taken at normal incidence for experimental reasons. The angle of incidence was 13°. The result differs very little from those taken at normal incidence (see Section 5-3.1).
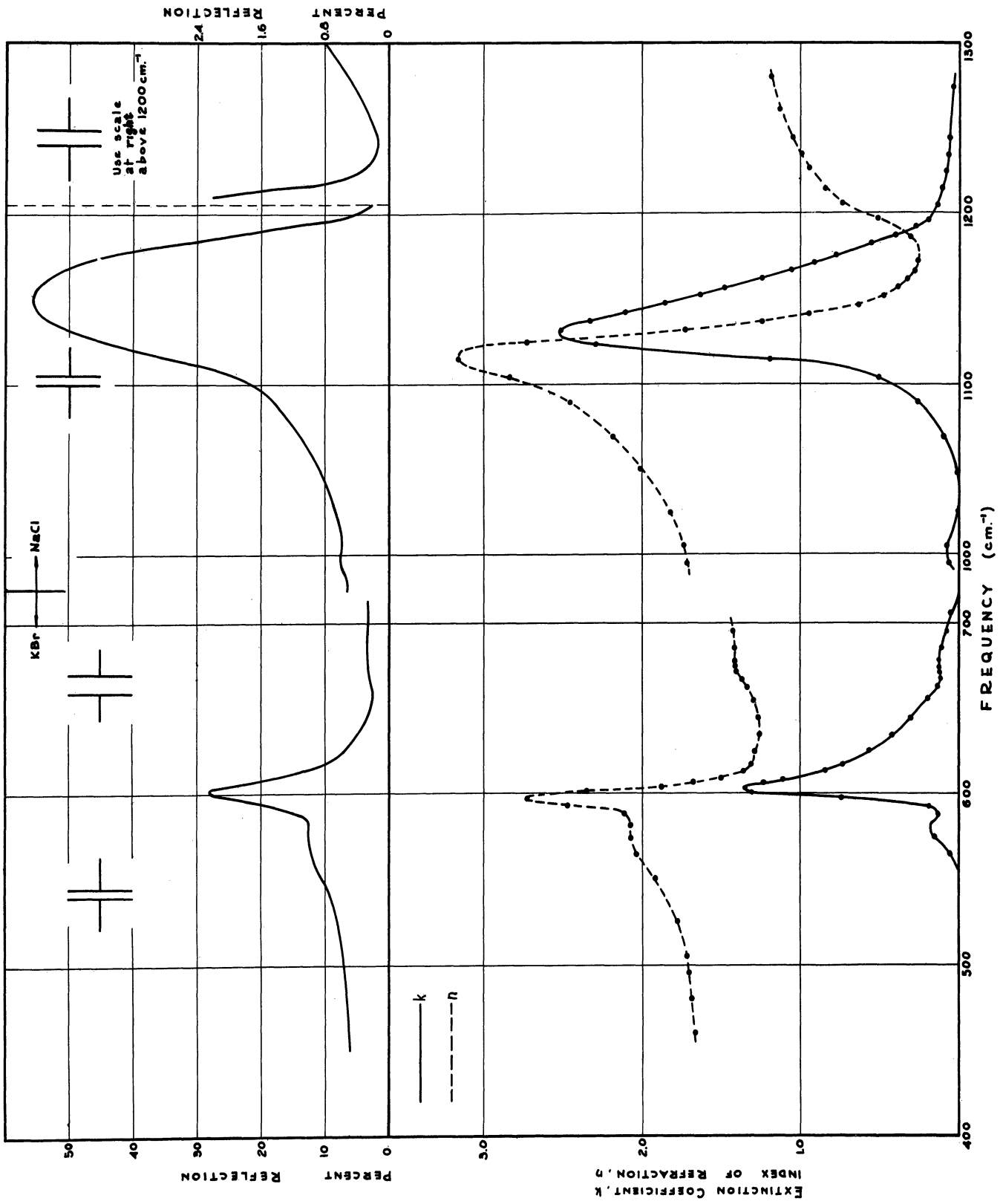
57

Figure 20. Reflecting powers and corresponding optical constants (450-1300 cm⁻¹). (ī0l) section; E∥b.

58
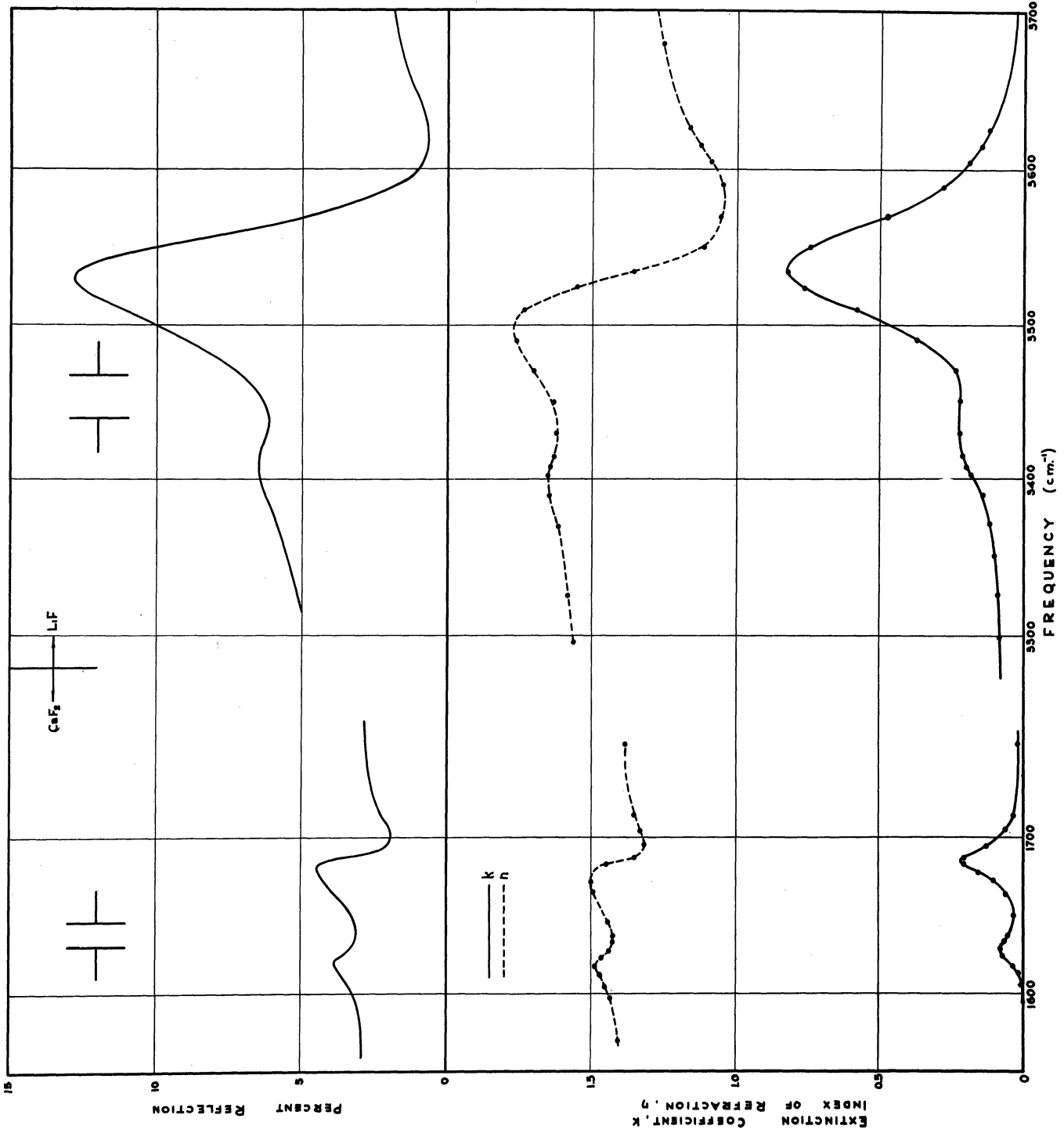

Figure 21. Reflecting powers and corresponding optical constants (1600-3700 cm^{-1}) ($\bar{1}$01) sections; E$\parallel$b.

for a typical sample of gypsum. The reflection bands are asymmetric with a minimum in the reflectivity on the high frequency side. At very low and very high frequencies, the reflectivity is constant.

The optical constants n and k show large variations in the vicinity of a reflection band. For the weaker reflection bands (less than 40%) the frequencies of the reflection and absorption maxima occur within 10 cm^{-1}. For very strong reflection bands (maximum reflectivity above 40%) the frequency of the absorption maximum may be displaced from that of the reflection maxima by about 10-25 cm^{-1}. For the bands studied, specific information is contained in Table 14.

As stated in the previous section, for analysis on a digital computer it is necessary to express the reflection spectrum in digital form. To do this, each reflection spectrum was divided into a series of 116 straight line segments covering the range of observation of 450 - 4000 cm^{-1}. The values of the reflecting powers and frequencies of the end points of these line segments were fed into the computer. The output consisted of the optical constants n and k at the midpoints of these line segments. These midpoints are represented by the black dots on the n and k curves in Figures 20 and 21. The actual calculations were carried out on MIDAC, Michigan Digital Automatic Computer (University of Michigan Engineering Research Institute Publication UMM 101), a general purpose digital computer constructed at the Willow Run Research Center. In its engineering and logical design, MIDAC is very similar to SEAC, the National Bureau of Standards Eastern Automatic Computer. The time required for the calculation of a reflection spectrum of 116 points on MIDAC is about one hour.

It would be desirable to compare absorption spectra as derived from the reflection spectrum with results obtained directly by transmission. Unfortunately, this can not be done with gypsum, as even a weak reflection

band corresponds to a very intense absorption band in transmission. It

has not been possible to secure samples thin enough to enable a comparison.

The thinnest samples used in this work were 15 μ thick. Samples of the

order of one micron or less would be required to make this comparison.

Robinson[48] was able to compare results by reflection and transmission

with polythene. For a film 2.0 μ thick, Robinson obtained absorption max-

ima with k = 0.25 and 0.42 at 2850 and 2920 cm^{-1}, respectively, in good

agreement with k = 0.24 and 0.41 at 2848 and 2922 cm^{-1}, respectively, deduced

from the reflection spectrum.

CHAPTER 4

EXPERIMENTAL APPARATUS AND MATERIALS

4-1 Infrared Spectrometers

A Perkin-Elmer Model 12C single-beam infrared recording spectrometer

was used for all reflection spectra and for transmission spectra from

450-750 cm^{-1} and from 2000-4000 cm^{-1}. A Perkin-Elmer Model 21 double-

beam infrared recording spectrometer equipped with an NaCl prism was used

for transmission spectra from 660-4000 cm^{-1}. The Model 12C instrument

contains a single-pass monochromator with provision for rapid prism in-

terchange. In Table 12, the regions in which the various prisms were

used for reflection spectra are given along with the spectral slit widths

(defined as one-half the total frequency interval passing across the exit

slit). Graphs given by the Perkin-Elmer Corporation were used to calcu-

late the spectral slit widths.[69] Where large spectral slit widths are

TABLE 12

PRISM DATA

Prism	Range cm^{-1}	Slit Width cm^{-1}
KBr	450-750	5
	680-750	11
NaCl	900-1300	5
	1200-1250	9
CaF_2	1400-1900	16
LiF	2800-4000	27

given the reflectivity is low. This requires the use of larger mechanical slits in order to allow sufficient energy to fall on the detector. The reflected energy was low on the high frequency side of strong reflection bands. When the reflectivity was low the background and sample measurements were taken at the same mechanical slit widths, but at different amplifier gains. The ratio of the amplifier gains was obtained by inserting a test signal into the system. This is provided for on the amplifier.

Atmospheric absorption was reduced by blowing dry nitrogen through the Model 12C monochromator housing. Scattered radiation at long wavelengths was diminished by replacement of the diagonal mirror after the exit slit by a frosted aluminized glass surface.

The Model 12C spectrometer was calibrated with known absorption bands of CO_2, H_2O, CH_3OH, NH_3, CH_4, and CO.[70] Sufficient points from the rotational fine structure were available in the regions of interest to allow linear interpolation except below 750 cm^{-1}, where a Friedel-McKinney[71] interpolation was employed. On the Model 21 instrument, the absorption bands of polystyrene checked within 0.01 μ (3 cm^{-1}) in the 6 μ region.

4-2 Auxillary Apparatus

4-2.1 Reflection Sample Holder

The optical arrangement for reflection measurements is shown in Figure 22. Since very large crystals were available, the first diagonal mirror of the spectrometer was replaced by the reflecting sample face. (The author would like to thank Professor D. Wood for suggesting this arrangement.) A diagram of the sample holder is shown in Figure 23.

Entrance
Slit

Monochromator

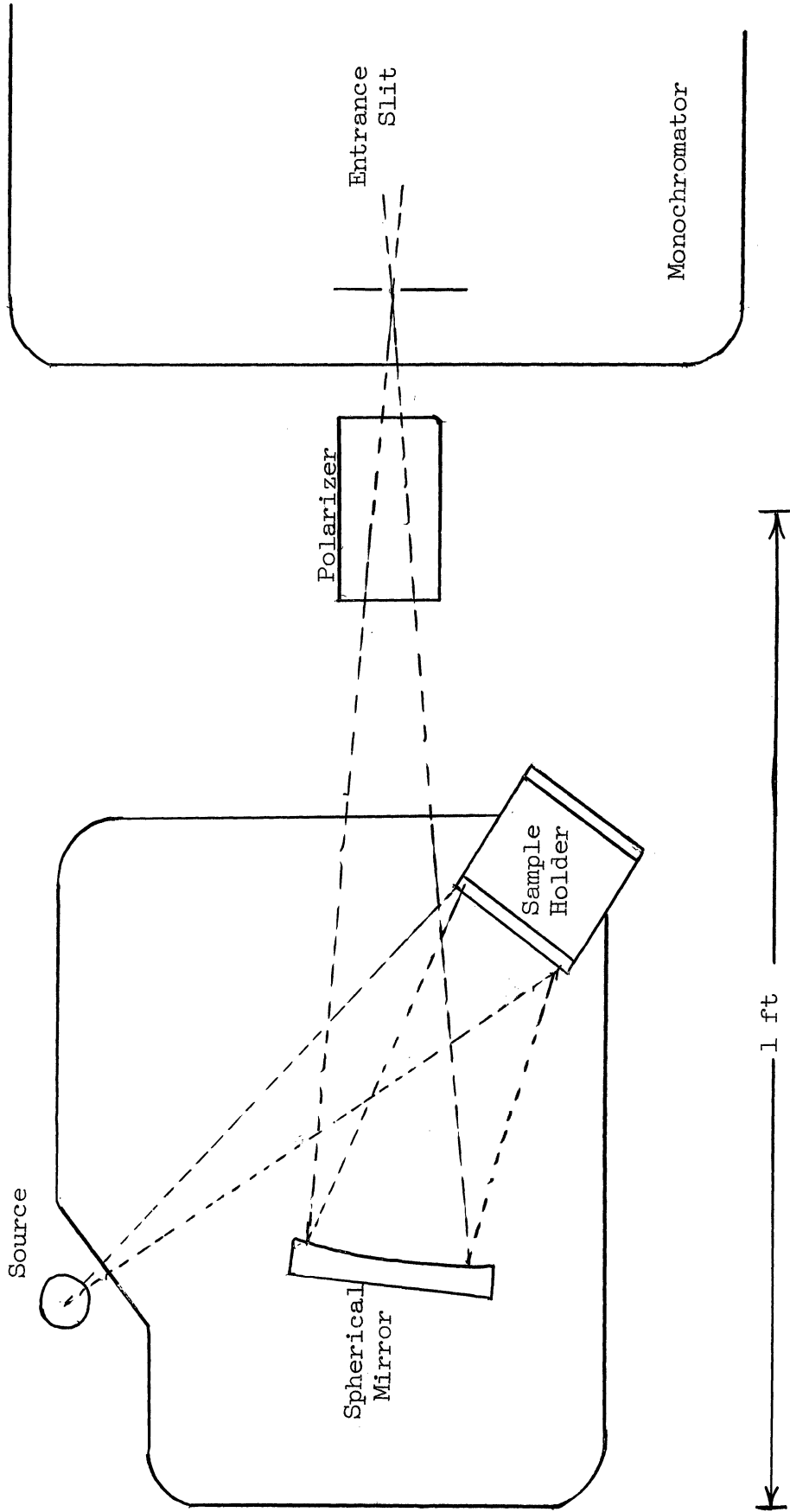Polarizer

Sample
Holder

Source

Spherical
Mirror

1 ft

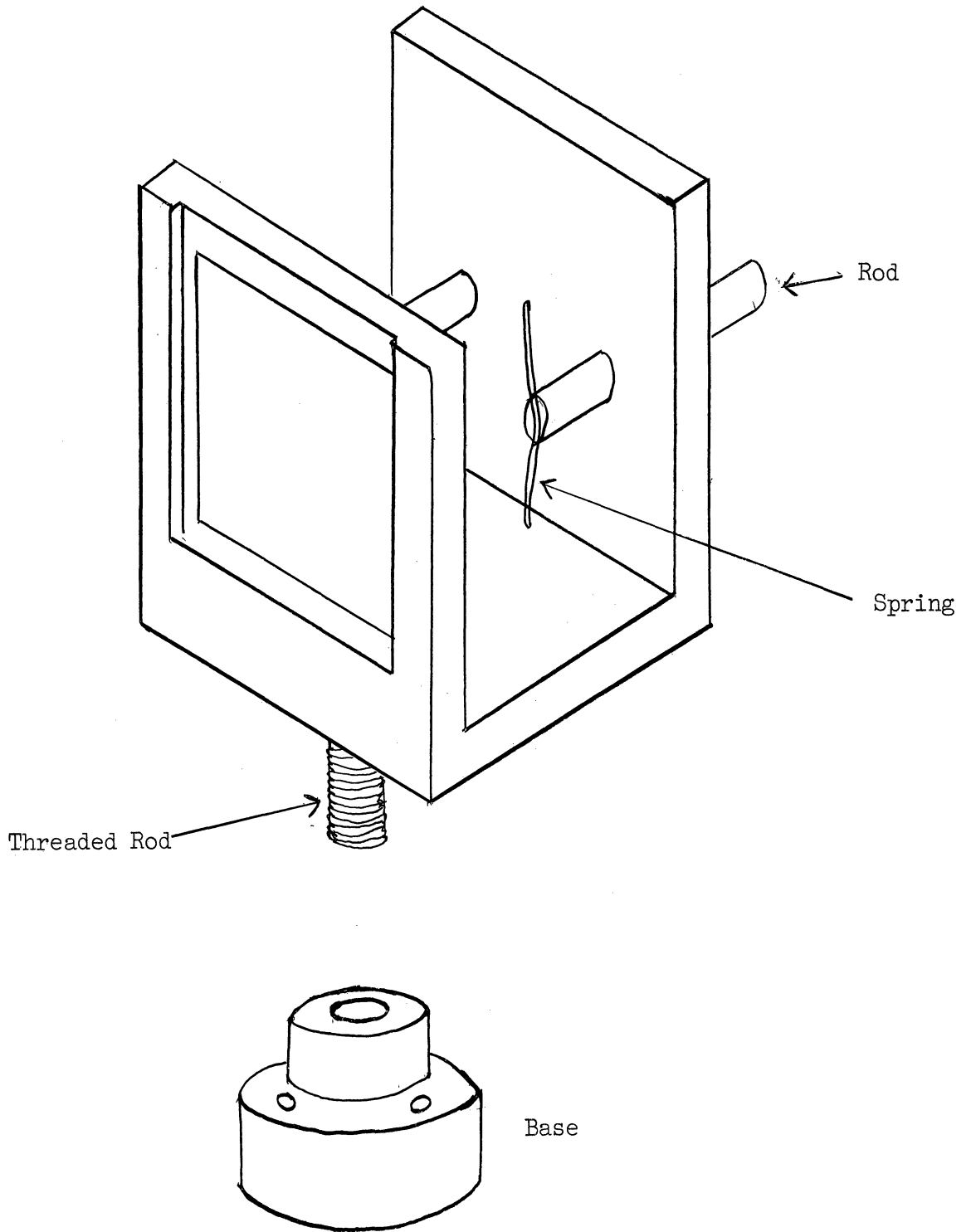Figure 22. Optical Arrangement for Reflection Spectra

Figure 23. Reflection Sample Holder

The sample holder base was constructed so that holes in the Model 12C spectrometer base provided for the first diagonal mirror mount could be used. A slot in the front enabled a diaphragm to be be placed in front of the sample. This was only necessary for the (100) (K) sections which were slightly smaller than the diagonal mirror. The dimensions of this mirror are 1-1/2" x 1-3/4".

The optical arrangement consisted of a divergent beam emerging from the source incident on the sample. The light was reflected off the sample into a spherical mirror which focused the light on the slit. The half-angle of the cone of the light was 7° and the angle of incidence was 13°. For reasons to be explained in Section 5-3.2, the plane of the electric vector was always arranged perpendicular to the plane of incidence, and the sample rotated to change the orientation. Although the angle of incidence is small, it would be desirable to achieve normal incidence. This can be done with a beam-splitter.[72] Although the beam-splitter discards more than half of the energy, it does have the advantage that the difference between polarization parallel and perpendicular to the plane of incidence no longer exists and the sample may remain fixed while the polarizer is rotated. If this were done at a finite angle of incidence, the resulting spectra would appear different.

Where only small samples are available, an optical arrangement whereby an image of the source is focused on the sample can be constructed.[47,73] For even smaller samples, a microscope for reflecting off the surface has been described.[50] The samples of gypsum used in this investigation were sufficiently large so that these modifications of the optical system were unnecessary.

4-2.2 Low-Temperature Cell

The low-temperature infrared transmission cell was constructed

following the design of Wagner and Hornig.[74] A diagram of the cell is

shown in Figure 24. The cell consists of a copper cooling block, coolant

reservoir, and an enveloping jacket. The coolant reservoir terminated

in a commercial copper-to-glass Housekeeper seal. The copper cooling

block was soft-soldered to the Housekeeper seal. The block was con-

structed from a solid piece of copper in which a rectangular hole was

machined. This was done in such a way as to leave a shoulder. The sam-

ple was placed between two KBr windows which fitted against the shoulder.

These windows were held in place by an annular copper ring wrapped with

lead foil to assure a snug fit. A thin layer of vacuum grease between

the copper and KBr increased thermal contact. A hole drilled in one of

the KBr windows holding the samples and in a corresponding place in the

copper cooling block allowed a small copper-constantan thermocouple to

be placed close to the sample. The thermocouple was brought out of the

vacuum system through a wax seal. The outer windows of KBr were attached

to the enveloping jacket with red Glyptal lacquer.

In using the low-temperature cell, the source optics cover of the

spectrometers was removed in order to allow sufficient space for both

the polarizers and cell.

4-2.3 Polarizers

Various kinds of polarizers were employed in this work, depending

on the spectrometer and type of measurement. These are listed below:

1. Silver Chloride. This consisted of six sheets of silver chlor-

ide inclined at an angle of $65°$ to the beam ($0° =$ normal inci-

dence).[75]

2. Silver Chloride. These consisted of a matched pair designed

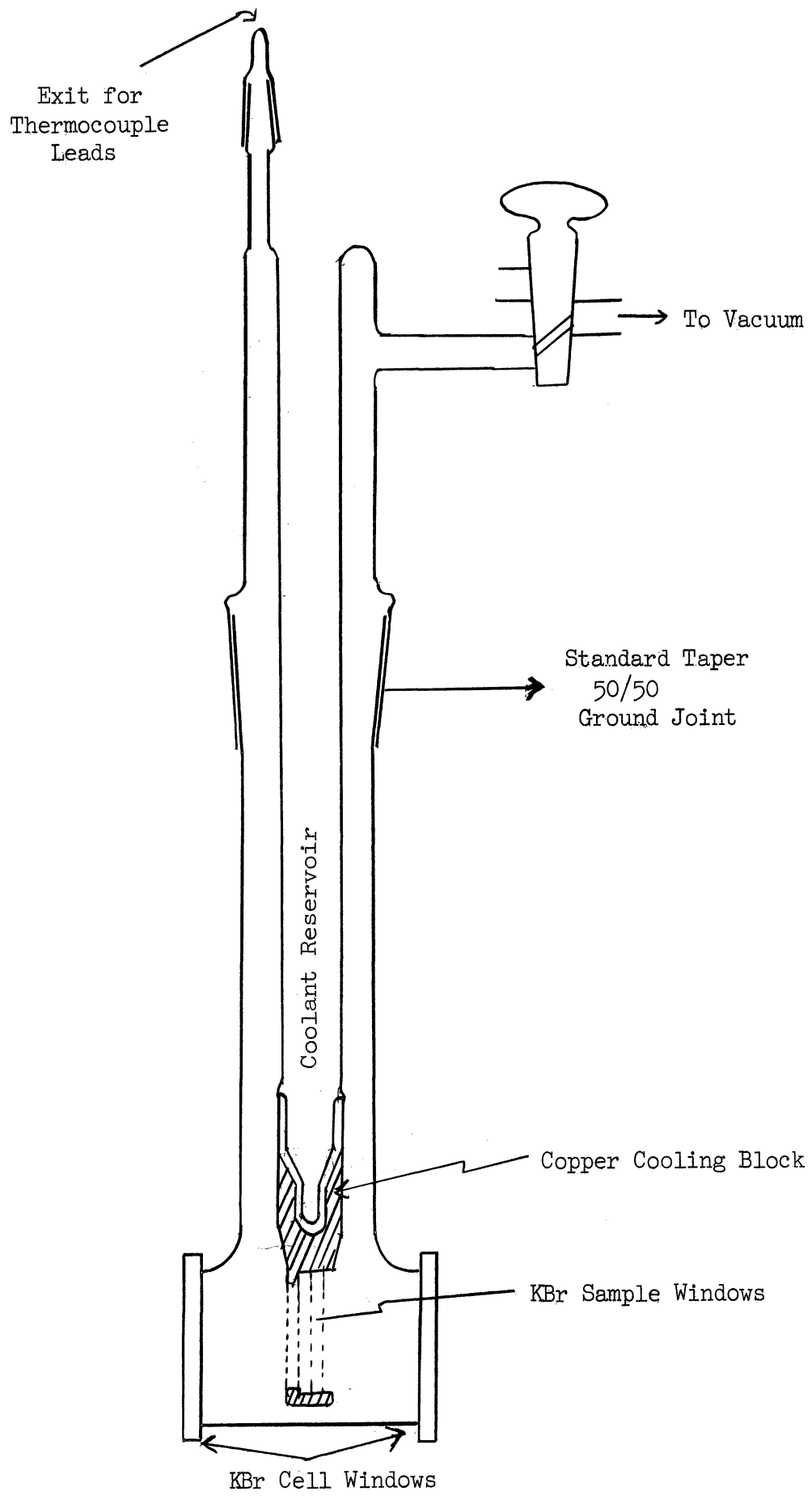for a double-beam spectrometer and were constructed by Kessler[76]

Figure 24. Low Temperature Cell

from the design of Vallance-Jones.[77]

3. Selenium.[78] This consisted of five sheets of evaporated selenium inclined at an angle of 68-1/2° and was constructed by Professor D. Wood.

For all of the reflection measurements, polarizer (1) was employed. For transmission measurements the polarizers used in the various regions are shown in Table 13.

For reflection measurements the plane of the electric vector was always chosen perpendicular to the plane of incidence. For transmission measurements the sample was held fixed and the polarizer rotated.

TABLE 13

POLARIZERS FOR TRANSMISSION MEASUREMENTS

Region cm^{-1}	Instrument	Temperature	Polarizer
450-750;2000-4000	12C	Room	3
450-750;2000-4000	12C	Liq.N$_2$	1
750-2000	21	Room	2
750-2000	21	Liq.N$_2$	2

4-3 Preparation of Samples

The variety of gypsum known as selenite can be obtained commercially in large transparent pieces. Crystals up to five feet in length have been known to occur naturally.[1] The selenite used in this research was purchased from Ward's Natural Science Establishment, Rochester, New York, and came from Washington County, Utah. Gypsum is one of the few natural products that do now show any significant variation in chemical composition. Only trace amounts of Ba and Sr may substitute for Ca.[1]

The three characteristic cleavage directions are easily recognized in gypsum. These directions were verified using a polarizing microscope. For transmission measurements a thin section parallel to the (010) plane was cleaved with a razor blade. With care and practice, samples at least 2mm x 15mm in area and about 15 microns thick could be obtained. These completely filled the entrance slit of the spectrometer. Larger samples are required for the low-temperature cell since the sample can not be placed next to the entrance slit. For this reason larger samples about 50 microns thick had to be employed at low temperatures.

A photograph of the samples used for reflection measurements is shown in Figure 1. These were cut into pieces of convenient size with a mineralogical saw. The (010) principal cleavage face has a natural polish and was used without further treatment. The ($\bar{1}$01) and (100)(K) sections were ground wet on a glass plate with American Optical abrasive M303. They were then polished with rouge on a slightly moist cloth stretched flat over a piece of glass. It was possible to polish sufficiently well so that newsprint could be read when reflected off the surface. Some cracks parallel to the principal cleavage developed; however, these occupied a very small percentage of the total area. The ($\bar{1}$01) and (100)(K) sections could be ground quite flat. Due to buckling of the layers the (010) section was not quite flat, and some fraction ranging from 0-40% of the incident light was lost. The effect of this on the results is discussed in Section 5-2.1.

4-4 Selection of Orientations

The selection of crystal orientations has been discussed by Newman

and Halford.[79] Their arguments are presented clearly and will be quoted

directly.

> . . . any fundamental mode which is capable of absorbing radiation
> must be accompanied by an oscillating electric moment. This lat-
> ter, because it is a vector quantity, will develop along a well-
> defined direction in the medium, a direction that is specified in
> the general theory, and will be incapable of absorbing radiation
> that is polarized in the plane perpendicular to that direction.
> This is the origin of polarized spectra, whose significances lie
> in the possibilities of identifying the characteristic direction
> associated with an absorption, correlating the latter with a mode
> of motion, and of interpreting these directions for different
> modes in terms of molecular and crystalline structures.
>
> In order to realize the possibilities just noted we must first
> solve a crucial problem: the structurally significant directions
> are defined inside the absorbing medium whereas the plane of polar-
> ization of the radiation, and its direction of propagation, are
> easily identified only outside the medium. If we are to translate
> the latter directions, determined outside the medium, into knowl-
> edge of the former ones, defined inside the medium, we must, if
> possible, select orientations for our crystal such that plane polar-
> ized radiation may traverse it without suffering either refraction
> or change of polarization character (plane to elliptical, etc.).
> Otherwise, if plane polarized radiation is incident upon a plate of
> anisotropic crystal in an entirely arbitrary way, it will* suffer
> refractions not in accordance with any simple law and, furthermore,
> for a non-absorber at least, the electric vector of the light will
> be resolved along directions in the medium peculiar both to the di-
> rections of propagation of the light through the crystal and to the
> frequency of the light.
>
> In certain special orientations, however, the requirements we
> must impose upon the behavior of the light inside the medium can**
> be met. These occur* for a non-absorber when the light is incident
> normal to a plate, whose surface is parallel with a plane contain-
> ing two principal axes of the dielectric ellipsoid of the crystal,
> and when the electric vector strikes parallel with one or the other
> of those principal axes. The orientation of the principal axes
> within the medium can depend, however, upon the frequency of the
> light. For an absorber we must* replace the real, dielectric ten-
> sor by the sum of it and an imaginary, conductivity tensor. Unless
> we can specify that the eigenvectors of these two tensors are par-
> allel, which we sometimes can, the situation becomes highly involved.
> In the situations noted below where the two sets of eigenvectors are

---

* M. Born, Optik (Julius Springer, Berlin, 1933).

** Met theory but not strictly so in practice. The actual light
is neither entirely parallel, nor perfectly polarized, nor all inci-
dent normal to the crystal face. However, the distribution of light
across the beam, the placement and small size of the specimen, all
make for a good practical approximation to the ideal.

parallel, it is still necessary to say that the resolution of the
electric vector of arbitrarily incident light takes place "along"
two ellipses rather than definite directions. But, when the pre-
viously prescribed conditions of incidence are met, and the eigen-
vectors of the two tensors are parallel, the requirements we have
had to place upon the light as it enters the medium will then be
fulfilled. It is clear that severe difficulties may attend the
interpretation of polarized spectra when they are obtained with
crystal mosaics or partially oriented microcrystals.

As was noted above, the directions of the eigenvectors for
the dielectric and conductivity ellipsoids can depend upon the
frequency of the light. This circumstance may give rise to diffi-
culties, especially if the two sets of eigenvectors depend differ-
ently upon the properties of the light, but also even when they
change directions together. For example, suppose that the char-
acteristic directions for monochromatic, visible light, normally
incident, are determined with crossed Nicol prisms. It could
happen, when we get into the region of infra-red absorption, that
the principal axes would become rotated by some large undetermined
angle from the positions observed with visible light. If the
angle were near to 45° and infra-red spectra were observed with
light polarized first along one, then along the other of the axes
found in the visible light, these spectra would appear to be iden-
tical. In contrast, spectra properly obtained might show extreme
differences.

For many forms of crystals, fortunately, the directions of
the aforementioned, polarization axes are fixed by symmetry and
become independent of the frequency of the light. In uniaxial
crystals of the hexagonal, trigonal, and tetragonal systems, and
for biaxial crystals of the orthorhombic system, all distinguish-
able polarization axes are symmetry fixed along crystallographic
axes. Spectra observed along these axes will assume a funda-
mental significance, the ones for other conditions of incidence
being representable as superpositions of them. For crystals of
the regular system there are, of course, no polarized spectra.

For monoclinic crystals, one axis is symmetry fixed but the
other two are unrestricted. There are no restrictions upon the
axes in some kinds of fibers, films, and other quasicrystalline
materials. Particular pains will be required, when working with
these latter kinds of substances to resolve these potential dif-
ficulties.

Newman and Halford[79] have pointed out the desirability of selecting

orientations of the crystal such that plane polarized radiation may

traverse it without suffering refraction or change in polarization char-

acter. For crystals belonging to the hexagonal, trigonal, tetragonal,

and orthorhombic systems, these orientations are fixed by symmetry and

related to the crystallographic axes. In monoclinic crystals (such as gypsum) the only orientation for which this is fixed by symmetry is for a crystal plate which is parallel to the $\underline{b}(C_2)$ axis of the crystal and when the electric vector of the light normally incident on this crystal face is polarized parallel to the $\underline{b}(C_2)$ axis. When the electric vector of the incident light is polarized perpendicular to the $\underline{b}(C_2)$ crystal a axis, then it _may_ undergo a change in polarization character on traversing the crystal. If plane polarized light did undergo a change in polarization character on traversing the crystal, then it would not be possible to observe a completely polarized absorption band (a completely polarized absorption band is one in which no absorption occurs perpendicular to the direction of maximum absorption). Observation of a completely polarized band for light incident normal to the (010) crystal face of a monoclinic crystal is evidence for absence of any change in the polarization character. Observation of a partially polarized band would require a more complicated explanation.

CHAPTER 5

EXPERIMENTAL RESULTS

5-1 Presentation of Data

In Chapter 2 certain predictions about the infrared spectrum were
made from a consideration of the structure. It was pointed out that the
infrared absorption bands could be divided into two species designated
as A_u and B_u. The transition moments of the A_u bands are parallel to
the $\underline{b}(C_2)$ crystal axes and the transition moments of the B_u bands lie in
the plane perpendicular to the $\underline{b}(C_2)$, i.e., the (010) plane. The various
crystal orientations were selected so as to isolate those bands belonging
to either species and to find the direction of the transition moment in
the (010) plane.

The transmission spectrum is shown in Figure 25. Although the sam-
ple is only 15 μ thick the absorption is too strong in the region of the
fundamentals to obtain quantitative data. However, the transmission spec-
trum serves very well to locate the direction of the transition moments
in the (010) plane. On preliminary examination it appeared that for all
the bands maximum absorption occurred when the electric vector was within
10° of being either parallel or perpendicular to the $\underline{c}(K)$ axis. In order
to define this direction quantitatively the angle $\emptyset$ introduced in Chap-
ter 2 will be used in which $\emptyset = 0°$, corresponding to a direction parallel
to the $\underline{c}(K)$ axis.

From the transmission spectrum it can be seen that very thin samples

would be required in order to procure satisfactory spectra. It is probably impossible to obtain single crystals of gypsum thin enough for good transmission spectra. The use of very thin samples can be avoided by measuring the reflection spectrum instead of the transmission spectrum as reflection bands occur wherever there are strong absorption bands. The conversion of reflection spectra into absorption spectra can be carried out according to the method described in Chapter 3.

The crystal sections for reflection were cut and polished parallel to the planes (010), ($\bar{1}$01), and (100)(K). The electric vector for the reflection spectrum of the (010) section was so chosen as to be either parallel to the c(K) axis ($\phi = 0°$) or perpendicular to the c(K) axis ($\phi = 90°$). Reflection measurements on the (100)(K) section were taken with the electric vector parallel to the b axis (A_u bands only) and also parallel to the c(K) axis (B_u bands only). With the ($\bar{1}$01) section the electric vector could be set parallel to the b axis or perpendicular to the b axis. In this way the measurements with the electric vector along the b axis and along the c(K) axis were taken on two different crystal orientations. The reflection measurements were taken at an angle of incidence of 13°. It will be shown in the next section that very little error is introduced since the angle of incidence is small.

The various transmission and reflection measurements are described as follows:

1. Incident beam normal* to (010) plane, i.e., direction of propagation along $b(C_2)$ crystal axis. Only B_u bands will be viewed.

   a) Reflection

      1) Electric vector parallel to c(K) axis corresponding to $\phi = 0°$. Reflection data summarized in Table 15B. Absorption spectrum derived from reflection spectrum from 3200-3700 cm^{-1} in Figure 28B. Other regions not shown.

---

*The beam is 13° off normal for the reflection spectra. This will be ignored in listing the results.

2) Electric vector perpendicular to $\underline{c}$(K) axis corresponding
to $\phi = 90°$. This is parallel to the projection of the
water symmetry axes on the (010) plane.
Reflection data summarized in Table 16B.
Absorption spectra derived from reflection spectra from
450-750 cm^{-1} in Figure 27B and from 1550-1750 cm^{-1} and
3200-3700 cm^{-1} in Figure 28B. Other regions not shown.

b) Transmission (thickness: 15 μ)

1) Electric vector parallel to $\underline{c}$(K) axis corresponding to
$\phi = 0°$ from 400-2800 cm^{-1} and electric vector set to
$\phi = -10°$ from 2800-4000 cm^{-1}.
Data summarized in Table 17 and spectra given in Fig-
ures 25, 27C, and 28C.

2) Electric vector perpendicular to $\underline{c}$(K) axis corresponding
to $\phi = 90°$ from 400-2800 cm^{-1} and electric vector set to
$\phi = 80°$ from 2800-4000 cm^{-1}.
Data summarized in Table 17 and spectra given in Figures
25, 27C, and 28C.

2. Incident beam normal to (100)(K) plane.

a) Reflection

1) Electric vector parallel to $\underline{b}$ axis (only A_u bands).
Reflection data summarized in Table 14A.
Absorption spectra derived from reflection spectra not
shown.

2) Electric vector parallel to $\underline{c}$(K) axis (only B_u bands)
corresponding to $\phi = 0°$. This is the same direction as
that in 1(a)(1).
Reflection data summarized in Table 15A.
Absorption spectrum derived from reflection spectrum
shown in Figure 27B from 450-750 cm^{-1} and in Figure 28B
from 1550-1750 cm^{-1}. Other regions not shown.

b) Transmission spectrum not measured.

3. Incident beam normal to ($\overline{1}$01) plane.

a) Reflection

1) Electric vector parallel to $\underline{b}$ axis. This is the same
direction as in 2(a)(1).
Reflection data summarized in Table 14A.
Absorption spectrum derived from reflection spectrum
shown in Figures 27A and 28A. Reflecting powers and
corresponding optical constants are given in Figures
20 and 21.

2) Electric vector perpendicular to $\underline{b}$ axis corresponding
to $\phi = 66°$. This direction is parallel to the projec-

tion of the lines joining the proton pairs in the water
molecules. This direction is only slightly different
from that in 1(a)(2).
Reflection data summarized in Table 16A.
Absorption spectrum derived from reflection spectrum shown
in Figures 27B and 29.

b) Transmission spectrum not measured.

4. Additional observations on transmission spectrum (sample thick-
ness about 50 μ).

   a) Incident beam not normal to (010).
   The sample was tilted about the $\underline{a}$ axis so that both A_u and
   B_u bands will be seen.
   The new bands are listed in Table 17.
   Spectrum shown in Figure 28D.

   b) Spectrum at temperature of liquid nitrogen.
   The bands are listed in Table 17 and the spectrum is shown
   in Figure 26 and for comparison purposes in Figure 28E.

The Figures 27A-C and 28A-E are arranged to enable rapid comparison

of the various experimental results over a given frequency region. Part

A of each figure contains the absorption spectrum derived from reflection

measurements with the electric vector polarized parallel to the $\underline{b}$ axis.

This will consist only of A_u bands. Part B contains the absorption spec-

trum derived from reflection measurements where the electric vector is

always polarized perpendicular to the $\underline{b}$ axis. This will consist only of

B_u bands. The dotted curve is for the case where the electric vector is

parallel to the $\underline{c}(K)$ axis ($\phi = 0°$), and the solid curve is for the case

where the electric vector is polarized perpendicular to the $\underline{c}(K)$ axis

($\phi = 90°$). Part C contains the corresponding transmission spectra for a

sample 15 μ thick. Below 2800 cm^{-1} the polarizations are the same as for

Part B. Above 2800 cm^{-1} the angle $\phi = -10°$ and 80° were employed since

it was found that these angles represent maximum and minimum transmission.

Part D of Figure 5-4 contains the directly observed transmission spectrum

of a sample which was tilted in the beam. In this way it is possible to

reveal A_u bands. The tilting axis was so chosen that the nearby B_u bands interfere as little as possible. There is a correspondence between Part A and Part D for the A_u bands. In Part E the spectrum at the temperatures of liquid nitrogen is given for $\phi = -10°$. The absorption for $\phi = 80°$ is so intense that no fine structure can be seen. At the low temperature, definite absorption peaks are obtained corresponding to bands which only appear as shoulders at room temperatures. Figure 29 is the view of the $(\bar{1}01)(K)$ section with the electric vector perpendicular to the $\underline{b}$ axis. This corresponds to an angle $\phi = 66°$. This section yields approximately the same results as those given in Figure 27B and 28B for $\phi = 90°$.

The transmission results are given in Figure 25 at room temperature for a 15-μ-thick sample and in Figure 26 at liquid nitrogen temperature for a sample about 50 μ thick. A thinner sample could be used at room temperature, since it could be small and placed right next to the entrance slit. At low temperatures a larger (and necessarily thicker) sample was required. The low temperature spectrum was drawn so as to be able to compare it to the room temperature spectrum. At low temperatures the shoulders near 3300 cm^{-1} become quite distinct (see Figure 28E). In addition, the intensity of the broad bands near 450 cm^{-1} and 600 cm^{-1} is reduced considerably. The results of the transmission spectra at room temperature and at low temperatures are summarized in Table 17. The dashes represent bands which are observed for normal incidence at room temperature and without any noticeable changes under different conditions. Where some change is noticed or some new band appears, the frequency is indicated. Dots indicate absence of a band. The direction of the electric vector ϕ is that for when maximum absorption takes place except in the 3400 cm^{-1}. Here maximum absorption takes place at $\phi = 80°$ and is so intense that no fine structure can be seen. Some fine structure is visible
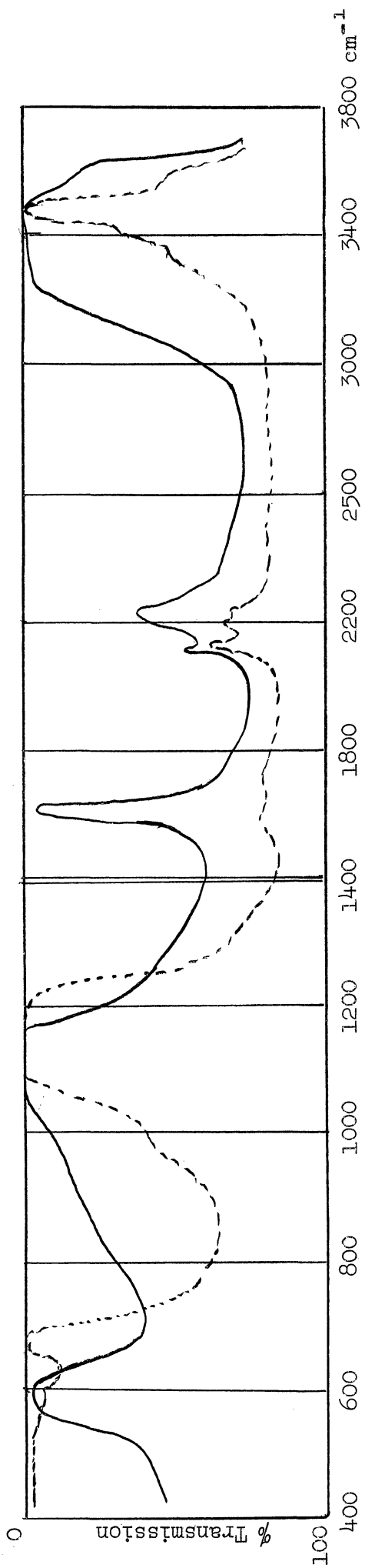
Figure 25. Transmission Spectrum of Gypsum (010) Section
(Room Temp.)
—— ∅ = 90°   ---- ∅ = 0°
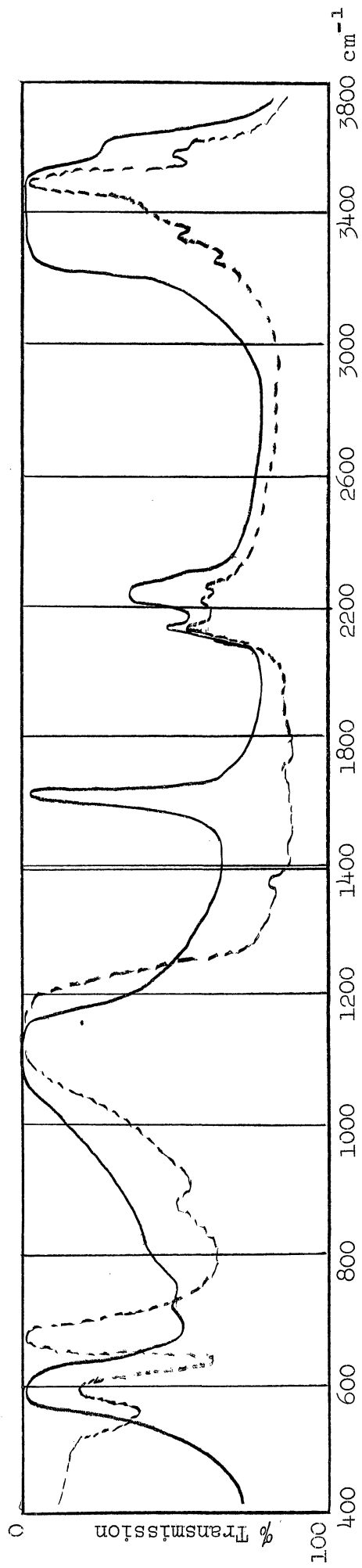
Figure 26. Transmission Spectrum of Gypsum (010) Section
(Liquid Nitrogen Temp.)
—— ∅ = 90°   ---- ∅ = 0°
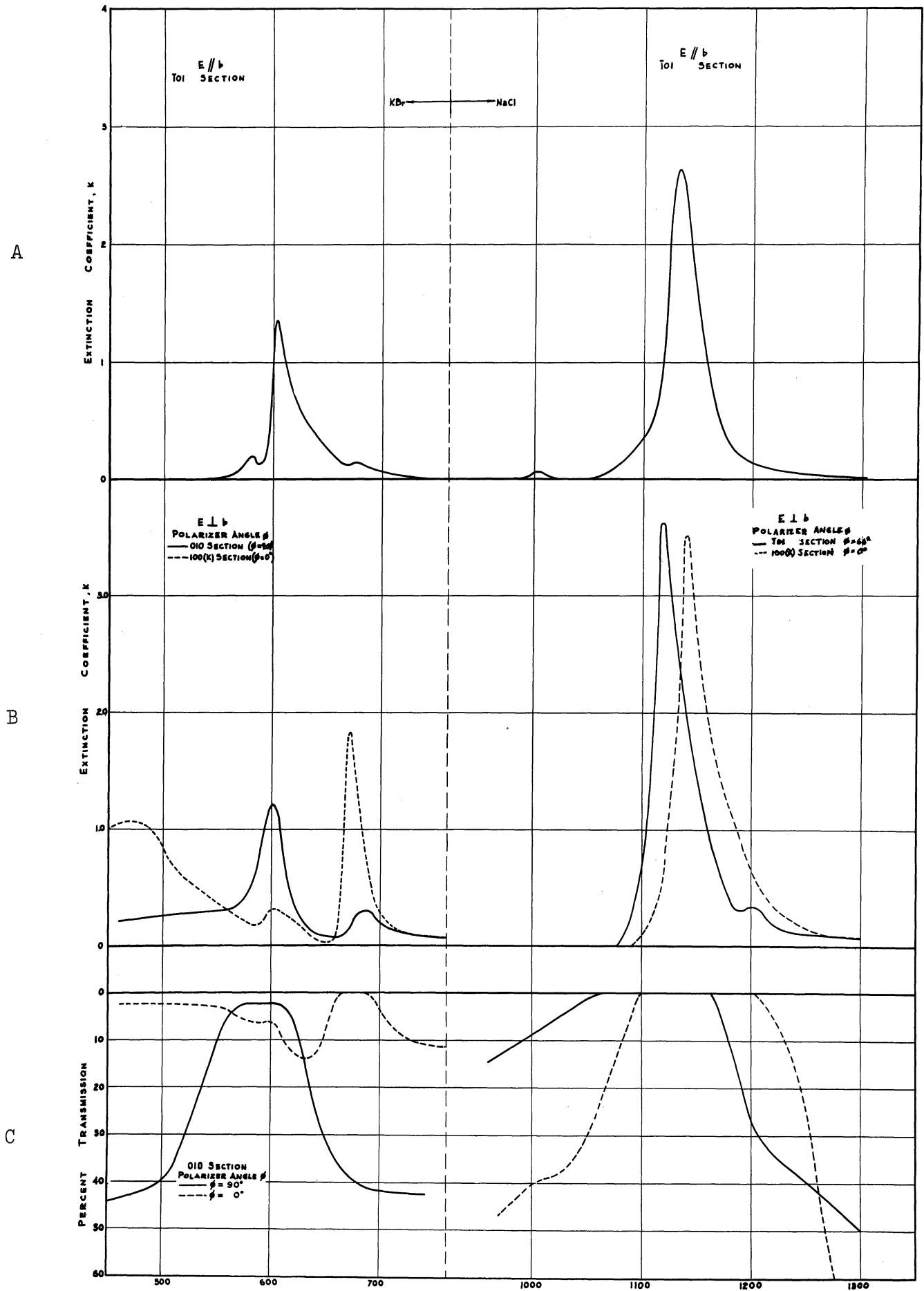
Figure 27. Absorption spectra of gypsum (450-750 cm^{-1} and 1000-1300 cm^{-1})
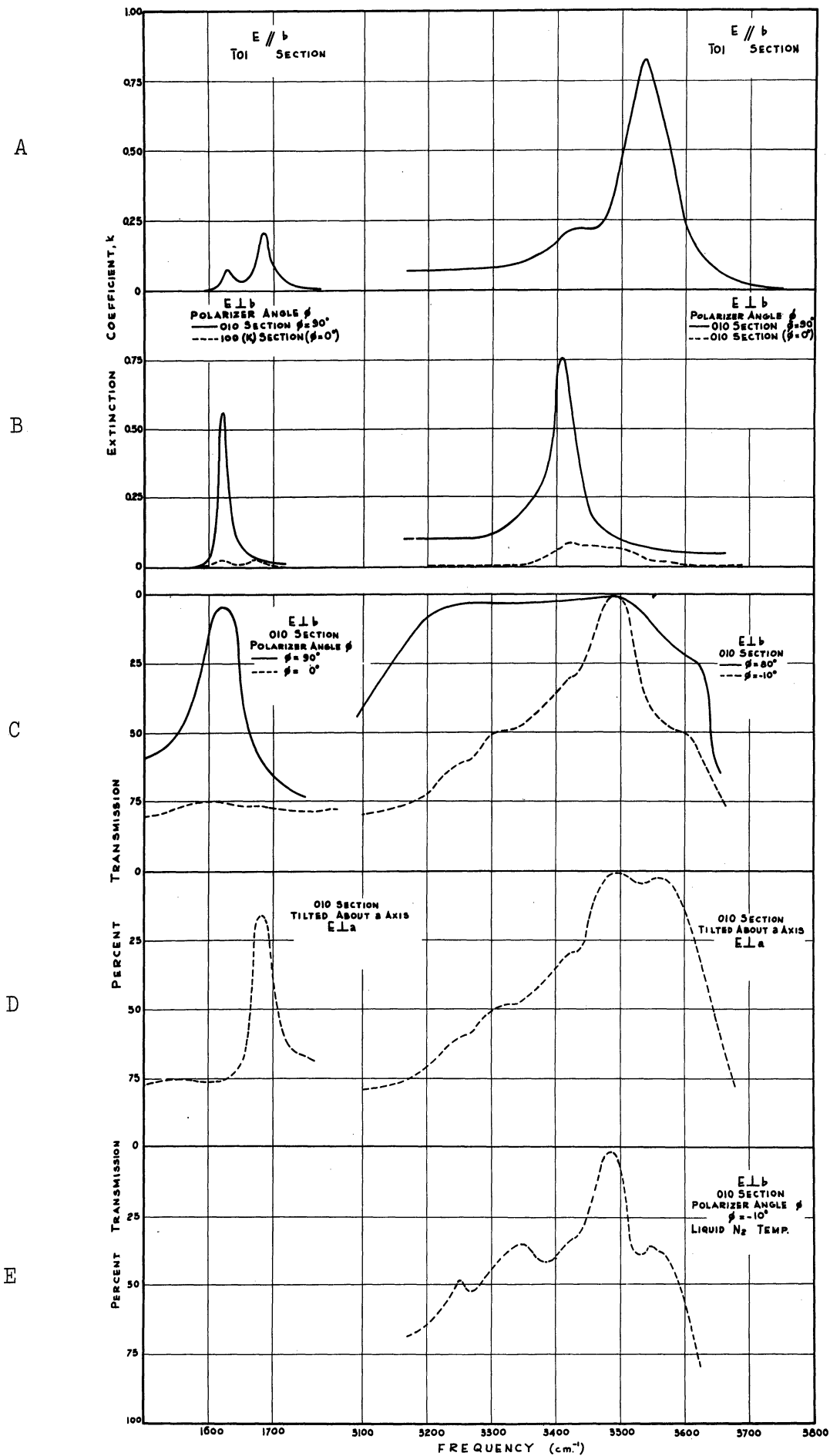
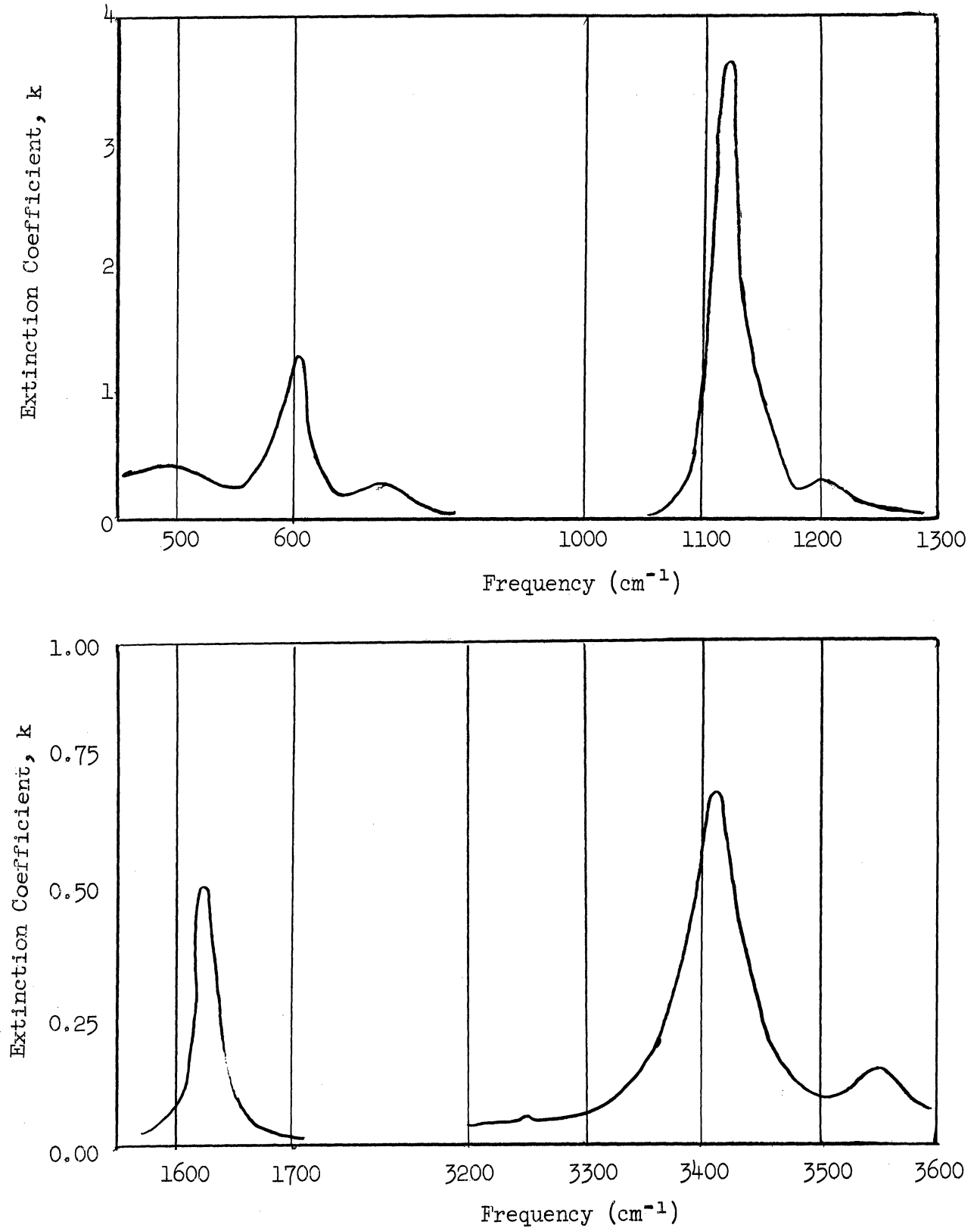Figure 28. Absorption spectra of gypsum (1550-1750 cm^{-1} and 3200-3700 cm^{-1})

Figure 29. Absorption spectrum of gypsum
derived from reflection spectrum off ($\bar{1}$01)
face. E⊥b.

when the electric vector is parallel to the direction of minimum absorption or $\phi = -10°$.

Tables 14A and 14B, 15A and 15B, and 16A and 16B have been arranged in the following way. Tables 14A and 14B contain the results of the analysis of reflection spectra of the ($\bar{1}$01) and (100)(K) faces with the electric vector of the incident light parallel to the $\underline{b}$ axis in both cases. Consequently, both tables are expected to be identical. Tables 15A and 15B contain the results of reflection off the (100)(K) and (010) faces with the electric vector polarized parallel to the c(K) axis. Both tables are expected to be identical. Tables 16A and 16B contain the results of two slightly different orientations. The electric vector is perpendicular to the $\underline{b}$ axis in both cases, but the angle ϕ is 90° for the (010) section and $\phi = 66°$ for the ($\bar{1}$01) section.

These tables give the frequency of the reflection maximum ν, the maximum reflecting power of the bands r^2_{max}, the reflection band widths g, the frequency of the derived absorption maxima ν, the maximum extinction coefficient of the band k_{max}, the integrated extinction coefficient $k_{int} = \int k \, d\nu$, and the absorption band width g. The extinction coefficient k is related to the more familiar absorption coefficient α (appearing in Lambert's law (T = $e^{-\alpha x}$, where T is the fractional transmission) by the expression

$$\alpha = \frac{4\pi k}{\lambda} \, ,$$

where λ is the wavelength of the light. Where the data are enclosed in parentheses, the band is believed to be due to a slightly inefficient polarizer (see Section 5-2.1). The assignments given will be discussed in the next chapter.

TABLE 14

REFLECTION SPECTRA OF GYPSUM

E ‖ $\underline{b}$ Axis

Section	Assignment		Reflection			Absorption			
			$\overline{\nu}$ cm^{-1}	r^2_{max} %	g cm^{-1}	ν cm^{-1}	k_{max}	k_{int} cm^{-1}	g cm^{-1}
		A							
$\overline{1}01$ A_u bands	$\nu_{R''}$ (H_2O)		580	....	....	580	0.1	....	....
	ν_{4b} (SO_4)		602	28	15	602	1.20	38	17
	ν_1 (SO_4)		1000	....	....	1000	0.06	....	....
	ν_{3b} (SO_4)		1153	56	70	1132	2.54	95	32
	ν_2 (H_2O)		(1620	3.9	....	1625	0.08	3	....)
	ν_2 (H_2O)		1680	4.5	....	1685	0.22	7	26
	ν_1 (H_2O)		(3400	....	....	3430	0.12	....	)
	ν_3 (H_2O)		3530	12.9	68	3537	0.77	60	68
		B							
100(K) A_u bands	$\nu_{R''}$ (H_2O)		580	....	....	570	0.1	....	....
	ν_{4b} (SO_4)		601	24	17	603	1.07	24	17
	ν_4 (SO_4)		(674	8.3	....	677	0.30	6	....)
	ν_1 (SO_4)		1000	....	....	1000	0.05	....	....
	ν_{3b} (SO_4)		1157	67	70	1130	2.90	110	35
	ν_2 (H_2O)		(1620	3.8	....	1625	0.04	....	....)
	ν_2 (H_2O)		1680	4.7	....	1684	0.22	6	23
	ν_1 (H_2O)		(3430	....	....	3430	0.10	8	....)
	ν_3 (H_2O)		3530	14	62	3538	0.75	60	65

TABLE 15

REFLECTION SPECTRA OF GYPSUM

E ∥ $\underline{c}$(K) Axis

Section	Assignment	Reflection			Absorption			
		cm^{-1}	r^2_{max} %	g cm^{-1}	cm^{-1}	k_{max}	k_{int} cm^{-1}	g cm^{-1}
				$\underline{A}$				
100(K) $\phi = 0°$ B_u bands	$\nu_R{}'$ (H$_2$O)	> 500	....	....	....	....	....	....
	ν_4 (SO$_4$)	(600	4.5	....	604	0.18	5	....)
	ν_{4c} (SO$_4$)	675	40	25	672	1.95	37	15
	ν_{3c} (SO$_4$)	1155	65	74	1141	3.52	130	27
		1179	....	....	....	....	....	....
	ν_2 (H$_2$O)	(1618	....	....	1618	0.02	....	....)
	ν_2 (H$_2$O)	(1680	....	....	1680	0.03	....	....)
	ν_1 (H$_2$O)	3480	....	....	3490	0.04	....	....
	ν_1 (H$_2$O)	(3530	....	....	3550	0.07	....	....)
				$\underline{B}$				
010 $\phi = 0°$ B_u bands	$\nu_R{}'$ (H$_2$O)	> 500	....	....	....	....	....	....
	ν_4 (SO$_4$)	(605	....	....	605	....	....	....)
	ν_{4c} (SO$_4$)	674	36.2	23	671	1.64	33	16
	ν_{3c} (SO$_4$)	1155	45	80	1143	2.06	80	....
		1180	....	....	....	....	....	....
	ν_2 (H$_2$O)	(1630	....	....	1630	0.08	....	....)
	ν_1 (H$_2$O)	(3405	....	....	3440	0.08	....	....)
	ν_3 (H$_2$O)	3480	....	....	3500	0.06	....	....

85

TABLE 16

REFLECTION SPECTRA OF GYPSUM

E $\perp$ b Axis

Section	Assignment	Reflection			Absorption			
		ν cm^{-1}	r^2_{max} %	g cm^{-1}	ν cm^{-1}	k_{max} cm^{-1}	k_{int}	g cm^{-1}
					A			
	$\nu_{R'}$ (H$_2$O)	>500	....	....	....	....	....	....
	ν_{4a} (SO$_4$)	606	23.5	15	606	1.15	31	17
	ν_4 (SO$_4$)	(680	6	....	685	0.25	6	....)
$\overline{1}$01(K) $\emptyset$ = 66°	ν_{3a} (SO$_4$)	1140	70	75	1118	3.64	120	32
		1206	....	....	1205	....	....	....
B$_u$ bands	ν_2 (H$_2$O)	1620	8.4	20	1624	0.48	9	15
		3240	....	....	3240	0.02	....	....
	ν_1 (H$_2$O)	3403	12.1	40	3410	0.61	38	48
	ν_3 (H$_2$O)	(3530	2.8	....	3535	0.07	....	....)
					B			
	ν_{4a} (SO$_4$)	604	22.5	20	603	1.00	31	22
	ν_4 (SO$_4$)	(675	....	....	682	0.2	6	....)
010 $\emptyset$ = 90°	ν_{3a} (SO$_4$)	1130	40		1127	1.84	80	29
		1145	41.5	77	....	....	....	....
B$_u$ bands		1195	....	....	1195	....	....	....
	ν_2 (H$_2$O)	1620	10.5	20	1623	0.57	12	17
		3240	....	....	....	....	....	....
	ν_1 (H$_2$O)	3404	11.8	40	3410	0.66	42	50

TABLE 17

TRANSMISSION SPECTRA OF GYPSUM

(010) Section

Assignment	Direction of Elect. Vector ϕ, degrees	Absorption Maxima		
		Normal Incidence		Tilted
		Room Temp cm^{-1}	Low Temp cm^{-1}	Room Temp cm^{-1}
$\nu_R{}'(H_2O)$	0	500(br)	---	---
$\nu_R{}''(H_2O)$	90	590(br)	---	---
$\nu_{4a}(SO_4)$				
$\nu_{4c}(SO_4)$	0	670	---	---
?		...	890	...
$\nu_{3a}(SO_4)$	0			
$\nu_{3c}(SO_4)$	90	1150(br)	---	---
$\nu_2(H_2O)\ B_u$	90	1620	---	---
$\nu_2(H_2O)\ A_u$		...	...	1686
$\nu_3(SO_4) + \nu_1(SO_4)$	80	2112	---	---
$\nu_3(SO_4) + \nu_1(SO_4)$	-25	2130	---	---
$\nu_R{}''(H_2O) + \nu_2(H_2O)B_u$	90	2198	2210	---
$\nu_R{}''(H_2O) + \nu_2(H_2O)A_u$	90	2235	2240	---
(H_2O)	80	3400	---	---
$\nu_2(A_g) + \nu_2(B_u)\ (H_2O)$	-10	3250(sh)	3248	---
$\nu_2(A_u) + \nu_2(B_g)\ (H_2O)$	-10	3340(sh)	3350	---
$\nu_1\ (H_2O)\ B_u$	-10	3420(sh)	3410(sh)	
	-10	3495	3495	
	-10	3560(sh)	3560	---
$\nu_3\ (H_2O)\ A_u$		...	...	3560

br = broad
sh = shoulder

5-2 Internal Consistency of Results

5-2.1 Internal Consistency of Reflection Spectra

If the reflection spectra were self-consistent, then Tables 14A and

14B would be identical, since the electric vector of the incident light

is parallel to the b axis in both cases. Similarly, Tables 15A and 15B

would be expected to be identical since the electric vector is parallel

to the c(K) axis in both cases. In Tables 16A and 16B, the orientations

are slightly different so that exact agreement would not be expected.

On the whole, good qualitative agreement for the cases described above is

obtained. However, some differences are observed and these will now be

discussed.

Corresponding reflectivities in Tables 14A and 14B are not exactly

the same. In particular, the bands near 600 cm^{-1} and 1620 cm^{-1} are stronger

for the ($\bar{1}$01) section in Table 14A, while the band near 670 cm^{-1} is stronger

in the (100)(K) sections. These differences can be explained by incomplete

polarization of the incident light by the polarizer. This can be illus-

trated by considering the case where the light is normally incident on the

XY plane of a crystal in either a transmission or reflection experiment.

$$
\begin{array}{c}
Y \\
| \\
| \\
\underline{\quad\quad\quad|\quad\quad\quad} X \\
| \\
| \\
|
\end{array}
$$
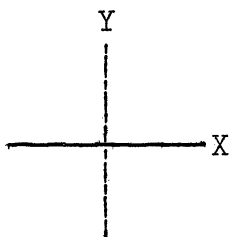
If the transition moment lies in the X direction, then, using polarized

light of the absorbing frequency, maximum absorption will be obtained when

the electric vector is parallel to the X axis, and no absorption will

occur when the electric vector is parallel to the Y axis. If the polar-

izer is not perfect, then a small amount of "absorption" will be indicated

by the spectrometer when the polarizer is set so that the electric vector is parallel to the Y axis. Similarly, the amount of absorption indicated when the polarizer is set in the X direction will be less than the true value. If, however, the transition moment lies in the Z direction (perpendicular to both X and Y), then no absorption will occur even in unpolarized light since the electric vector of the light is always perpendicular to the transition moment.

In the case of the 670 cm^{-1} band, the transition moment lies along the c(K) axis. In Table 14B for the (100)(K) section, the bc(K) plane is viewed with the electric vector set perpendicular to the c(K) axis. Since the polarizer is not perfect, some reflection occurs due to the band with the transition moment along the c(K) axis. This absorption does not occur for the (101) section listed in Table 14A, since the transition moment is nearly perpendicular to the electric vector and parallel to the direction of propagation, regardless of the orientation of the polarizer. The reverse situation occurs for the band near 1620 cm^{-1} where the reflection in the (101) section is stronger than for the (100)(K) section. The transition moment of this band is perpendicular to both the b and c(K) axes and lies nearly in the plane of the (101) section (see Table 16). If the polarizer were perfect this band would be completely absent from Table 14A.

In Tables 15A and 15B, giving the absorption along the c(K) axis, there are two strong bands near 670 cm^{-1} and 1150 cm^{-1}. The maximum reflecting power of the band near 670 cm^{-1} is 40% for the (100)(K) section and 36% for the (010) section. This difference is small enough to be explained by cracks in the sample. However, for the band near 1150 cm^{-1} the reflecting power of the (100)(K) section is 65% and that of the (010) section is only 45%. This difference is too large to be explained by

incomplete polarization of the light or by cracks in the sample. Earlier investigators achieved reflectivities near 70% for these sections.[8,12,25] The discrepancy here is believed to be due to the imperfect optical quality of the samples used. The (010) plane is parallel to the principal cleavage and thin sheets tend to buckle somewhat. It may seem strange that this effect yields poor agreement only with the 1150 cm^{-1}, while satisfactory results are obtained with all the other bands. One possible clue is offered by the fact that bands near 1150 cm^{-1} are the strongest ones in the infrared spectrum. The penetration of light into the crystal is small for a strong band. The penetration distance δ is defined as the distance in which the light intensity drops to $(1/e)$th of its initial value and is given by

$$\delta = \frac{\lambda}{4\pi k} .$$

For the band near 1150 cm^{-1}, the penetration distance is approximately 0.2 microns. However, for the band near 670 cm^{-1} the penetration distance is approximately 0.7 microns. This result indicates that the error in the reflection power due to surface irregularities will be larger for greater absorption.

5-2.2 Comparison of Reflection and Transmission Spectra

Both transmission and reflection spectra of the (010) section have been measured. With one notable exception (occurring at 3495 cm^{-1}), the reflection bands correspond to strong absorption bands appearing in the transmission spectrum. This exception will be discussed shortly.

It would be desirable to compare the value of the extinction coefficient calculated from the reflection spectrum with the value directly measured by transmission. Unfortunately, the sample could not be cleaved

thin enough for this measurement. It was thought that the band near 1620 cm^{-1} could be used. The percent transmission calculated from the reflection spectrum is about 0.000003% for a sample 15 μ thick. The observed value is 4%. The discrepancy may be attributed to the efficiency of the polarizer. If the polarizer is 96% efficient, a maximum of 96% of the energy can be absorbed by a completely polarized band. For this reason, an unpolarized band may often appear to be stronger than a polarized band having the same intrinsic absorption coefficient.

The outstanding disagreement between the reflection and transmission spectrum occurs for the band centered at 3495 cm^{-1} (see Figure 28C). This appears strongly in transmission and is apparently unpolarized. No strong reflection maximum appears to correspond to this band. Only a weak band occurs in reflection (see Figure 28B). It is the opinion of the author that the transmission spectrum in this case is misleading. Pain, Duval, and Lecomte[17] reported a strong band at 3491 cm^{-1} and weaker bands [probably shoulders] at 3244, 3334, and 3580 cm^{-1} for gypsum crystal in unpolarized light. However, on examining the powder where random orientations are present, very strong bands are reported[17] at 3402 cm^{-1} and 3533 cm^{-1}. No mention is made of any band near 3491 cm^{-1}. This suggests that the intensity of the band at 3491 cm^{-1} is actually much weaker than that of the polarized bands at 3402 cm^{-1} and 3533 cm^{-1}. The strong bands in the reflection spectrum found in this work are at 3410 cm^{-1} and 3537 cm^{-1}, which is in good agreement with the powder studies.

Only thin crystal sections parallel to the (010) plane could be obtained. Transmission spectra taken at normal incidence will reveal only B_u bands. However, by tilting the sample in the beam, it is possible to reveal the presence of A_u bands. In this way it is possible to compare results obtained by transmission and reflection for the A_u bands.

Strong A_u bands occur near 1680 cm^{-1} and 3450 cm^{-1}. They are shown in reflection in Figure 28A and in transmission in Figure 28D. The electric vector is set so that bands whose transition moments lie along the $\underline{b}$ axis will absorb (or reflect) radiation. An additional check on the A_u band is provided by inspection of the spectrum of powdered gypsum, where random orientations are present. A weak band near 1680 cm^{-1} has been reported,[19,20] as well as a strong band[17] near 3537 cm^{-1}.

5-3 Analysis of Errors of the Reflection Method

The influence of experimental errors on the determination of the optical constants will be discussed briefly. The calculation of the optical constants from the reflecting powers by the Robinson method is a complicated one and depends on the detailed shape and intensity of the absorption band. For this reason it is not possible to give definite limits of error applicable to all cases.

5-3.1 Influence of Error in the Reflecting Power

The fundamental formulas for the calculation of the optical constants are the following:

$$n = \frac{1 - r^2}{1 + r^2 - 2r \cos \theta_c} \qquad k = \frac{-2r \sin \theta_c}{1 + r^2 - 2r \cos \theta_c} \quad , \quad (3\text{-}6)$$

in which the value of θ_c is obtained from the integral

$$\theta_c = \frac{1}{\pi} \int_0^\infty \frac{d \ln r}{d\omega} \ln\left|\frac{\omega + \omega_c}{\omega - \omega_c}\right| d\omega \quad . \qquad (3\text{-}27)$$

The quantities r and ω are observed experimentally. The influence of an error in ω will be ignored. Errors in r can be attributed to loss of a constant fraction of the energy over the entire frequency range, shift

of the zero energy line, or scattering and other effects due to surface irregularities. The error due to scattering and surface irregularities will not be considered here. Scattering is probably small for infrared wavelengths. The errors in r due to a loss of a constant fraction of the energy or to a shift of the zero energy line are probably the most important ones.

The effect of a loss of a constant fraction of the energy is easily shown to introduce no error in the phase angle θ_c. If the true reflecting power r^2 were actually altered by some factor "a" such that the quantity ar^2 is observed, then

$$\frac{d \ln \sqrt{ar}}{d\omega} = \frac{d \ln \sqrt{a}}{d\omega} + \frac{d \ln r}{d\omega} = \frac{d \ln r}{d\omega} ,$$

so that the value of the integrand in (3-27) remains unchanged. The error in the extinction coefficient k can be found from equation (3-6). As an example, the reflection band near 3540 cm^{-1} [assigned as $H_2O \; \nu_3(A_u)$] and shown in Figure 21 will be calculated. The reflecting power at the maximum in the absorption is 12.8%. The derived extinction coefficient is 0.82. If the reflectivity were actually 13.8%, then the extinction coefficient would be 0.86.* This gives some idea of the magnitude of the error introduced.

The calculation of the error due to a shift in the zero energy line involves an integration over the entire reflection spectrum and would be a very difficult statistical problem, and will not be given here. The error introduced in the optical constants would be greatest on the high frequency side of the band since the reflection coefficient has a minimum here.

---

*The phase angle θ_c can be obtained from the reflection equation (3-6), knowing n and k.

5-3.2 Error Due to Non-normal Incidence

The reflection spectra were taken at an average angle of incidence of 13°. This angle is only an average, since the optical arrangement involved a divergent beam with an angle of divergence of 7°, as discussed in Section 4-2.1. If the beam is assumed parallel, it will be shown that the error introduced by non-normal incidence is negligible.

For anisotropic crystals it is advisable to choose the electric vector perpendicular to the plane of incidence (the plane containing the incident and reflected ray) for the following reason. In Figure 30 the plane of incidence is the plane of the paper. Any transition moments will be assumed to lie in one of the three mutually perpendicular directions X, Y, or Z. The X and Y directions lie in the plane of incidence and the Z direction is perpendicular to it. If the incident light is polarized so that the electric vector is perpendicular to the plane of incidence, it will be parallel only to the Z axis and perpendicular to the X and Y axes. If the incident light is polarized so that the electric vector is parallel to the plane of incidence, it will have a component along both the X and Y directions. In order to view one direction at a time, the light was always polarized so that the electric vector was perpendicular to the plane of incidence.

The correction for non-normal incidence can be made in the following manner given by Robinson and Price.[49] The reflection coefficient of light polarized perpendicular to the plane of incidence is given by Fresnel's equation

$$R_s = \frac{\sin (\varphi - \chi)}{\sin (\varphi + \chi)} , \qquad (5-1)$$

in which φ is the angle of incidence and χ is the angle of refraction. The angles φ and χ are related by Snell's law
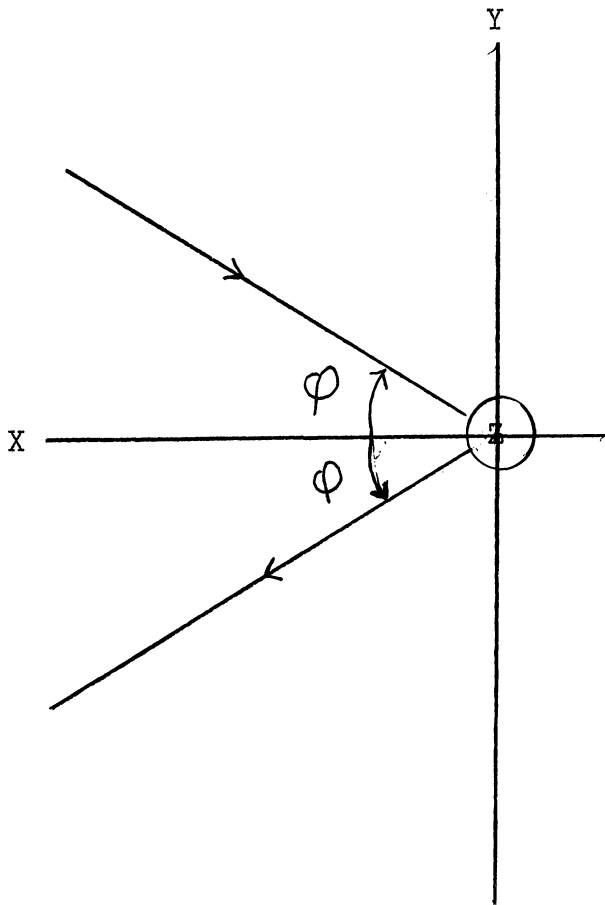
Figure 30. Angles of incidence. The incident
and reflected ray lie in the plane of the paper.

$$\sin \varphi = \underline{N} \sin \underline{\chi} \ , \tag{5-2}$$

where $\underline{N}$ and $\underline{\chi}$ will be considered complex. By eliminating the angle $\underline{\chi}$ between these two equations, the following result can be obtained.

$$\underline{R_s} = \frac{\underline{N_s} - 1}{\underline{N_s} + 1} \tag{5-3}$$

where

$$\underline{N^2} = \underline{N_s}^2 \cos^2 \varphi + \sin^2 \varphi \ . \tag{5-4}$$

The complex number

$$N_s = n_s - ik_s \tag{5-5}$$

is obtained from the reflection spectrum, while

$$N = n - ik$$

is the desired result. Solving for n and k in terms of n_s and k_s in the two equations, the following relations are obtained:

$$n^2 + k^2 = (n_s^2 + k_s^2)\cos^2 \varphi + \sin \varphi \tag{5-6}$$

$$nk = n_s k_s \cos \varphi \ .$$

To a first order approximation, let

$$n = n_s - \Delta n$$
$$k = k_s - \Delta k \ , \tag{5-7}$$

so that

$$\frac{\Delta n}{n_s} = \frac{\sin^2 \varphi}{2} \left(1 - \frac{1}{n_s^2 - k_s^2}\right)$$

$$\frac{\Delta k}{k_s} = \frac{\sin^2 \varphi}{2} \left(1 + \frac{1}{n_s^2 - k_s^2}\right) \ . \tag{5-8}$$

Except where n_s and k_s are about the same value, this first approximation is valid for small angles. Since $\varphi = 13°$, $\frac{\sin^2 \varphi}{2} = 0.025$, and

since the term $\dfrac{1}{n_s^2 - k_s^2}$ is usually greater than unity, this correction term was ignored.

5-3.3 Error Due to Limited Range of Measurement

The calculation of the phase angle involves an integration over all frequencies from zero to infinity. However, whenever the reflectivity is constant over a frequency interval, the contribution of this section of the reflection spectrum is zero since $\dfrac{d \ln r}{d\omega} = 0$. The range of integration may be replaced by finite limits when the reflectivity remains constant on both the high and low frequency sides of an reflection band. A constant reflectivity in these regions corresponds to absence of absorption. For gypsum the absorption is effectively constant from about 4000 cm^{-1} to the ultraviolet. For low frequencies ($> 450 \ cm^{-1}$), the absorption is still finite for some orientations. The extinction coefficient can not be calculated exactly near the limits of integration. In fact, if the limit of integration is close to a reflection band, failure to include all of the band can result in an error in the phase angle over the rest of the spectrum. This small error in the phase angle is believed to account for one obvious error in certain absorption curves derived from reflection spectra. In some cases where the transmission spectra indicated no absorption, the derived extinction coefficient differed from zero. This difference was not greater than ± 0.1. When this occurred, the extinction coefficients reported in the tables were found by drawing in a zero line connecting the high and low frequency sides.

5-3.4 Integral Approximation

In the phase calculation, a continuous curve is approximated by a series of straight line segments. The use of straight line segments to approximate a continuous curve can alter the results. In principle, this

error can be minimized by use of many line segments at the expense of additional computation. This difficulty could be avoided with the aid of an analog computer in which the input would be a continuous arbitrary curve.[80] A general-purpose digital computer was used because of its availability. An additional advantage is gain in the use of a more flexible digital computer in that other parts of the calculation such as the reflection equation can be solved at the same time.

In this work, 116 points on a reflection spectrum extending from 450-5000 cm^{-1} were used. These were chosen so that many points were located near a reflection band; very few were used in the regions between bands. The points chosen are shown in Figures 20 and 21.

5-3.5 Error Due to Limited Spectral Resolution

Robinson and Price[49] noticed that absorption spectra derived from reflection spectra showed a shift in the frequency of the absorption maximum compared to those obtained directly from the transmission spectra. The frequencies of the absorption maxima derived from reflection were higher than those measured directly by transmission. Empirically, Robinson and Price found this shift to amount to one-quarter of the effective spectrometer slit width.

In transmission spectra the effect of limited spectral resolution is to change the apparent extinction coefficient of the band. If the absorption band is symmetric, the frequency of the absorption maximum will not be affected. Reflection bands are asymmetric. Consequently, limited spectral resolution will affect both the frequency of the absorption maximum and derived reflection maximum.

5-4 Problems of Crystal Optics

In Section 4-4 it was pointed out that there are certain difficulties associated in analysing bands belonging to the B_u species. These difficulties are absent for completely polarized bands. It has been found that all of the B_u fundamentals are either completely polarized or nearly completely polarized. The bands near 670 cm^{-1} and 1623 cm^{-1} are completely polarized. The other fundamentals show nearly complete polarization. The overtone near 2200 cm^{-1} shows only partial polarization.

For the fundamentals examined, the transition moments of fundamentals belonging to the A_u species must lie parallel to the b axis and the transition moments of bands belonging to the B_u species must lie in the plane perpendicular to the b axis, i.e., the (010) plane. The directions in the (010) plane of the B_u transition moments are found experimentally to be within 10° of being either parallel or perpendicular to the c(K) axis for all of the fundamentals. It is interesting to point out that one of the principal axes of the dielectric ellipsoid measured at radio frequencies lies within 2° of the c(K) axis.[81] On the other hand, the smallest angle between the c(K) axis and one of the principal axes of the index of refraction ellipsoid measured in visible light is 38°.

CHAPTER 6

INTERPRETATION OF THE INFRARED AND RAMAN SPECTRUM

6-1   The Sulfate Frequencies

6-1.1   Discussion of the Infrared Spectrum
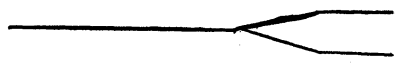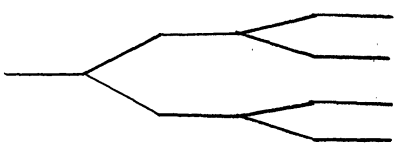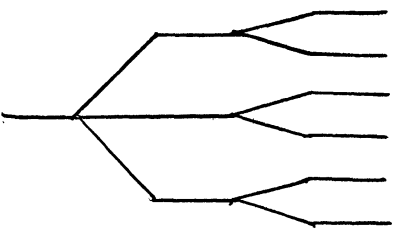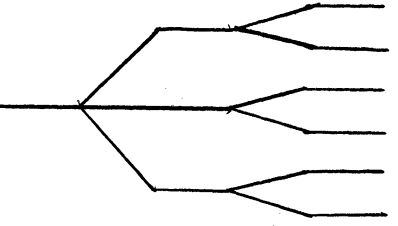
In Section 2-3 certain predictions were made about the distribution

of internal sulfate fundamentals of gypsum among the various symmetry

species. These predictions are summarized in Table 18. The values of

the observed infrared and Raman frequencies are shown along with the Raman

bands measured for sulfate ion in aqueous solution. A chart with a linear

frequency scale illustrating these results is given in Figure 31.

In the crystal, all of the infrared-active bands belong to one of

two species, A_u or B_u. The transition moments of the A_u bands lie parallel

to the $\underline{b}(C_2)$ crystal axis, while the transition moments of the B_u bands

lie in the plane perpendicular to the $\underline{b}(C_2)$ axis. Bands belonging to these

two species can be distinguished experimentally by the use of various cry-

stal orientations and by the use of polarized light with the electric vec-

tor set either parallel or perpendicular to the $\underline{b}(C_2)$ axis.

The A_u bands are shown in Figure 27A. Five internal sulfate funda-

mentals belong to the A_u species, one each corresponding to the molecular

fundamentals ν_1, ν_3, and ν_4, and two corresponding to ν_2. The fundament-

als ν_3 and ν_4 are infrared-active for the free ion and would be expected

to be strongly infrared active in the crystal. On the other hand, the

fundamentals ν_1 and ν_2 are infrared inactive for the free ion and become

TABLE 18

CRYSTAL FREQUENCIES OF SULFATE IONS

Isolated Ion		Crystal		
981	ν_1	A_g	1006	
		A_u	1000	(...)
451	ν_2	A_g	492	
		A_u	...	
		A_g	413	
		A_u	...	
1104	ν_3	A_g	1144	
		A_u	1131	(100)
		B_g	1138	
		B_u	1142	(130)
		B_g	1117	
		B_u	1118	(120)
613	ν_4	A_g	621	
		A_u	602	(30)
		B_g	669	
		B_u	672	(35)
		B_g	623.5	
		B_u	604	(30)

g = Raman, u = infrared
Infrared intensities given in pa   s
Raman assignments of Rousset and Lochet[28]
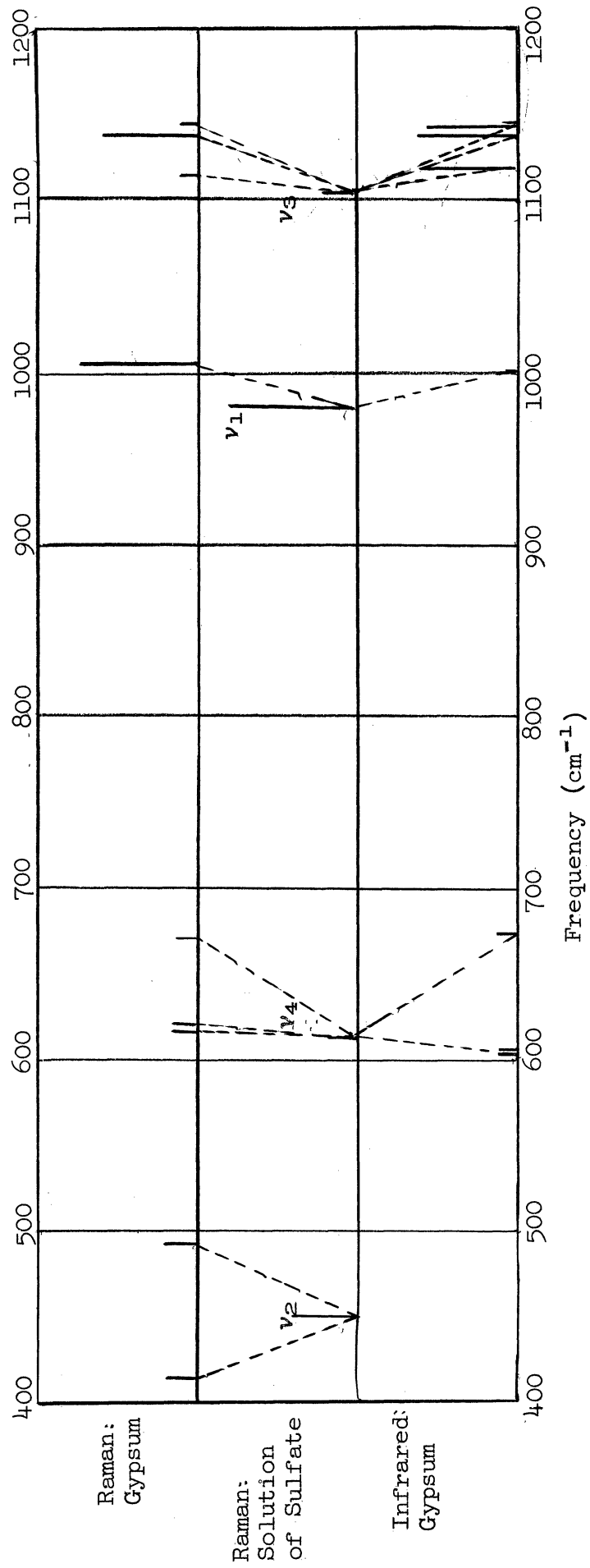
Figure 31. Comparison of Sulfate Frequencies

active only in the perturbing field of the crystal. For this reason ν_1 and ν_2 should appear weakly or not at all. Strong bands are observed at 1131 cm^{-1} and 602 cm^{-1} corresponding to the fundamentals ν_3 and ν_4, respectively, and a weak band appears at 1000 cm^{-1} corresponding to ν_1. No bands are observed corresponding to ν_2 within the range of measurement.

Absorption bands belonging to the B_u species are shown in Figure 27B. The transition moments of these bands must lie somewhere in the (010) plane. However, the particular direction in this plane may be different for different vibrations. It was found experimentally that the transition moments were either parallel ($\phi = 0°$) or perpendicular ($\phi = 90°$) to the $\underline{c}(K)$ axis.* Two crystal fundamentals arise from each of the molecular fundamentals ν_3 and ν_4. All four B_u absorption bands are observed in the infrared spectrum.

The labeling of the crystal fundamentals corresponding to ν_3 and ν_4 is carried out according to the direction of the transition moment. Those bands in which the transition moment is parallel to the $\underline{b}$ axis are designated as ν_{3b} and ν_{4b}; those in which the transition moment is parallel to the $\underline{c}(K)$ axis are designated as ν_{3c} and ν_{4c}; and those in which the transition moment is perpendicular to both the $\underline{b}$ and $\underline{c}(K)$ axes are designated as ν_{3a} and ν_{4a}.

The ν_3 absorption bands are the most intense found in the infrared spectrum. From Figure 14, giving the form of the normal vibrations of the isolated ion, it can be seen intuitively that the ν_3 bands would be expected to be quite intense since this vibration involves a motion of the four oxygens moving in unison against the central sulfur.

The ν_4 bands are not as intense as the ν_3 bands. Both ν_{4a} (604 cm^{-1}) and ν_{4b} (602 cm^{-1}) occur within two cm^{-1} of each other. This difference

---

*This observation is somewhat uncertain for the ν_3 band, due to overlapping of ν_{3a} and ν_{3c}.

is within experimental error. The ν_{4c} (672 cm^{-1}) band is completely polarized along the $\underline{c}$(K) axis. The ν_{4a} (604 cm^{-1}) is not as completely polarized. The ν_{4a} and ν_{4b} are obscured by a broad band, which is presumably a rotary lattice frequency of water and will be discussed later. Since the sulfate bands are considerably sharper they are easily distinguishable from the water rotary lattice band as shown in Figure 27B. The water band may in some way be responsible for the asymmetric shape of the derived absorption spectrum.

The classification of the observed bands has been carried out quite satisfactorily using the factor group analysis given in Chapter 2. Seven of the nine infrared active internal fundamentals due to the sulfate ions have been found and these can be unambiguously assigned. The direction of the transition moment of each of these fundamentals has been determined, using polarized radiation. From these directions, information about the force fields in gypsum can be obtained. The force field will be discussed in Section 6-1.3 after a discussion of the Raman spectrum.

6-1.2 Discussion of the Raman Spectrum

The Raman lines due to the internal sulfate fundamentals can be classified in terms of the crystal symmetry species A_g or B_g by the use of polarized light. Before presenting this data, the selection rules for Raman activity given in Chapter 2 will be repeated. The components of the change in polarizability tensor α are distributed in the following way:

$$
A_g \qquad
\begin{array}{c|ccc}
 & x & y & z \\
\hline
x & \alpha_{xx} & --- & \alpha_{xz} \\
y & --- & \alpha_{yy} & --- \\
z & \alpha_{xz} & --- & \alpha_{zz}
\end{array}
$$

$$
B_g \qquad
\begin{array}{c|ccc}
 & x & y & z \\
\hline
x & \text{---} & \alpha_{xy} & \text{---} \\
y & \alpha_{xy} & \text{---} & \alpha_{yz} \\
z & \text{---} & \alpha_{yz} & \text{---}
\end{array}
$$

The axes x, y, and z are chosen with respect to the sulfate ion, while the experimental measurements are taken with the electric vector of the scattered light parallel to the principal axes 1, 2, and 3 of the index of refraction ellipsoid in visible light. The axis 2 of the index ellipsoid and the y axis of the sulfate ion will always be chosen parallel to the $\underline{b}(\underline{C_2})$ axis of crystal, because of symmetry considerations. However, the only constraints imposed by symmetry on the x and z axes as well as the 1 and 3 axes is that they lie in the plane perpendicular to the crystal $\underline{C_2}$ axis, i.e., the (010) plane. The diagram given in Figure 32 shows the relation of the index axes to the sulfate ion. Since the y direction and the 2 direction are determined by symmetry considerations only, it should be possible to distinguish between the A_g and B_g bands without knowing the directions of the x and z axes. The fact that the x and z directions need not coincide with the 1 and 3 directions will not change any selection rules.

The results of Rousset and Lochet[28] are shown in Table 19. It can be seen that the observed bands fall into two classes. By comparing with the selection rules given previously, each Raman line can be classified as belonging to either the A_g or B_g species. The number and distribution of the Raman bands is in agreement with the factor group analysis given in Chapter 2.

6-1.3 Relation to the Structure

The following experimental observations about the infrared and Raman
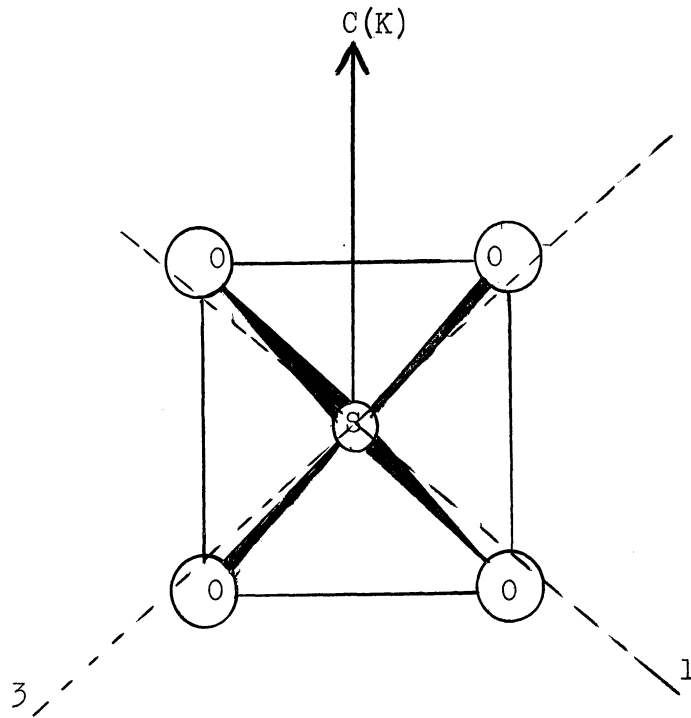
Figure 32. Projection of the sulfate ion on the (010) plane.
The C_2 axis of the sulfate ion is perpendicular to the plane
of the paper and passes through the sulfur atom. Two of the
oxygens lie above the plane of the paper and two lie below
the plane.

TABLE 19

RAMAN INTENSITY DATA (SULFATE)[28]

1006 cm^{-1} (A_g)

ν_1

	1	2	3
1	s	-	-
2	-	s	-
3	-	-	s

413 cm^{-1} (A_g)

ν_2

	1	2	3
1	s	-	w
2	-	s	-
3	w	-	m

492 cm^{-1} (A_g)

	1	2	3
1	-	-	s
2	-	m	-
3	s	-	s

621 cm^{-1} (A_g)

ν_4

	1	2	3
1	-	-	-
2	-	-	-
3	-	-	m

623.5 cm^{-1} (B_g)

	1	2	3
1	-	-	-
2	-	-	s
3	-	s	-

669 cm^{-1} (B_g)

	1	2	3
1	-	m	-
2	m	-	s
3	-	s	-

1144 cm^{-1} (A_g)

ν_3

	1	2	3
1	s	-	w
2	-	m	-
3	w	-	s

1117 cm^{-1} (B_g)

	1	2	3
1	-	-	-
2	-	-	m
3	-	m	-

1138 cm^{-1} (B_g)

	1	2	3
1	-	s	-
2	s	-	s
3	-	s	-

s = strong
m = medium
w = weak

spectrum of gypsum have been established.

1. The ν_1 non-degenerate molecular fundamental splits into two crystal fundamentals, one belonging to species A_g (Raman) and the other to species A_u (infrared), with a difference of only six cm^{-1} between them.

2. The ν_2 doubly-degenerate molecular fundamental splits into four crystal fundamentals: two belong to species A_g and differ by about 75 cm^{-1} in the Raman spectrum, and two belong to species A_u. The A_u modes could not be observed in the infrared spectrum.

3. The ν_3 triply-degenerate molecular fundamental splits into six crystal fundamentals distributed among all four crystal symmetry species with a maximum splitting of about 25 cm^{-1}.

4. The ν_4 triply-degenerate fundamental splits into six crystal fundamentals with a splitting of about 70 cm^{-1} among the infrared active modes $(A_u + B_u)$ and a splitting of about 50 cm^{-1} among the Raman active modes $(A_g + B_g)$.

5. One of the two B_u fundamentals corresponding to the molecular fundamental ν_4 has its transition moment parallel to the $\underline{c}(K)$ axis. The other band has its transition moment perpendicular to the $\underline{c}(K)$ axis. A similar result holds for the ν_3 crystal fundamentals.

6. For a given molecular fundamental there is no general rule as to whether the infrared or Raman fundamental occurs at a higher frequency.

In order to seek an explanation for these observations, the theory of crystal spectra applicable to this case will be discussed. According to Hornig,[82] the complete harmonic potential function may be written in the following way:

$$V = V_L + \sum_j (V_j^\circ + V_j') + \sum_j \sum_k V''_{jk} + V'''_{Lj} ,$$

in which V_L, the lattice potential, includes terms involving the center

of gravity and orientation of the molecules; V_j^0 is the potential energy

function of the free molecules, and V_j', V_{jk}'', and V_{Lj}''' are perturbations.

The term V_j' represents the change in V_j^0 due to the equilibrium field of

the crystal. The terms V_{jk}'' account for the interaction between the dis-

placement coordinates of the jth and k^{th} molecules, while V_{Lj}''' accounts

for the interaction between the internal and lattice coordinates. The

term V_j' has the site symmetry of the jth molecule. When the site sym-

metry is lower than the point symmetry of the isolated molecule, inclu-

sion of this term can account for splitting of degeneracies and changes

in the selection rules. This term can also account for shifts in the

frequency between the gaseous and solid state.

If ther are $\underline{p}$ molecules in the unit cell, each non-degenerate nor-

mal vibration results in a $\underline{p}$-fold degenerate crystal mode in the zeroth

order. Introduction of a coupling term V_{jk}'' can account for a splitting

of this degeneracy. The remaining term V_{Lj}''' can be expected to be negli-

gible when the frequency separation between the lattice and internal vi-

brations is large.

In the case of gypsum, this would imply that the large splitting of

$\nu_2(A_g)$ and $\nu_2(A_g)$, and $\nu_{4a}(B_u)$ and $\nu_{4c}(B_u)$ is due to some local perturb-

ing potential. However, differences between the infrared and Raman spec-

trum of bands like $\nu_{3b}(A_g)$ and $\nu_{3b}(A_u)$ are attributed to coupling of the

molecules in the unit cell.

Since the splitting of the ν_2 vibration is extremely large, Rousset

and Lochet[28] suggested that the sulfate ion is distorted from a tetra-

hedral configuration into one of lower symmetry. According to this view

this distortion is too small to have been detected by x-ray diffraction.

The depolarization studies are said to indicate that this lower symmetry

is C_2. In the opinion of the author, the Raman and infrared spectrum of

gypsum can be adequately explained without stating whether the sulfate ions lose their tetrahedral configuration in the equilibrium position. The Raman and infrared results from the motions of molecules. The motions of the sulfate ions in the crystal may be thought to resemble those of a system subject to a potential energy function of symmetry $\underline{C_2}$. However, it is not possible to make any statement about the equilibrium sulfate configuration in this case.

The infrared polarization studies suggest that there might be a perturbing field parallel or perpendicular to the $\underline{c}(K)$ axis, since the transition moments of the B_u bands appear to lie parallel or perpendicular to this direction. From Figure 5 it can be seen that the calcium and sulfate ions are arranged in rows parallel to the $c(K)$ axis in the following way:

```
        2.57    O O  2.57              O O               O O               O O
   Ca           S       Ca             S      Ca         S      Ca         S
        2.59    O O  2.59              O O               O O               O O
```
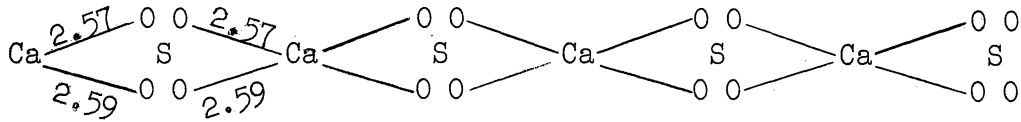
in which the Ca - O distances are 2.57 and 2.59 A.U. It is possible that this arrangement may induce a perturbing force parallel to the $\underline{c}(K)$ axis. On the other hand, in Table 2 a short Ca-O "bond" of 2.38 A.U. is listed. The projection of this "bond" on the (010) plane occurs at an angle $\emptyset = 80.5°$, or nearly perpendicular to the $c(K)$ axis. This "bond" links calcium and sulfate ions in adjacent rows. Either or both of these structural features may result in a perturbation which influences the direction of the transition moments.

6-2 The Water Frequencies

6-2.1 Discussion of the Infrared Spectrum

In Section 2-2, certain predictions were made concerning the distribution of the internal water fundamentals among the various species. This classification is summarized along with the frequencies of the observed bands in Table 20. These assignments are tentative. Each molecular fundamental splits into four crystal fundamentals, each belonging to one of the four factor group species. The A_u bands are shown in Figure 28A, while the B_u bands are given in Figure 28B.

TABLE 20

CRYSTAL FREQUENCIES OF WATER OF CRYSTALLIZATION

3657.1	ν_1	A_g	3404.5
		A_u	3430(8)
		B_g	3402.5
		B_u	3410(42)
1595	ν_2	A_g	....
		A_u	1685(6.5)
		B_g	....
		B_u	1623(12)
3755.8	ν_3	A_g	3496.5
		A_u	3537(60)
		B_g	3498
		B_u	3490(2)

Raman assignments of Cabannes, Couture, and Mathieu[33]
Raman bands: subscript g; infrared bands: subscript u

From a knowledge of the structure it is possible to predict the
ratio of the infrared intensities of the A_u to B_u bands (dichroic ratio)
corresponding to each of the molecular fundamentals. A comparison of
the observed and predicted values is shown in Table 21.

TABLE 21

PREDICTED AND OBSERVED INFRARED WATER DIRECTIONS

Fundamental	$\cot^2 \Theta = \dfrac{k_{Au}}{k_{Bu}}$		ϕ	
	Predicted	Observed	Predicted	Observed
ν_2	0.61	0.54 ±0.1	89.5°	90°
ν_1	0.61	0.2	89.5°	80°
ν_3	1.40	30	66°	...

In this table k_{Au}/k_{Bu} refers to the dichroic ratio (using integrated in-
tensities). The angle ϕ initially defined in Section 2-3 gives the angle
of the electric vector in the (010) plane for maximum absorption. From
this table it can be seen that good results are obtained for the ν_2 funda-
mentals and very poor agreement is obtained for the ν_1 and ν_3 fundamentals.

The two sharp bands near 1623 cm^{-1} and 1684 cm^{-1} are assigned to $\nu_2(B_u)$
and $\nu_2(A_u)$ modes, respectively. The B_u band shows maximum absorption when
the electric vector is perpendicular to the $\underline{c}$(K) axis ($\phi = 90°$). This
direction of maximum absorption is parallel to the projection of the water
symmetry axes on the (010) plane and is exactly what one would expect from
structural considerations. Good results for the intensity and direction
of polarization are obtained for the ν_2 fundamental. The large splitting
of about 60 cm^{-1} between $\nu_2(A_u)$ and $\nu_2(B_u)$ indicates appreciable inter-
action among the various molecules of water in the unit cell. For this

reason it is surprising that the "oriented gas" approximation on which these predictions are based works so well. In addition, the fact that the effective spectrometer slit width is of the same order of magnitude as the observed band width might be expected to give erroneous intensities.

In the region of the ν_1 and ν_3 fundamentals, two strong infrared reflection bands are observed, one with the transition moment parallel to the $\underline{b}(C_2)$ axis near 3540 cm^{-1}, and the other with the transition moment perpendicular to the $\underline{b}(C_2)$ axis near 3410 cm^{-1}. On examining the reflection spectrum closely, a weak plateau near 3430 cm^{-1} and a weak band near 3490 cm^{-1} can be discerned. These four bands are assigned to $\nu_3(A_u)$, $\nu_1(B_u)$, $\nu_1(A_u)$, and $\nu_3(B_u)$ as shown in Table 20. However, in view of the discrepancy between the predicted and observed intensities given in Table 21, it appears that the "oriented gas" approximation is inadequate to explain the observed results.

The transmission spectrum of gypsum displays an anomaly at 3495 cm^{-1}. A strong band appears in transmission and is apparently unpolarized. No corresponding strong band appears in reflection. This discrepancy has been discussed in Section 5-2.2, where it was concluded that this band is weak compared to the strong reflection bands. No satisfactory explanation can be given as to why this band is unpolarized. In the transmission spectrum there is a shoulder near 3560 cm^{-1}, which can be resolved into a definite band at low temperatures. This band is not completely polarized. No satisfactory assignment can be given. The other weaker bands are satisfactorily explained as combinations and will be discussed in Section 6-2.3.

Some broad bands are present in reflection near 450 cm^{-1} and 600 cm^{-1}. The polarization properties indicate that the lower frequency band designated as ν_R, ($\sim$450 cm^{-1}) absorbs more strongly when the electric

vector is parallel to the $\underline{b}$ axis. In transmission, broad bands are found near both of these frequencies. At low temperatures these bands become reduced in intensity (see Figure 28E). Krishnan[29] reported two broad bands in the Raman spectrum with frequency shifts of 565 cm^{-1} and 588 cm^{-1} which are presumably also rotary lattice modes.

6-2.2 Discussion of the Raman Spectrum

The Raman spectrum of the water of crystallization of gypsum has been examined closely by several investigators. A marked dependence on orientation, as well as polarization, has been noted. A summary of the more recent results is given in Table 22. The assignments are those of Cabannes, Couture, and Mathieu.[33]

TABLE 22

RAMAN LINES DUE TO WATER OF
CRYSTALLIZATION IN GYPSUM (cm^{-1})

Assignment	Cabannes, Couture, Mathieu[33] (1953)	Stekhanov[33] (1953) (low temp)	Krishnan[29] (1945)	Roop* Kishore (1942)
ν_2	1632		1631(2)	1622
		3230	3258(3)	3244
		3273		3309
		3349	3334(3)	
$\nu_1(B_g)$	3402.5	3408	3406(30)	3410
$\nu_1(A_g)$	3404.5			
$\nu_3(A_g)$	3496.5	3486	3495(30)	3480
$\nu_3(B_g)$	3498			
		3564		3584
		3626	3606(3)	
		3673	3680(2)	

The figures given within brackets represent visual estimates of the relative intensities by Krishnan.

*See summary by Krishnan for reference and additional studies.

The intensities of the components of the two strong Raman bands have been given by Cabannes, Couture, and Mathieu and are shown in Table 23. The crystal was cut in the shape of a rectangular parallelepiped with the edges parallel to the axes of the index of refraction ellipsoid. The directions 1, 2, and 3 are the same as for the sulfate spectra discussed in the previous section. This investigation was more thorough than the one for sulfate. The light was incident normal to one of the faces of the parallelepiped and plane-polarized parallel to one of the edges. The direction of propagation of the scattered light was perpendicular to the direction of propagation of the incident light. The scattered light was analysed parallel to one of the edges. This is shown in Figure 33, in which E_2 and E_3 can represent different directions of the electric vector of the incident light, and M_1 and M_3 can represent different directions for analysis of the scattered light.

TABLE 23

RAMAN INTENSITY DATA (WATER OF CRYSTALLIZATION)

$v_1(A_g + B_g)$

	1	2	3
1	64	10	19
2		14	2.5
3			14

$v_3(A_g + B_g)$

	1	2	3
1	2	8.5	2.5
2		240	14
3			6

It is possible to calculate the relative intensities of the tensor components of the $v_3(A_g + B_g)$ band in a similar way as for the infrared calculations for the ratio of intensities of the A_u to B_u bands. It is also possible to calculate the relative intensities of the $v_1(A_g + B_g)$
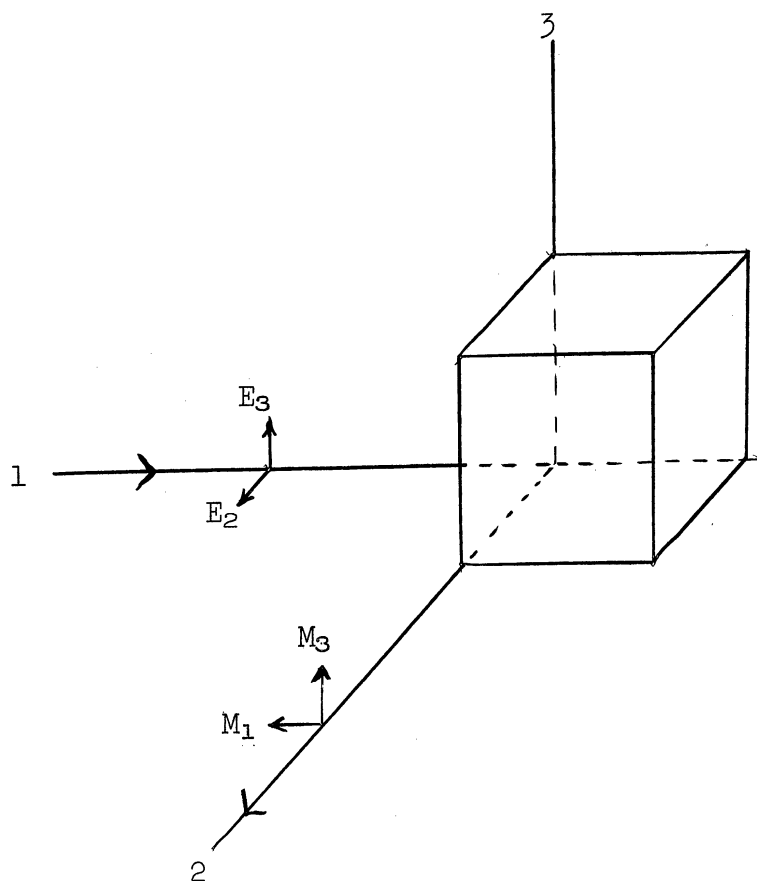
Figure 33. Orientation of crystal for
studies of the Raman effect. Directions
1, 2, 3 are parallel to the principal
axes of the index of refraction ellipsoid.

band if some assumption is made about the ratio of the tensor components of the individual molecules. A large difference exists between the observed and predicted values for both ν_1 and ν_3.

The high intensity of the band attributed to the ν_3 fundamental is disturbing. In the free molecule the Raman activity of this band is due to the off-diagonal tensor components, while that of the ν_1 vibration is due to diagonal terms. However, the intensity of the band attributed to ν_3 is equal to or greater than that of the ν_1 band. This has led Cabannes, Couture, and Mathieu to the conclusion that the two OH bonds are not equivalent and that it is not possible to argue for or against the Wooster structure for gypsum on the basis of the observed Raman spectrum.

6-2.3 Relation to the Structure

If the positions of the water molecules in gypsum are known, then it is possible to predict certain specific details of the infrared and Raman spectrum due to these molecules. These predictions are in good agreement with the infrared experimental results for the ν_2 (deformation) fundamental and in poor agreement for the ν_1 and ν_3 (stretching) fundamentals. The experimental results in the Raman spectrum are also in poor agreement for the ν_1 and ν_3 bands. Sufficient Raman data for the ν_2 fundamental have not been obtained to be able to draw any conclusions concerning it.

This disagreement can be attributed to one of two causes:

1. The assumed structure is incorrect.

2. The assumptions inherent in predicting the spectrum are not applicable.

Since there is no other reason for suspecting that the assumed structure is incorrect, it appears that a re-examination of the assumptions used

in predicting the spectrum is warranted. One principal assumption made is that every crystal fundamental is composed of the superposition of molecular fundamentals, with the phases so chosen as to satisfy the symmetry requirements. This assumption is justified if the interactions among the various molecules in the unit cell is small and if the crystal fundamentals belonging to the same symmetry species occur at widely separated frequencies.

In water vapor, the fundamentals ν_1 and ν_3 are located within 100 cm^{-1} of each other and the rotational fine structure overlaps. However, these fundamentals can not interact in the gaseous state since they belong to different symmetry species. In gypsum crystal, this restriction is removed. Each species of the factor group contains fundamentals arising from the ν_1 and ν_3 molecular fundamentals. Since the difference between ν_1 and ν_3 in the crystal is of the order of 130 cm^{-1}, and since this is of the order of crystalline splittings (the splitting between $\nu_2(A_u)$ and $\nu_2(B_u)$ is about 60 cm^{-1}), it might be expected that the character of the motions of ν_1 and ν_3 is quite different in the crystal than in the gas. The experimental observations will be reviewed in the light of this possibility.

On examining the spectroscopic data, a certain correspondence can be found between the infrared and Raman results:

1 (a) For the band assigned as ν_3, maximum absorption in the infrared occurs when the electric vector is parallel to the $\underline{b}(C_2)$ axis. The dichroic ratio is of the order of thirty.

(b) For the band assigned as ν_3 in the Raman spectrum, by far the largest tensor component is α_{22} (see Table 23). This corresponds to the incident electric vector parallel to $\underline{b}(C_2)$ axis. and the scattered light analysed with the electric

vector parallel to $\underline{b}(\underline{C}_2)$ axis.

2 (a) For the band assigned as ν_1, maximum infrared absorption

occurs when the electric vector lies in the plane perpendic-

ular to the $\underline{b}$ axis, i.e., the (010) plane. The dichroic

ratio is of the order of 1/5. The direction of the electric

vector in the (010) plane for maximum absorption is at the

angle $\phi = 80°$.

(b) For the Raman band assigned as ν_1, the largest tensor compo-

nents lie on the principal diagonal and where both the inci-

dent and scattered electric vectors lie in the (010) plane.

These experimental results are in accord with the following explana-

tion. From the model of the unit cell (see Figure 4) it can be seen that

there are two different types of OH bonds. Those which are nearly verti-

cal are designated as OH_3 and are within $12°$ of being parallel to the

$\underline{b}(\underline{C}_2)$ axis. Those which are nearly horizontal are designated as OH_1 and

are within $15°$ of being perpendicular to the $\underline{b}(\underline{C}_2)$ axis. The distance be-

tween the water oxygen and nearest sulfate oxygen is 2.70 for the OH_3 bonds

and 2.71 for the OH_1 bonds (see Table 2). This difference in distance may

or may not be significant, since it is within the experimental error. In

a simple valency force field treatment, the stretching force constants k_1

and k_3 can be assigned to the OH_1 and OH_3 bonds, respectively. In the

gaseous state, these force constants are equal. In gypsum crystal, it is

possible to think of an effective force constant consisting of an "intrin-

sic" force constant (the force constant in the gaseous state) and a term

taking into account the crystalline environment. The "intrinsic" part

will be the same for OH_1 and OH_3, but the environmental parts are differ-

ent. If the resultant effective force constant k_1 for the OH_1 bond were

somewhat different from the effective force constant k_3 of the OH_3 bond,

then the normal mode v_1 would be essentially an OH_1 vibration and the normal mode v_3 would be essentially an OH_3 vibration. The resulting transition moments will lie nearly parallel and perpendicular to the $\underline{b}(\underline{C_2})$ axis and will thus account for the infrared results. The projection of the OH_3 bonds on the (010) plane would give the direction of the transition moment of the B_u mode. This direction corresponds to an angle $\emptyset = 77°$ compared to the observed value of $\emptyset = 80°$. The Raman spectrum can also be explained very well on this basis. One would expect two strong Raman bands of approximately equal intensity, with large tensor components lying on the principal diagonal. This is exactly what is observed. The calculation of the exact magnitude of the inequality of k_1 and k_3 required to account for the experimental results would be a separate undertaking, but solution of a similar problem by Kohlrausch[83] suggests that this inequality need only be small to cause a large shift in the form of the normal vibrations without any appreciable shift in the frequencies.

Another structural feature revealed in the spectrum is the presence of hydrogen bonding. The v_2 (deformation) frequency is increased by about 30-90 cm^{-1} in gypsum crystal compared to the gaseous state. However, the v_1 and v_3 (stretching) frequencies are decreased by about 250 cm^{-1} in the crystal. This result is understandable since the O-O distance between the water and sulfate oxygens is 2.70 and 2.71 A.U. Lord and Merrifield[84] have shown that there is a correlation between the OH stretching frequency shift and O-O distance for a number of crystals which are thought to have strong hydrogen bonds. Using their data, one would expect to find a stretching frequency shift of about 800 cm-1 in gypsum. This would seem to indicate that the hydrogen bonds in gypsum are not as strong as in the substances investigated by Lord and Merri-

field. Absorption bands affected by hydrogen bonding are known to be broader than those not affected. The v_1 and v_3 bands are about 50-70 cm^{-1} wide (half-width), while all the other fundamentals range between 15-35 cm^{-1}. The half-widths of v_1 and v_3 are comparatively narrow compared to strongly hydrogen-bonded substances.

6-3 Combinations and Overtones

6-3.1 Origin and Selection Rules

In order to simplify the mathematical treatment of vibrations in solids, harmonic forces are assumed (i.e., only squared terms appear in the potential energy function). In this first order approximation the infrared active fundamentals appear as sharp lines. Combinations and overtones are not allowed. The appearance of combinations and overtones indicates the need for cubic or higher order terms to the potential energy function. In addition, the line shapes of fundamentals are found to be broader than might be expected from the harmonic picture.[82]

The general theory of crystal spectra (including anharmonicity) predicts essentially no selection rules for combinations and overtones.[85,86] However, in previous studies of crystal spectra it has been found that the factor group selection rules provide a successful guide for the classification of observed combinations and overtones.

The selection rules for combinations and overtones for the factor group of gypsum, C_{2h}^6, can be obtained from those listed in Herzberg[87] for the isomorphous point group C_{2h}, or these can be readily derived from the character table (Table 6). The results for binary combinations and overtones are listed in Table 24. The left side contains the species of all the possible simple binary combinations and the right side contains the species of the resultant.

In addition to classifying the bands, it would be useful to predict the direction of the transition moments. For the A_u bands these must lie parallel to the $\underline{b}(C_2)$ axis and for the B_u bands these must lie in the plane perpendicular to the $\underline{b}(C_2)$ axis, i.e., the (010) plane. For the water fundamentals it is possible to predict the direction of the transition moment in the (010) plane. It is not known how to predict this direction for the combination bands.

TABLE 24

MULTIPLICATION TABLE
(BINARY COMBINATIONS AND OVERTONES)

$$A_g \cdot A_g = A_g$$

$$A_u \cdot A_u = A_g$$

$$B_g \cdot B_g = A_g$$

$$B_u \cdot B_u = A_g$$

$$A_g \cdot B_g = B_g$$

$$A_u \cdot B_u = B_g$$

$$A_g \cdot A_u = A_u$$

$$B_g \cdot B_u = A_u$$

$$A_g \cdot B_u = B_u$$

$$A_u \cdot B_g = B_u$$

The experimentally observed frequencies and assignments are shown in Table 25 for the combinations bands. It is not always possible to calculate the frequency of a combination band by taking the sum of fundamentals. This is because the Raman bands corresponding to ν_R" and ν_2

TABLE 25

COMBINATION BANDS

Assignment	Calculated Frequency cm^{-1}	Observed Frequency cm^{-1}
SO_4 $\quad \nu_{4a}(B_u) + \nu_4(A_g)$ $602 \quad + \quad 621$	1223	
SO_4 $\quad \nu_4(B_g) + \nu_4(A_u)$ $623.5 + \quad 604$	1227.5	1205
SO_4 $\quad \nu_3(B_g) + \nu_1(A_u)$ $1117 \qquad 1000$	2117	
SO_4 $\quad \nu_{3a}(B_u) + \nu_1(A_g)$ $1118 \qquad 1006$	2124	2112
SO_4 $\quad \nu_3(B_g) + \nu_1(A_u)$ $1136 \qquad 1000$	2136	2130
SO_4 $\quad \nu_{3c}(B_u) + \nu_2(A_g)$ $1142 \quad + \quad 1006$	2148	
H_2O $\quad \nu_2(B_u) + \nu_{R''}(A_g)$ $1623 \quad + \quad ?$	....	2198
H_2O $\quad \nu_2(A_u) + \nu_{R''}(B_g)$ $1684 \quad + \quad ?$	....	2235
H_2O $\quad \nu_2(A_g) + \nu_{R''}(B_u)$ $? \quad + \quad 600$	....	
H_2O $\quad \nu_2(B_g) + \nu_{R''}(A_u)$ $? \quad + \quad 580$	....	
H_2O $\quad \nu_2(B_u) + \nu_2(A_g)$ $1623 \qquad ?$	....	3248
H_2O $\quad \nu_2(A_u) + \nu_2(B_g)$ $1684 \qquad ?$	....	3350
$?$	....	3560

have not been classified in terms of the crystal species. Broad bands have been observed in the Raman spectrum[29] near 565 and 588 cm^{-1}, which is close to the broad infrared band near 600 cm^{-1} assigned as $\nu_{R''}$. A weak Raman band which has been reported[29,33] near 1632 cm^{-1} is assigned as ν_2, but it has not been classified.

The weak reflection band near 1200 cm^{-1} (see Figure 27B) corresponds roughly in frequency to a combination of the sulfate internal fundamentals $\nu_2 + \nu_2$. As can be seen in Table 25, the observed band is about 25 cm^{-1} lower than that obtained by taking the sum of fundamentals so that the agreement is not outstanding.

The complex band near 2200 cm^{-1} was assigned by Coblentz to both the water and sulfate since both liquid water and anhydrite (anhydrous $CaSO_4$) have bands in this region. On examining the polarized spectrum it was found that this complex consists of two relatively sharp bands at 2112 cm^{-1} and 2130 cm^{-1} and several overlapping broad bands centered near 2230 cm^{-1}. The sharp bands are believed to be combinations of the sulfate internal fundamentals $\nu_1 + \nu_3$, while the broad bands suggest combinations of the water fundamentals $\nu_2 + \nu_{R''}$. Since the $\nu_{R''}$ rotary lattice fundamental is broad, it is not surprising that the combination band is also broad.

The two bands near 3248 cm^{-1} and 3350 cm^{-1} may be assigned as combinations of the water internal fundamental $\nu_2 + \nu_2$. It is not possible to calculate the expected position of the band since the ν_2 Raman band has not been classified. The weak band near 3560 cm^{-1} can not be satisfactorily assigned.

In conclusion, it can be seen that reasonable agreement can be obtained by considering the binary combinations of the observed fundamentals using the factor group selection rules.

6-4 Conclusion

The results of this investigation are of interest in evaluating infrared spectroscopy as a tool in structural investigations of solids. It was found that the infrared spectrum of the mineral gypsum, $CaSO_4 \cdot 2H_2O$, could be correlated with the crystal structure. Both the interpretation of the spectrum and the experimental methods may be of interest in similar problems.

Gypsum as well as many solids has intense absorption bands. The measurement of the reflection spectrum instead of the more usual transmission spectrum was found to be quite successful for obtaining the optical constants of highly absorbing materials. The chief difficulties with reflection methods in the past is that they are not suitable for anisotropic materials and the analysis of data to obtain the absorption spectrum is quite cumbersome. The method introduced recently by T. S. Robinson is quite suitable for anisotropic materials, but the calculations are complicated and tedious. Since the Robinson method has been employed in this investigation, the calculations have been carried out rapidly on an electronic digital computer. This method shows great promise for the spectroscopy of solids.

The various infrared active fundamentals of gypsum can be classified in terms of the symmetry species associated with the space group. Information about the magnitude and direction of crystal forces on the sulfate ion can be obtained from a study of bands which are degenerate in the isolated ion but are split to give non-degenerate bands in the crystal.

One of the principal purposes of this investigation was to attempt to locate the positions of the hydrogen atoms of the water of crystallization in gypsum, assuming a knowledge of the location of the heavy atoms

in the crystal. Assuming an "oriented gas" model, the ratios of the intensities of the two infrared active crystal fundamentals arising from each molecular fundamental can be predicted. Good agreement between the observed and predicted values was obtained for the ν_2 (deformation) fundamental and poor agreement was obtained for the ν_1 and ν_3 (symmetric and antisymmetric stretching) fundamentals. It appears that some additional factor must be taken into account in predicting the spectrum. The fact that the symmetry of the water molecules is different in the vapor and in gypsum crystal is believed to account for the discrepancy.

In general, this investigation shows that infrared spectroscopy provides a powerful method for examining the motions of molecules and ions in crystals. It is possible to obtain information about the force field in crystals from the infrared spectrum. However, any conclusions about the positions of atoms deduced from infrared intensities must be examined with care.

APPENDIX I

LOCATION OF SINGULARITIES

The location of the singularities of the functions to be considered
is of crucial importance. Functions such as the complex conductivity σ
can be treated in exactly the same way as the complex impedance of an
electrical networks. However, further consideration must be given to the
complex index of refraction $\underline{N}$ and complex reflection coefficient $\underline{R}$.

For a simple oscillator it is easy to show from expression (3-16),

$$\underline{\sigma} = \frac{n_0 e^2}{m} \frac{\omega e^{i(\phi + \pi/2)}}{\sqrt{(\omega_0^2 - \omega^2)^2 + g^2\omega^2}} , \qquad (3\text{-}16)$$

that no singularities lie on the right half of the complex frequency
plane. This is done for the equivalent case of a resonant circuit by
Bode.[88] Extension to a system of oscillators can be carried out in the
same way as for an electrical network[89] or more easily by writing down
the expression for the complex conductivity of the system. This will
consist of a sum of terms similar to (3-16). This is a rational func-
tion of ω and is said to be positive real.[90] The properties of positive
real functions are well known and include absence of singularities in
the right half of the complex frequency plane. Since the test for singu-
larities will be carried out on $\underline{N}$ and $\ln \underline{R}$, it will first be applied to
$\underline{\sigma}$ as an illustrative example.[91]

Singularities occur in functions when the derivative becomes infi-
nite. Positive real functions such as $\underline{\sigma}$ can be written as the quotient

of two polynomials,

$$\underline{\sigma} = \frac{M(p)}{D(p)} \quad , \tag{A-1}$$

which are functions of the complex frequency p. The derivative is given by

$$\frac{d\underline{\sigma}}{dp} = \frac{D\frac{dM}{dp} - N\frac{dD}{dp}}{D^2} \quad . \tag{A-2}$$

Since M and D are ordinary polynomials neither they nor their derivatives can become infinite for finite values of p. Only where D = C (the poles of the original function) can the derivative become infinite. Therefore, the singularities of a positive real function are its poles. These do not lie in the right half of the complex frequency plane.[91]

The complex index of refraction $\underline{N}$ in terms of $\underline{\sigma}$ is given by (3-19)

$$N = \sqrt{\frac{4\pi\sigma}{p} + 1} \quad . \tag{3-19}$$

The quantity under the square root sign is known as the complex dielectric constant and is also a positive real function. Letting

$$N = \sqrt{\frac{M'}{D}}$$

and differentiating the result

$$\frac{dN}{dp} = \frac{1}{2}\sqrt{\frac{D}{M'}} \frac{\left(D\frac{dM}{dp} - M'\frac{dD}{dp}\right)}{D^2} \tag{A-3}$$

is obtained. This derivative becomes infinite whenever M' or D vanishes. These are the zeros and poles of a positive real function and cannot lie in the right half of the complex frequency plane.[90] Consequently, no singularities of $\underline{N}$ lie in the right half of the complex frequency plane.

The reflection coefficient $\underline{R}$ is related to $\underline{N}$ by

$$\underline{R} = \frac{\underline{N} - 1}{\underline{N} + 1} . \qquad (3\text{-}5)$$

The derivative of $\ln \underline{R}$ is given by

$$\frac{d \ln \underline{R}}{dp} = \frac{2}{\underline{N}^2 - 1} \frac{d\underline{N}}{dp} . \qquad (A\text{-}4)$$

Substituting the value of $\underline{N}^2$ from (3-18) gives

$$\frac{d \ln \underline{R}}{dp} = \frac{p}{2\pi\underline{\sigma}} \frac{d\underline{N}}{dp} = \frac{p}{2\pi} \frac{D}{M} \frac{d\underline{N}}{dp} . \qquad (A\text{-}5)$$

This function becomes infinite at the zeros and poles of a positive real function and therefore the singularities are absent from the right side of the complex frequency plane.

It should be pointed out that the singularities of $\underline{N}$ and $\ln \underline{R}$ are not the poles of these functions, but are branch points.

APPENDIX II

RELATIONS BETWEEN REAL AND IMAGINARY PARTS
OF COMPLEX FUNCTIONS

The conditions under which the real and imaginary parts of a complex function

$$Z = X + iY$$

can be related are the following:[92]

1. The real component, X, is an even function of the frequency ω.*

2. The imaginary component, Y, is an odd function of the frequency ω.*

3. There are no singularities in the interior of the right half-plane.

4. Singularities at any finite point p_0 on the real frequency axis are of such a nature that $(p - p_0)Z$ vanishes as p approaches p_0. This admits logarithmic singularities and branch points but not poles on the real frequency axis (the real frequency axis is the $i\omega$ axis).

5. In general, it will be supposed that Z is analytic at infinity. For the theorem in question a singularity here is permitted, provided Z/p vanishes as p is made indefinitely great.

6. If Z is assumed to be analytic at zero and infinite frequency, the quantities X_0, Y_0, X_∞, Y_∞, etc., will be defined as the coefficients in the corresponding power series expansions,

$$Z = X_0 + iY_0 p + X_1 p^2 + iY_1 p^3 + \ldots\ldots$$

and

$$Z = X_\infty + i\frac{Y_\infty}{p} + \frac{X_1^!}{p^2} + i\frac{Y_1^!}{p^3} + \ldots\ldots$$

These conditions are fulfilled by the complex functions $\underline{\sigma}$, $\underline{N}$, and $\ln \underline{R}$ obtained by assuming a model consisting of Lorentz oscillators.

---

*The stringency of this condition has been questioned by Brachman and Macdonald.[93]

The conditions are fulfilled by positive real functions such as $\underline{\sigma}$. It was shown in Appendix I that the restriction on location of singularities is fulfilled by $\underline{N}$ and $\ln \underline{R}$. Satisfaction of the other conditions follows readily for a system of Lorentz oscillators.

From this point the derivation of the relations between the real and imaginary parts becomes a mathematical problem whose solution is relatively short and is a direct application of Cauchy's theorem. Let the value of X and Y at ω_c be denoted as X_c and Y_c, respectively. Consider the integral

$$\oint \left(\frac{Z - A_c}{p - i\omega_c} - \frac{Z - A_c}{p + i\omega_c} \right) dp = 0$$

evaluated over the path shown in Figure 34. The bounded area extends to very large values of p. Small indentations at $\pm\omega_c$ are made, since the integrand has poles at these points. By the method of contour integration, it is not difficult to show that the expression (A-6) reduces to[94]

$$Y_c = \frac{2\omega_c}{\pi} \int_0^\infty \frac{X - X_c}{\omega^2 - \omega_c^2} \, d\omega .$$

(A-7)

With slightly more labor this can be expressed in the alternate form

$$Y_c = \frac{1}{\pi} \int_0^\infty \frac{d \ln X}{d\omega} \ln \left| \frac{\omega + \omega_c}{\omega - \omega_c} \right| d\omega .$$

(A-8)

This form is more suitable for calculations near $\omega = \omega_c$ and was used for the calculations in reflection spectra.
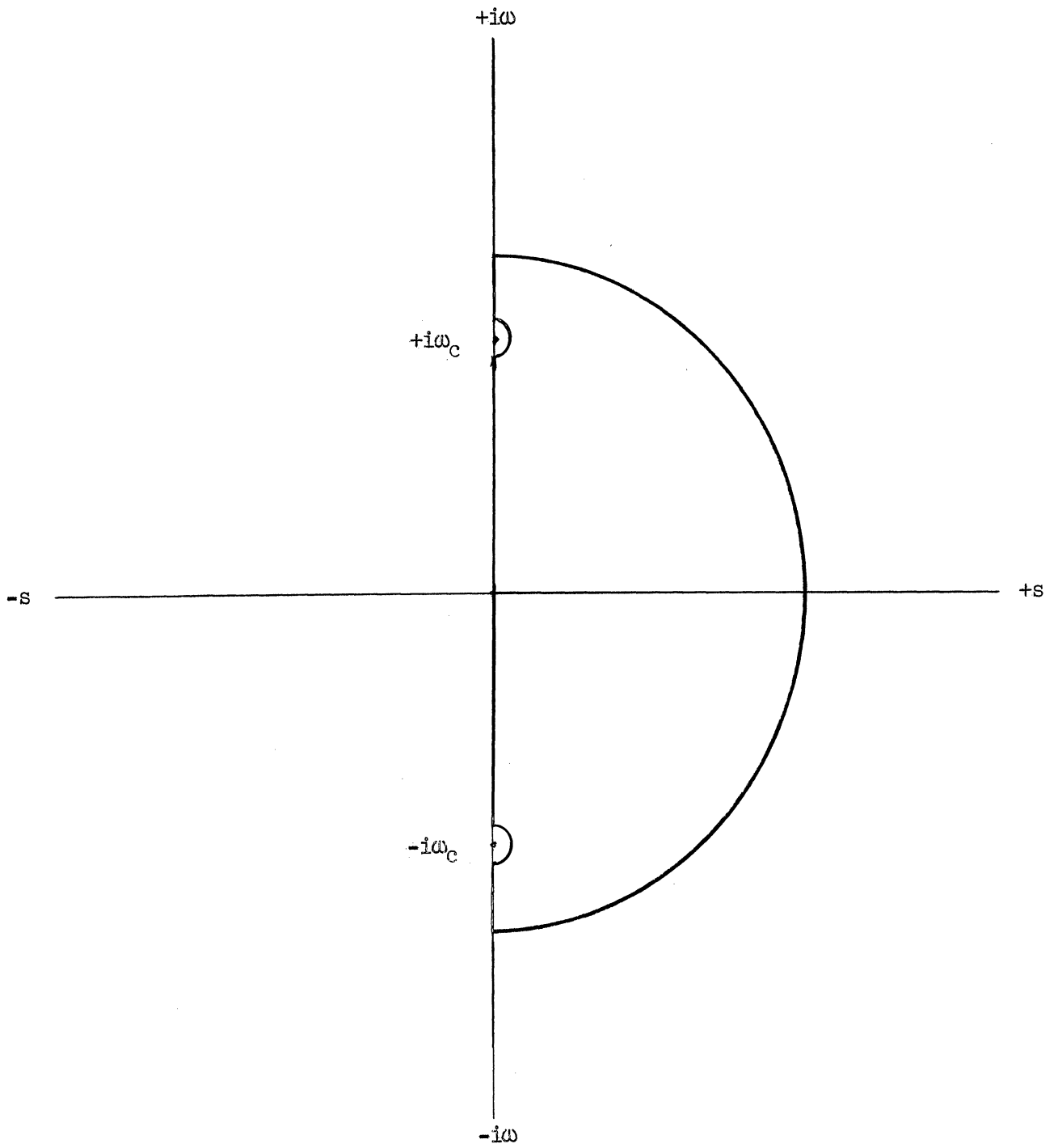
Figure 34. Region of Contour Integration

BIBLIOGRAPHY

1. Dana's System of Mineralogy, II, rewritten and enlarged by Palache, Berman, and Frondel. John Wiley and Sons, Inc., New York, 1953, p. 483.

2. Wooster, W. A. Z. Krist., 94, 375 (1936).

3. Bragg, W. L. Atomic Structure of Minerals. Cornell University Press, Ithaca, New York, 1937, p. 130.

4. de Jong, W. F. and Bouman, J. Z. Krist., 100, 275 (1938).

5. Bhagavantam, S. and Venkatarayudu, T. Theory of Groups and Its Application to Physical Problems, Andhra University, Waltair, India, 1951, second edition, p. 127.

6. Herzberg, G. Infrared and Raman Spectra of Polyatomic Molecules, D. Van Nostrand, New York, 1945, p. 489.

7. Pake, G. E. J. Chem. Phys., 16, 327 (1948).

8. Coblentz, W. W. Investigations of Infrared Spectra, Part III. Carnegie Institution of Washington, Washington, D.C., 1936, pp. 17-20.

9. Coblentz, W. W. Phys. Rev., 30, 322 (1910).

10. Coblentz, W. W. Bull. Bur. Standards, 7, 619 (1911).

11. Coblentz, W. W. Bur. Standards Sci. Papers, 17, 267 (1921).

12. Goens, E. Z. Physik, 6, 12 (1921).

13. Ellis, J. W. Phys. Rev., 38, 693 (1931).

14. Carrelli, A. Nuovo cimento, 14, 245 (1937).

15. Louisfert, J. J. phys. et radium, 8, 21 (1947).

16. Louisfert, J. J. phys. et radium, 8, 45 (1947).

17. Pain, C., Duval, C., and Lecomte, J. Compt. rend., 237, 238 (1953).

18. Webber, D. S. Phys. Rev., 96, 846 (1954).

19. Hunt, J. M., Wisherd, M. P., and Bonham, L. C. Anal. Chem., 24, 1478 (1952).

20. Miller, F. A. and Wilkins, C. H. Anal. Chem., 24, 1253 (1952).

21. Keller, W. D., Spotts, J. H., and Biggs, D. L. Am. J. Sci., 250, 453 (1953).

22. Aschkinass, E. Ann. Physik, 1, 42 (1900).

23. Koch, J. Ann. Physik, 26, 974 (1908).

24. Randall, H. M. Astrophys. J., 34, 308 (1911).

25. Schaefer, C. and Schubert, M. Ann. Physik, 50, 283 (1916).

26. Rubens, H. Z. Physik, 1, 11 (1921).

27. Cabannes, J. and Aynard, R. J. phys. et radium, 3, 137 (1942).

28. Rousset, A. and Lochet, R. J. phys. et radium, 6, 57 (1945).

29. Krishnan, R. S. Proc. Indian Acad. Sci., 22A, 274 (1945).

30. Gross, E. F. and Val'kov, V. I. Doklady Akad. Nauk S.S.S.R.
    67, 619 (1949); Chem. Abstracts, 48, 6829 (1954)
    68, 473 (1949); Chem. Abstracts, 44, 437 (1950)

31. Stekhanov, A. I. Doklady Akad. Nauk S.S.S.R., 92, 281 (1953),
    U.S. Atomic Energy Commission, NSF-tr-189.

32. Aynard, R. Compt. rend., 236, 1416 (1953).

33. Cabannes, J., Couture, L., and Mathieu, J. P. J. chim. phys., 50, C89 (1953).

34. Born, M. and Goeppert-Mayer, M. Handbuch der Physik, second edition, Vol. 24, Part 2, Julius Springer, Berlin, 1933, Chapter IV.

35. Bhagavantam, S. and Venkatarayudu, T. Proc. Indian Acad. Sci., 9A, 224 (1939).

36. Bhagavantam, S. and Venkatarayudu, T. Theory of Groups and Its Application to Physical Problems, Andhra University, Waltair, India, 1951, second edition, Chapter XII.

37. Halford, R. S. J. Chem. Phys., 14, 8 (1946).

38. Hornig, D. F. J. Chem. Phys., 16, 1063 (1948).

39. Winston, H. and Halford, R. S. J. Chem. Phys., 17, 607 (1949).

40. Bhagavantam, S. Proc. Indian Acad. Sci., 8A, 345 (1938).

41. Herzberg, G. Infrared and Raman Spectra of Polyatomic Molecules, D. Van Nostrand, New York, 1945, p. 281.

42. Benedict, W. S. and Plyler, E. K. Nat. Bur. Standards J. Research, 46, 246 (1951).

43. Fox, J. J. and Martin, A. E. Proc. Roy. Soc. (London), A174, 234, (1940).

44. Narayanaswamy, P. K. Proc. Indian Acad. Sci., 27A, 311 (1948).

45. Andreyev, S. N. and Balicheva, T. G. Doklady Akad. Nauk. S.S.S.R., 90, 149 (1953); U.S. Atomic Energy Commission, NSF-tr-66.

46. Kohlrausch, F. Ramanspektren, Hand- und Jahrbuch der chemischen Physik, Vol. 9, Part 6, Akademische Verlagsgesellschaft, Leipzig, 1943 (Reprinted: Edwards Brothers, Ann Arbor, Michigan, 1943) p. 151.

47. Simon, I. J. Opt. Soc. Amer., 41, 336 (1951).

48. Robinson, T. S. Proc. Phys. Soc., B65, 910 (1952).

49. Robinson, T. S. and Price, W. C. Proc. Phys. Soc., B66, 969 (1953).

50. Robinson, T. S. Thesis, University of London, 1953.

51. Bode, H. W. Network Analysis and Feedback Amplifier Design, D. Van Nostrand, New York, 1945, Chapter XIV.

52. Lorentz, H. A. The Theory of Electrons, B. G. Teubner, Leipzig, 1909, pp. 153, 307.

53. Seitz, F. The Modern Theory of Solids, McGraw-Hill Book Company, Inc., New York, 1940, Chapter XVII.

54. Bode, H. W., op. cit., p. 320.

55. Ibid., pp. 305-308, 312, 318.

56. Toll, J. S. and Wheeler, J. A., Unpublished.

57. Toll, J. S. Thesis, Princeton University, 1952.

58. Krönig, R. de L. J. Opt. Soc. Amer., 12, 547 (1926).

59. Kallman, H. and Mark, H. Ann. Physik, 82, 585 (1927).

60. Kramers, H. A. Atti del Congreso Internazional de Fisici, Como. Nicolo Zonichelli, Bologna, 1927, Vol. 2, p. 545.

61. Kronig, R. Ned. Tijdschr. Natuurk., 9, 402 (1942).

62. Kronig, R. Physica, 12, 543 (1946).

63. Schützer, W. and Tiomno, J. Phys. Rev., 83, 249 (1951).

64. von Kampen, N. G. Phys. Rev., 89, 1072 (1953).

65. Gell-Mann, M., Goldberger, M. L., and Thirring, W. E. Phys. Rev., 95, 1612 (1954).

66. Frohlich, H. _Theory of Dielectrics_, The Clarendon Press, Oxford, 1949.

67. Gorter, C. J. and Kronig, R. _Physica_, 3, 1009 (1936).

68. Pake, G. E. and Purcell, E. M. _Phys. Rev._, 74, 1184 (1948).

69. Instruction Manual for Perkin-Elmer Model 12C Infrared Spectrometer, Appendix. Perkin-Elmer Corporation, Norwalk, Connecticut, 1950.

70. Downie, A. R., Magoon, M. C., Purcell, T., and Crawford, B. _J. Opt. Soc. Amer._, 43, 941 (1953).

71. McKinney, D. S. and Friedel, R. A. _J. Opt. Soc. Amer._, 38, 222 (1948).

72. Murphy, G. M., Weiner, G., and Oberly, J. J. _J. Chem. Phys._, 22, 1322 (1954).

73. Couture-Mathieu, L., Ketelaar, J. A., Vedder, W., and Fahrenfort, J. _Physica_, 18, 762 (1952).

74. Wagner, E. L. and Hornig, D. F. _J. Chem. Phys._, 18, 296 (1950).

75. Newman, R. and Halford, R. S. _Rev. Sci. Instr._, 19, 270 (1948).

76. Kessler, H. B. Thesis, University of Michigan, 1953.

77. Vallance-Jones, A. Thesis, Cambridge University, 1949.

78. Elliot, A., Ambrose, E. J. and Temple, R. _J. Opt. Soc. Amer._, 38, 212 (1948).

79. Newman, R. S. and Halford, R. S. _J. Chem. Phys._, 18, 1276 (1950).

80. Scott, R. E. _Proc. Inst. Radio Engrs._, 40, 970 (1952).

81. Narayana Rao, D. A. A. S. _Proc. Indian Acad. Sci._, 27A, 177 (1948).

82. Hornig, D. F. _Discussions Faraday Soc._, 9, 115 (1950).

83. Kohlrausch, F. _Der Smekal-Raman Effect_, Erganzungsband, 1931-1937, J. Springer, Berlin, 1938, p. 136.

84. Lord, R. C. and Merrifield, R. E. _J. Chem. Phys._, 21, 167 (1953).

85. Born, M. and Blackman, M. _Z. Physik_, 82, 551 (1933).

86. Born, M. and Bradburn, M. _Proc. Roy. Soc._, A188, 161 (1947).

87. Herzberg, G., op. cit., p. 126.

88. Bode, H. W., op. cit., p. 26.

89. Ibid, p. 110.

90. Guillemin, E. A. _The Mathematics of Circuit Analysis_, John Wiley and Sons, New York, 1949, p. 409.

91. Bode, H. W., op. cit., p. 28.

92. Ibid, p. 278.

93. Brachman, M. K. and Macdonald, J. R. _Physica_, _20_, 1266 (1954).

94. Bode, H. W., op. cit., p. 307.